Chemie der Erde 74 (2014) 149–183

Contents lists available at ScienceDirect

Chemie der Erde

journal homepage: www.elsevier.de/chemer

Invited Review

The Almahata Sitta polymict breccia and the late accretion of asteroid 2008 TC_3

Marian Horstmann*, Addi Bischoff

Institut für Planetologie, Westfälische Wilhelms-Universität Münster, Wilhelm-Klemm-Str. 10, 48149 Münster, Germany

ARTICLE INFO

Article history:
Received 2 October 2013
Accepted 29 January 2014
Editorial handling - Prof. Dr. K. Heide

Keywords:
Almahata Sitta
Asteroid 2008 TC_3
Polymict ureilite
Polymict breccia
Ureilite
Ureilitic andesite
Enstatite chondrites
Late accretion
Impact mixing
Ureilite parent body

ABSTRACT

On October 7, 2008, a small asteroid named 2008 TC_3 was detected in space about 19 h prior to its impact on Earth. Numerous world-wide observations of the object while still in space allowed a very precise determination of its impact area: the Nubian Desert of northern Sudan, Africa. The asteroid had a pre-atmospheric diameter of ~4 m; its weight is reported with values between ~8 and 83 t, and the bulk density with ~2–3 g/cm^3, translating into a bulk porosity in the range of ~20–50%. Several dedicated field campaigns in the predicted strewn field resulted in the recovery of more than 700 (monolithological) meteorite fragments with a total weight of ~10.5 kg. These meteorites were collectively named "Almahata Sitta", after the nearby train station 6, and initially classified as an anomalous polymict ureilite. Further work, however, showed that Almahata Sitta is not only a ureilite but a complex polymict breccia containing chemically and texturally highly variable meteorite fragments, including different ureilites, a ureilite-related andesite, metal-sulfide assemblages related to ureilites, and various chondrite classes (enstatite, ordinary, carbonaceous, Rumuruti-like). It was shown that that chondrites and ureilites derive from one parent body, i.e., asteroid 2008 TC_3, making this object, in combination with the remotely sensed physical parameters, a loosely aggregated, rubble-pile-like object. Detailed examinations have been conducted and mineral-chemical data for 110 samples have been collected, but more work on the remaining samples is mandatory.

Detailed study of Almahata Sitta allows insights into the formation and evolution of ureilites and their parent body. These results support the catastrophic impact disruption of the ureilite parent body and re-accretion of the dispersed ureilitic material into second generation ureilite asteroids. Almahata Sitta shows that different chondritic materials were present in the region of re-accretion and mixed into the newly formed rubble-pile-like asteroid. Asteroid 2008 TC_3 was part of a late-formed ureilitic second generation body in the main belt and was liberated ~20 Ma ago, finally moving into Earth-crossing orbits that ultimately led to its impact on Earth. The abundant samples of Almahata Sitta, fragments of Asteroid 2008 TC_3, allow study of not only different types of meteorites, but offer the unique opportunity to gain further insights into processes in the asteroid belt of our Solar System such as migration, collision, mixing, and (re-)accretion of asteroidal bodies. Beyond that, this event has the potential to further the understanding of the meteorite–asteroid links, which is a major goal of meteorite science.

Contents

* Corresponding author. Tel.: +49 251 8336377; fax: +49 251 8336301.
E-mail address: marianhorstmann@uni-muenster.de (M. Horstmann).

http://dx.doi.org/10.1016/j.chemer.2014.01.004
0009-2819/

1. Introduction

Asteroids are generally accepted to be the parent bodies of the majority of meteorites in the world's meteorite collections. Establishing and understanding the link between meteorites available for study on Earth and their asteroidal parent bodies is one of the major goals of meteorite science. However, this is quite challenging and has, except for the Itokawa S-type asteroid and the LL ordinary chondrites via the Hayabusa space craft (Nakamura et al., 2011), not been successfully demonstrated by direct sampling of asteroidal material. Further albeit weaker links of meteorite classes and asteroids have been based on spectroscopic observations (e.g., Burbine et al., 2002). The Dawn mission was designed to further elucidate the proposed link between the largest achondrite group of HED (howardites, eucrites, diogenites) meteorites and asteroid 4 Vesta (e.g., McSween et al., 2010).

In October 2008, a one-of-a-kind event allowed for the first time the study of an asteroid in space that subsequently impacted Earth and allowed collection of numerous meteorite fragments, enabling a direct comparison of the asteroids properties obtained via remote sensing and detailed petrographic and mineral-chemical aspect of its meteorite remnants: On October 6th, 2008, Richard Kowalski at the automated Catalina Sky Survey telescope at Mt. Lemmon Observatory (Arizona) detected a small asteroidal body at 06:39 UTC (Kowalski, 2008; Yeomans, 2008; McGaha et al., 2008; Chesley et al., 2008). The object was designated asteroid 2008 TC_3. Subsequent orbital calculations predicted an impact on Earth in the Nubian Desert of northern Sudan about 19 h after the discovery (McGaha et al., 2008; Jenniskens et al., 2009a,b; Table 1).

After its impact, field campaigns organized by Peter Jenniskens and Muawia Shaddad (supported by staff from the University of Khartoum) and further independent search activities resulted in the collection of several hundred small meteorite fragments that were collectively named the Almahata Sitta meteorite, which is the Arabic translation for the nearby train station 6 (e.g., Goodrich et al., 2014; Jenniskens et al., 2009a,b; Bischoff et al., 2010b; Shaddad et al., 2010). To date more than 700 specimens with a total weight of roughly 10 kg have been collected, 25 of which (number refers only to those for which mineral-chemical data are available) were studied in a consortium led by P. Jenniskens. Fragments of about 80 different meteorites were investigated independently in cooperations organized by the Institut für Planetologie, Münster. A small number of additional samples were examined by other institutions. Overall, petrographic and mineral-chemical data have been collected for 110 samples (Table 2).

Table 1
Orbital parameters of asteroid 2008 TC_3 used to calculate the approach path. For details see Jenniskens et al. (2009b).

Symbol	Parameter	Value
α	Semimajor axis	1.308201 ± 0.000009 AU
q	Perihelion distance	0.899957 ± 0.000002 AU
ω	Argument of perihelion	$234.44897 \pm 0.00008^\circ$
Ω	Longitude of ascending node	$194.101138 \pm 0.000002^\circ$
i	Inclination	$2.54220 \pm 0.00004^\circ$
Tp	Perihelion time	2008 November 20.3989 ± 0.0001 UT

The Almahata Sitta meteorite, originally classified as a anomalous polymict ureilite (Jenniskens et al., 2009b), soon turned out to be a complex polymict breccia consisting of various ureilites and chondrites showing a broad range of textures, mineral abundances and compositions (Bischoff et al., 2010a,b). Combined with remote sensing data, these results made asteroid 2008 TC_3 a prime example of a rubble pile asteroid, although the different lithologies appear to be weakly welded together (Popova et al., 2011, and below). This is different from the classical case of a rubble pile, in

Table 2
Compilation of mineral-chemical data for 110 Almahata Sitta samples, including ureilites, ureilite-related samples, and the various chondrite classes.

Frag-No.	Frag. Mass	Shock[a]	W[b]	Typical grain size[c]	Ol cores	Ol range	Px cores	Px range	Px (Wo)	Comments	Refs.
Coarse-grained ureilitic fragments											
AHS 1	4.412 g							En61–99	1–37	range for low-Ca and Ca-rich Px	1
AHS 4	14.592 g			Ol ≤200 μm, Px ≤500 μm	down to Fa13.1	Fa6.9–13.1		En78–85	2–6		1
AHS 15	75.536 g					Fa5.6–8.5		En83.6–84	4.8–5	schreibersite (~2.5 wt% Ni)	1,2
AHS 22	115.32 g				Fa19.7		En79/En73.9		4.7/9.5	two distinct low-Px populations	3
AHS 24	92.76 g				Fa3–7		En52		6		1
AHS 27	283.84 g				Fa14.7/14.8		En82.1/81.5		4.7/5.1		3,4
AHS 39	5.661 g				Fa17.7–21.5	Fa4.1–21.5		En74.2–47.8	6.8–7.2	low abundance of Ol	1
AHS 44	2.291 g				Fa16–21		Fs28.5		11.1	metal (wt%): Ni = ~4.9, Co = ~0.4, P = 0.35, Si = 1.5	1–3
AHS 48	152.11 g				Fa13–21					only one small grain	1
AHS 54	121.22 g					Fa10–21				only one small grain	1
AHS S138	2.812 g				Fa3.5–17.3	Fa17–17.3		En75–85	5–10		1
MS-16	4.31 g	S3	W0/1	500–800 μm	Fa5–6	Fa2–6	Fs5–6	Fs5–6	3–4.5#	Px-dominating; 4–5 wt% Ni in metal	5
MS-153	7.43 g	S2	W0/1	100–300 μm	Fa10–12	Fa8–13	Fs10–11.5	Fs3.5–11.5	4–5#	Px-rich	5
MS-156	16.00 g	S2	W0	>1 mm	Fa17–19	Fa4–19	Fs11–12.5	Fs4–12.5	1–8#	zoned Ol with fine-grained network of metals and FeS	5
MS-157	3.68 g	S2	W0/1	0.8–1.2 mm	Fa12–13	Fa2–13	Fs10–11	Fs2–11	4.5–5#		5
MS-160	8.39 g	S3	W0	>1 mm	Fa17–19	Fa1–19				Px-poor	5
MS-162	4.74 g	S3	W0/1	400–600 μm	Fa16–18	Fa1.5–18	Fs6–7	Fs2–7	4–4.5#	grains up to 2.5 mm	5
MS-167	49.14 g	S3	W0/1	0.6–1.5 mm	Fa20.5–22	Fa2–22	Fs17–18.5	Fs1–18.5	11–11.5#		5
MS-169	26.29 g	S3	W0	300–600 μm	Fa11–12.5	Fa1–12.5	Fs10.5–11	Fs0.5–11	5–9#	Px-rich	5
MS-170	26.81 g	S3	W0/1	400–800 μm	Fa20–22	Fa1–22	Fs17–19	Fs3–19	6–7#		5
MS-171	34.35 g	S2	W0	100–300 μm	Fa15–16.5	Fa5–16.5	Fs12–14	Fs9–14	2–9#	variable grain size	5
MS-173	32.30 g	S3	W0/1	0.8–1.2 mm	Fa11.5–13.5	Fa6–13.5	Fs10.5–11.5	Fs0.5–11.5	4.5–5.5#	Px-rich	5
MS-175	7.46 g	S2	W0/1	300–600 μm	Fa10–12	Fa2–12	Fs8–10	Fs2–10	4.5–5#	Px-rich	5
MS-178	52.27 g	S3	W0/1	500–800 μm	Fa10.5–12	Fa2–12	Fs10–13.5	Fs1–13	1.3–13#		6,7
MS-180	84.12 g	S3	W0	~600 μm	Fa12.5–17	Fa2–17	Fs10.5–15	Fs3–15	3–10#		6,7
MS-182	19.33 g	S2	W0/1	0.3–1 mm	Fa4.5–10	Fa3–10	Fs3–4.5	Fs0.4–4.5	1–3.5#	Ol-rich	6,7
MS-183	17.49 g	S2	W0/1	up to 2 mm			Fs3–7	Fs2–7	2.5–4.5#	Px-rich, no Ol	6,7
MS-187	6.31 g	S2	W0	200–900 μm	Fa10–11.5	Fa3–11.5	Fs10–13	Fs1.5–13	5.5–9#	Px-rich	6,7
MS-193	3.18 g	S3	W0		Fa13–16.5	Fa6–16.5		Fs13.5–15.5	10#		6,7
MS-194	2.77 g	S2	W0	0.6–1.2 mm	Fa9.5–17	Fa3–17	Fs9–10.5	Fs2.5–10.5	5–8#	Px-rich	6,7
MS-202	1.90 g	S2	W0	0.7–1.2 mm	Fa20–21	Fa4–21				no Px, zoned Ol with fine-grained network of metals and FeS	6,7
MS-204	1.03 g	S3	W0/1	0.3–1.6 mm	Fa17–20.5	Fa2.5–20.5	Fs14–17	Fs6–17	4.5–11#		6,7
MS-206	0.30 g	S2	W0	0.3–2 mm	Fa6–10	Fa2.5–10	Fs8.5–9.5	Fs2.5–9.5	5–8.5#	Px-rich	6,7
MS-MU-005	13.30 g			0.4–2 mm	Fa9–10	Fa1–10	Fs7–9	Fs2-9		Px-rich	this study
MS-MU-006	13.58 g			0.4–2 mm	Fa10–12	Fa4–12	Fs9–12	Fs5–12		large graphite (up to ~0.6 mm)	this study
MS-MU-008	5.90 g	S2	W0/1	0.5–1.5 mm	Fa15–18	Fa2–18	Fs15–16	Fs10–16	~5#		8
MS-MU-010	9.60 g	S3	W0/1	0.3–2 mm	Fa19–22	Fa3–22	Fs17–18	Fs1–18	~11#	Ol grains frequently >1 mm	8
IM-UNM-1	155.5 g				Fa20	Fa3–20	Fs11		5	Ca-rich Px	9

Table 2 (*Continued*).

Frag-No.	Frag. Mass	Shock[a]	W[b]	Typical grain size[c]	Ol cores	Ol range	Px cores	Px range	Px (Wo)	Comments	Refs.
Fine-grained ureilitic fragments											
AHS 3	5.938 g			10–20 μm		Fa12–23		En78–85	2–6	termed #3–1 in [1], Px veins up to ~200 μm in width	10
AHS 7	1.52 g			10–20 μm	Fa13.4–13.6	Fa7.6–16.4		En80–90	3–10	rare crystals up to ~1 mm, augite: En57Wo40	1
MS-20	3.55 g	recry. Ol	W0/1	<30 μm	Fa8–9	Fa0–9	Fs12–15	Fs0–15	1.5–8#	metal-rich areas with niningerite	5
MS-28	37.92 g	recry. Ol	W0/1	<20 μm	Fa11–13	Fa3–13	Fs13–16	Fs2–16	2–6.5#		5
MS-61	16.55 g	recry. Ol	W0/1	<20 μm	mainly: Fa14–16	Fa2–19	Fs14–17	Fs3–17	3.5–7#	cores in some areas Fa_{18-19}	5
MS-124	34.02 g	recry. Ol	W0/1	mostly: <20 μm	Fa19–21	Fa3–21	Fs16–18	Fs1–18	3–10#	contains coarser-grained fragment	5
MS-152	9.13 g	recry. Ol	W0/1	<30 μm	Fa18–21	Fa2–21	Fs14–16	Fs7–16	3.5–6#	reduced fragment: $\sim Fa_1$	5
MS-154	4.18 g	recry. Ol	W0/1	<20 μm	Fa11–14	Fa0–14	Fs6–8	Fs1.5–8	1–10#	areas with olivine cores of $\sim Fa_{<5}$ dominate	5
MS-161	4.88 g	recry. Ol	W0/1	<30 μm	Fa18–19.5	Fa1–19.5	Fs14.5–15.5	Fs12–15.5	3.5–9#	suessite	5
MS-165	2.63 g	recry. Ol	W0/1	<20 μm	Fa15–18	Fa2.5–18	Fs12–14	Fs0–14	3–6#	area with niningerite	5
MS-168	33.18 g	recry. Ol	W0/1	<20 μm	mainly: Fa8–11	Fa0–21	Fs8–14	Fs0–14	1.5–4#	areas with 18–20.5 mol% Fa and $Fa_{<5}$ occur	5
MS-185	7.49 g	recry. Ol	W1	<10 μm	Fa0–1.5	Fa0–1.5	Fs8–12	Fs0.5–12	1–5.5#	ultra-fine-grained, niningerite, Ca-rich Px	6,7
MS-186	6.44 g	recry. Ol	W0	<20 μm	Fa17–21	Fa1–21	Fs13–14.5	Fs4–14.5	3.5–11#	Ca-rich Px	6,7
MS-195	3.02 g	recry. Ol	W0	<30 μm	Fa18–22.5	Fa1–22.5				no Px	6,7
MS-198	1.82 g	recry. Ol	W0/1	<50 μm	Fa14–19	Fa0.5–19	Fs15.5–25.5	Fs2.5–25.5	0.5–5.5#		6,7
MS-203	1.30 g	recry. Ol	W0	<30 μm	Fa21–24	Fa6–24	Fs16.5–18.5	Fs4–18.5	0.5–3#		6,7
MS-MU-001	9.50 g	recry. Ol		<10 μm	Fa19–22	Fa9–22	Fs17–20	Fs9–20			this study
AS-H109		recry. Ol				Fa2–15	Fs19	Fs3–19	1.3–5.6		4
IM-UNM-2	24.40 g					Fa12–18		Fs9	5	Ca-rich Px	9
Fine-grained ureilite fragments with variable grain sizes											
AHS 53	95.342 g					Fa14-21	Fs19	Fs25-28	6-7	only average Px cores	11
MS-25	1.59 g	S3	W0/1	50–500 μm	Fa15.5–16.5	Fa0.5–16.5	Fs14–14.5	Fs2.5–14.5	0.5–10.5#	Px-rich, relics of large Ol and Px	6,7
MS-184	7.83 g	S2	W0	50–700 μm	Fa11–13.5	Fa7.5–13.5	Fs10–11.5	Fs9–11.5	3.5–5.5#	Px-rich	6,7
MS-188	5.12 g	S3	W1		Fa13–19	Fa2.5–19	Fs11–12	Fs4.5–12	2–7.5	Ca-rich Px	6,7
MS-190	4.39 g	S2	W0/1	50–500 μm	Fa11.5–21	Fa1.5–21	Fs17.5–21	Fs2.5–21	0.5–12.5#	Px-rich, Ca-rich Px	6,7
MS-191	4.13 g	recry. Ol	W0/1	Ol <30 μm, Px ≤500 μm	Fa17.5–23	Fa3–23	Fs18–20	Fs4–20	3.5–6#	grain size: Px > Ol, Ca-rich Px	6,7
MS-205	0.64 g	recry. Ol	W0/1	<30 μm and 30–100 μm	Fa19–22.5	Fa3–22.5	Fs14–17	Fs6.5–17	0.5–10.5#		6,7
MS-MU-004	10.32 g			0.4–1.0 mm	Fa~22	Fa2–22	Fs~20	Fs3–20		Px-rich	this study
Ureilite fragments with unknown texture											
AHS 29	55.417 g						Fs17–19		11	only average Px cores	1,11
AHS 32	130.40 g				Fa18–21		Fs8				1,11
AHS 33	76.444 g						Fs9.5			only average Px cores	11
AHS 36	57.88 g				Fa2–10		En86.6/82.3		5.0/9.2	only average Ol, two distinct low-Px populations	1,3

Table 2 (*Continued*).

Frag-No.	Frag. Mass	Shock[a]	W[b]	Typical grain size[c]	Ol cores	Ol range	Px cores	Px range	Px (Wo)	Comments	Refs.
Ureilite fragments with unknown texture											
AHS 49	61.149 g				Fa21					only one small grain	1
AHS 50	25.312 g				Fa21					only one small grain	1
AHS 51	20.197 g							Fs8.5–18	9	only average Px cores	3,11
Metal-sulfide dominated fragments with ureilitic portions											
MS-158	9.05 g	recry. Ol	W0/1	<20 μm	Fa17–20	Fa10–20	not analyzed			data for the fine-grained portion	5,12
MS-166	3.25 g	recry. Ol	W0/1	up to 120 μm	Fa12–14	Fa2–14	Fs13–15	Fs2–15		coarse-grained Ol inclusion; Ni-rich metals	5,12
Ureilite-related andesite											
MS-MU-011	24.20 g									plagioclase-rich rock (andesite), see text for details	13

Frag-No.	Frag. Mass	Class	Shock[a]	W[b]	Ol (av.)	Ol (range)	Px (av.)	Px (range)	Sulfides	Metal		Comments	Refs.
										Ni (wt%)	Si (wt%)		
Enstatite chondrites													
AHS 16		EL6					Fs1	Fs0.4–3.1	tro, ferroan ala		≤1.24		1
AHS 41		EH5 or EH6					Fs2.9	Fs1.4–4.9	tro		≤2.93		1
AS-H32		EL6					Fs0.21		tro, old, ferromagnesian ala		0.75		4
MS-D	17.34 g	EL6	S2	W0/1			Fs < 0.3		old, tro, keil, ala	5.5–7.1	0.7–0.9	breccia, Zn-rich sulfide (Rudashevskyite?)	5,12
MS-7	8.73 g	EL5/6	S2	W0/1			Fs < 0.3		old, tro, keil	6.9	0.8	breccia?	5
MS-13	5.02 g	EH IMR*	S3	W0/1			Fs0.6 ± 0.4	Fs0-1.6	old, tro, nin, keil	5.5–7.5	2.4–2.7	shock-darkened	5,12
MS-14	4.69 g	EH3	S3	W0/1			Fs2.9 ± 3.7	Fs0-13	old, tro, dau, nin	3.5–6.5[§]	2.4–3.3	perryite, schreibersite	5,12
MS-17	4.22 g	EL3/4	S2	W0/1	Fa0.2 (1 grain)		Fs0.5 ± 0.3	Fs0-1	old, (Zn-)ala, tro, rare keil	4.3–8.4[§]	0.2–0.9	sinoite, schreibersite	5,12
MS-52	18.17 g	EL6	S2	W0/1			Fs < 0.3		tro, old, ala, keil	6.4–7.2	0.7–0.9	Zn-rich sulfide (rudashevskyite?)	5,12
MS-79	14.71 g	EL6	S2	W0			Fs < 0.4		tro, old, ala	6.4	0.9		5
MS-150	25.46 g	EL IMR*	S2	W0/1			Fs < 0.3		old, tro, keil, dau	6.3	1.5	schreibersite	5,14
MS-155	3.11 g	EH IMR*	S3	W0/1			Fs0.4 ± 0.2		old, tro, nin, keil	4.7–7.3	2.7–4.8	shock-darkened	5
MS-163	9.94 g	EH IMR*	S2	W0/1			Fs1.1 ± 0.6	Fs0.1-1.9	tro, keil, nin, old	6.5	3.3	shock-darkened	5
MS-164	8.90 g	EL3/4	S2	W0			Fs0.4 ± 0.5	Fs0-2	tro, old	5.6–7.2	1.2–1.4	schreibersite	5,12
MS-172	45.52 g	EL IMR*	S2	W0/1			Fs < 0.3		tro, keil, old, ala	6.5–7.3	1.1–1.2		5,12
MS-174	12.24 g	EL6	S2	W0/1			Fs < 0.3		tro, old, ala, keil	6.3	0.8	breccia	5
MS-177	19.02 g	EL3	S3	W0			Fs0.6 ± 1.3	Fs0–8	tro	6.9	0.6	Ca,Al-rich inclusion	6,15
MS-179	8.70 g	EL3-5					Fs0.8 ± 1.2	Fs0.1–12.3	ala, tro, old	6.4	0.6	breccia	6
MS-189	4.89 g	EL3	S2	W0/1	Fa0.1 (1 grain)		Fs0.7 ± 0.5	Fs0.2–2.3	ala, tro, old	6.2	0.7		6,15
MS-192	4.18 g	EH4/5	S2	W1			Fs0.4 ± 0.3	Fs0.1–1.5	tro, nin, old, djer	6.1			6,15
MS-196	2.96 g	EL5	S3	W1			Fs0.3 ± 0.3	Fs0.1–1.4	tro, old	6.8	1.7		6,15
MS-200	2.56 g	EL3/4	S2	W1			Fs0.6 ± 0.9	Fs0.1–4.6	tro, old	7.2	1.2		6,15
MS-201	1.99 g	EL5	S2	W0/1			Fs0.6 ± 0.5	Fs0.1–2.2	tro, old	5.8	1.4		6,15
MS-MU-002	3.00 g	EL3				Fa0-1.5		Fs0–7	tro, old, ala, keil		1.4	Ol in chondrules	this study
MS-MU-003	15.40 g	EL breccia							tro, old, keil		1.7		this study
MS-MU-007	15.57 g	EL6	S2	W0/1			Fs0.3		tro, old, nin	7.3	0.9	graphite aggregates, sinoite	6,8
MS-MU-009	14.30 g	EH4/5	S2	W0/1			Fs1.2		tro, old, nin	5.8	3.3		6,8

Table 2 (*Continued*).

Frag-No.	Frag. Mass	Class	Shock[a]	W[b]	Ol (av.)	Ol (range)	Px (av.)	Px (range)	Sulfides	Metal		Comments	Refs.
										Ni (wt%)	Si (wt%)		
Ordinary chondrites													
AHS 25	221.95 g	H5	S3		Fa18.1 ± 0.4	Fa17.7–18.2	Fs16.2 ± 0.4	Fs16.7-28.4	tro			martensite with 14.1 ± 5.0 wt% Ni	1,4
AHS A100	11.356 g	L4			Fa24.2	Fa23.6–25.5	Fs21.6	Fs18.6-23.9	tro				1
MS-11	6.88 g	H5/6	S3	W0/1	Fa16.5		Fs14		tro	7.6	<0.2	Co in metal: ~0.8; shock-melted areas	5
MS-151	4.78 g	H5	S2	W0/1	Fa20.5		Fs17.5		tro	8.2	<0.1	Co in metal: ~0.7; shock-darkened	5
MS-197	2.45 g	LL4/5	S3	W0	Fa29.9		Fs23.4		tro				15
Carbonaceous chondrite													
MS-181	58.6 g	CB_a		W0		Fa3-4	Fs2.7 ± 1.1	Fs0.9-5.9	Cr-bearing tro	6–8, rarely up to 31		troilite: 0.6–10.8 wt% Cr, tiny Ni-rich metal grains	6,16
Rumuruti-like chondrite													
MS-CH	5.68 g	unique	S2	W0/1	mainly: Fa35–37	Fa19–38	Fs14.4 ± 7.5	Fs3-26	tro	mainly:~38; Co:~2	<0.2	matrix: ~40 vol%	17

[a] Shock metamorphism determined based on the classification schemes for ordinary and enstatite chondrites by Stöffler et al. (1991) and Rubin et al. (1997); recry. Ol = recrystallized olivine.

[b] Weathering grade W0/1 (Wlotzka, 1993) assigned based on the slight brownish taint in restricted areas of the thin section as observed in transmitted light.

[c] For the coarse-grained ureilitic fragments the grain size determination can only be a rough estimate, because of the limited sample size. In some cases only a few grains were available.

#) only Px cores;

*) Horstmann (2013) suggests a re-classification of at least some of these samples as non-IMR (see this reference for details).

[§] Metal in MS-14 and MS-17 has small, micron-sized Ni-rich patches with Ni concentrations up to ~24 wt% and ~12 wt%, respectively.

Please note that ureilite samples characterized as "porous" and "compact" in Zolensky et al. (2010b) are listed here as fine-grained and coarse-grained, respectively. tro = troilite, ala = alabandite, old = oldhamite, keil = keilite, nin = niningerite, dau = daubreelite, djer = djerfisherite. Sample locations: MS and MS-MU = Institut für Planetologie, Münster; AHS = Collection Almahata Sitta Consortium; AS-H = Haberer-Meteorites; IM-UNM = Institute of Meteoritics, Albuquerque. References: (1) Zolensky et al. (2010b); (2) Goodrich et al. (2010a); (3) Ross et al. (2011a); (4) Warren and Rubin (2010); (5) Bischoff et al. (2010b); (6) Horstmann et al. (2012a); (7) Roggon (2012); (8) Treutler (2013); (9) Hutchins and Agee (2012); (10) Mikouchi et al. (2010b); (11) Herrin et al. (2010b); (12) Horstmann (2013); (13) Bischoff et al. (2013a); (14) Hoffmann et al. (2012b); (15) Hain (2012); (16) Bischoff et al. (2012); (17) Horstmann et al. (2010).

which the different fragments are bonded by gravitation, which is negligible in the ~4 m sized asteroid 2008 TC_3.

In addition to a detailed examination of the various Almahata Sitta meteorites with respect to their (thermal) histories, the study of meteoritic breccias such as Almahata Sitta – as reviewed by, e.g., Bischoff et al. (2006) – are of considerable importance for unraveling the formation and evolutionary pathways of both meteorites and asteroids. As noted by Bischoff et al. (2010b), "the existence and abundance of foreign and exotic fragments in meteorites give some measure on the degree of mixing among asteroids in the asteroidal belt. [. . .] The relative abundance of different types of material in different meteorite breccias may reveal something about the abundance of certain materials at different times and places in the asteroid belt." Mixing of chondritic and achondritic material further allows to place constraints on (at least relative) time-scales of asteroid formation, also hinting at the late accretion of such bodies.

The present review paper attempts to compile all research performed on the Almahata Sitta meteorites and asteroid 2008 TC_3. However, particular emphasis will be placed on the mineralogical and chemical characterization of the large variety of different types of meteoritic material found among the Almahata Sitta individuals, the division of which is partly adopted from earlier publications (Bischoff et al., 2010b; Horstmann et al., 2010).

The compiled data will be used to extract information on the formation and evolutionary pathway of asteroid 2008 TC_3, its late parent body accretion by mixing of different types of meteoritic ingredients, and the ureilite parent body, in particular.

2. Discovery of asteroid 2008 TC_3, studies in space, and its atmospheric entry

After asteroid 2008 TC_3 was detected in space on October 6th, 2008, numerous worldwide astronomical observations enabled very precise determinations of its orbit and impact trajectory and site on Earth (Table 1; Fig. 1a). This allowed to constrain the impact location: the Nubian Desert of northern Sudan, North Africa (Fig. 1b; e.g., McGaha et al., 2008; Jenniskens et al., 2009a,b; Shaddad et al., 2010).

The impact was observed by several eyewitnesses in Wadi Halfa at the Sudanese border to Egypt and at a train station, named Station 6, in the Nubian Desert between Wadi Halfa and Khartoum (Figs. 1b and 2), that described a "rocket-like fireball with an abrupt ending" (Jenniskens et al., 2009b). Some detailed reports from eyewitnesses are given in Shaddad et al. (2010); e.g., attendant Abdel Moniem Magzoub from Station 6 heard a sound about 2–3 min after the fireball observation and saw the dust cloud produced by the fireball for 10–15 min. Additionally, the pilot of a plane flying over Chad in more than 1000 km distance saw several light flashes at the time the asteroid exploded (Kwok, 2009). Asteroid 2008 TC_3 traveled from the geodetic longitude of 31.80381°E and latitude of +20.85787°N at an altitude of 50 km to 32.58481°E and +20.70569°N at 20 km altitude (Jenniskens et al., 2009b). More details on the approach trajectory are given by Shaddad et al. (2010).

The more than 500 astronomical observations at about 60 different locations on Earth before the asteroid entered the Earth's umbra revealed information on the object's brightness variations. Its absolute visual magnitude at the equatorial aspect in the Johnson-V-band was determined, which is a measure of the asteroid's size (Pravec and Harris, 2007; Jenniskens et al., 2009b). Using the objects Johnson-V-band geometric albedo of 0.046 ± 0.005, measured for the dark phase of the object, the determined absolute visual magnitude of 30.9 ± 0.1 translates to an asteroid diameter of 4.1 ± 0.3 m (Jenniskens et al., 2009b). If a low density of the meteorite samples of about 2.3 g/cm^3 is assumed (see also below), a pre-atmospheric

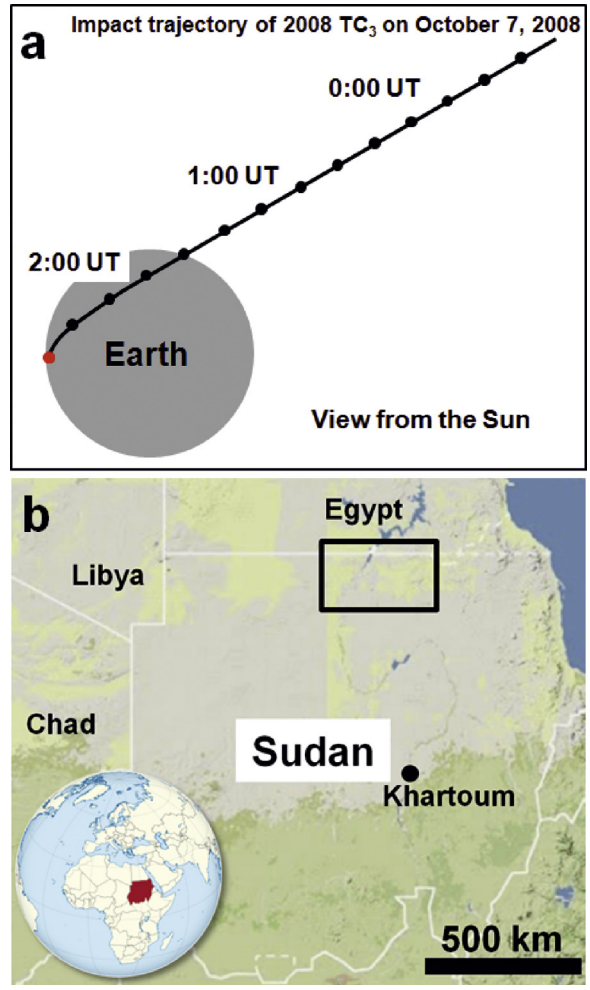

Fig. 1. (a) Calculated trajectory of asteroid 2008 TC_3 on October 7th, 2008, as seen from the sun (redrawn after http://neo.jpl.nasa.gov/news/2008tc3.html; accessed 08/12/2013). (b) Map of Sudan and adjacent countries (compiled from *maps.google.de* and *de.wikipedia.org/wiki/Sudan*; accessed 08/12/2013). The black box outlined (not to scale) shows the predicted impact area with the strewn field of asteroid 2008 TC_3. A detailed image of the strewn field is shown in Fig. 2. The terrestrial globe inlay at the left bottom highlights Sudan in Africa.

mass of the bolide of 83 ± 25 t can be calculated, having a kinetic energy of the impact in the range of $(6.4 \pm 1.9) \times 10^{19}$ J at 50 km altitude (Jenniskens et al., 2009b). Scheirich et al. (2010) constrained the volume of the asteroid to 25 ± 10 m^3, corresponding to an average radius of 1.8 ± 0.2 m. Based on the measured concentrations of cosmogenic radionuclides, Welten et al. (2010a) determined an effective radius of 300 g cm^{-2} (radius × density). With the absolute radius of 1.8 m determined by Scheirich et al. (2010), this value corresponds to a bulk density of 1.66 ± 0.25 g/cm^3, and a bulk porosity of 50 ± 7%, resulting in a total mass of about 41 t for asteroid 2008 TC_3.

A calibrated light curve was obtained before the meteoroid impacted Earth from over 1700 images of the asteroid (Kozubal et al., 2011; Fig. 3). Using the light curve characteristics and taking several other physical parameters into account (e.g., kinetic energy), Kozubal et al. (2011) estimated the asteroid to be ~4.1 m in diameter, 28 m^3 in volume, and 51 t in mass. Further constraints on the size, mass, and density can be found in Section 6.3.

Scheirich et al. (2010) studied the shape and rotation of asteroid 2008 TC_3 and found that the rotational and precession periods were 99.20 and 97.00 s, respectively. These authors also found "two approximately mirror solutions of orientation of its angular

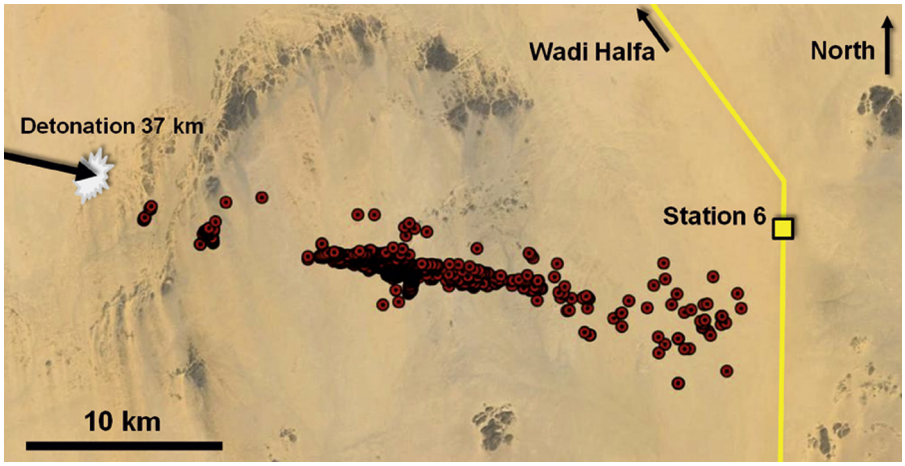

Fig. 2. Map of the fall location of asteroid 2008 TC_3 in the Nubian Desert, northern Sudan. The black arrow represents the direction of the asteroid's fireball and the position of final detonation is shown with the star. Red spots indicate the exact positions of all meteorites recovered and listed with coordinates in Shaddad et al. (2010). The yellow line shows the local train track with Station 6 labeled, after which the meteorite is named. Basic background image modified after Google Earth. Data from Shaddad et al. (2010) were converted and imported into Google Earth. Figure based on Jenniskens et al. (2009b).

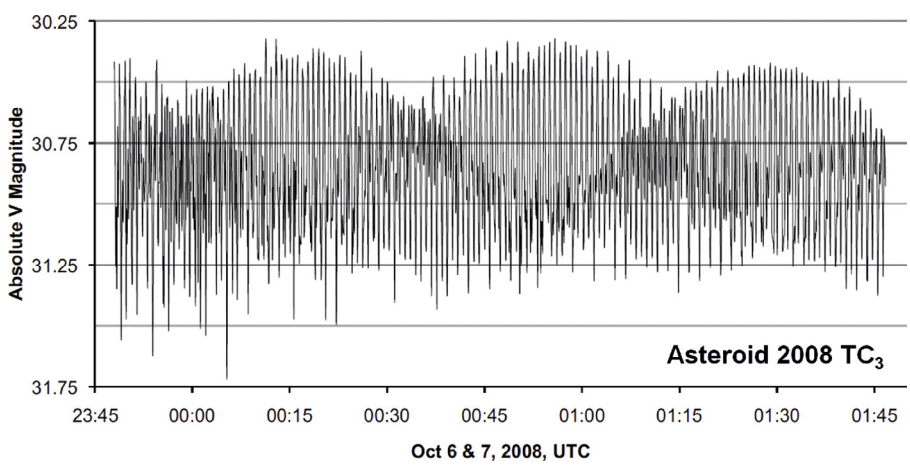

Fig. 3. Unfiltered V-band light curve for asteroid 2008 TC_3, corrected for atmospheric extinction. Figure modified after Kozubal et al. (2011).

momentum vector" and they revealed its shape using convex modeling of photometric data: The shape of the asteroid had an axial ratio of approximately 1:054:036.

Sensors onboard U.S. government satellites detected the impact of the asteroid first at 02:45:40 UT (Brown, 2008; Chesley et al., 2008). Borovička and Charvát (2009) wrote that the fireball was captured in the 2:45 UT images in four near infrared channels at a height of 45 km and in eight mid-infrared channels at a height of 33 km. Based on satellite observations, the object was first discovered at about 65 km altitude after its atmospheric entry and then started to disintegrate at an altitude of ~46–42 km. The final detonation that destroyed the bolide took place at an observed height of about 37 km (Jenniskens et al., 2009a,b). The weather satellite *Meteosat 8* took a picture of the impact location right at the moment of its final detonation and the coordinates were reported as 32.16°E longitude and +20.97°N latitude (Fig. 4a; Borovička and Charvát, 2008). The altitudes of detonation determined correspond to ram pressures of only 0.2–0.3 MPa (~46–42 km) and 1 MPa (~37 km), respectively (Jenniskens et al., 2009b), pointing to rather fragile material constituting asteroid 2008 TC_3. Given the impact conditions, it was not expected that any of the obviously very fragile material would survive the flight through the atmosphere and reach the Earth's surface (Jenniskens et al., 2009b). According to the fireball PE-criterion (Ceplecha and McCrosky, 1976), the object's final parameters would rather argue for cometary debris than asteroidal or meteoritical material. Jenniskens et al. (2009b) mentioned that the unusual Tagish Lake C2 meteorite that fell in Canada in 2000 was similar in its parameters to asteroid 2008 TC_3, but penetrated much deeper into the atmosphere, breaking up at 40–29 km altitude, and continuing ablation until 27 km altitude (Brown et al., 2002).

The mid-infrared channels of *Meteosat 8* and *9* also detected two dust clouds in the atmosphere at altitudes of 44 and 36 km, resulting from the disruption of the asteroid in the atmosphere (Fig. 4b; Borovička and Charvát, 2009). Independently, Jenniskens et al. (2009b) measured a dust cloud altitude of ~35–42 km. At 45 and 37.5 km heights the fireball had a brightness of −18.8 and −19.7 mag, respectively, and a color temperature of 3650 ± 100 K at an altitude of 45 km (Borovička and Charvát, 2009). It was also found that at first the dust cloud (Fig. 4b) was made of re-condensed amorphous silicates and that some minutes later the silicates in the dust cloud, having a total mass of 3100 ± 600 kg, were largely crystalline. Borovička and Charvát (2009) suggested that at this time the silicate smoke temperature exceeded 1000 K and that much more cold dust particles totaling up to about 10 t were produced during the atmospheric entry. From the radiated energy they estimated a total mass of 35–65 t and an asteroid 2008 TC_3 bulk porosity of about 50%, based on the altitude of fragmentation.

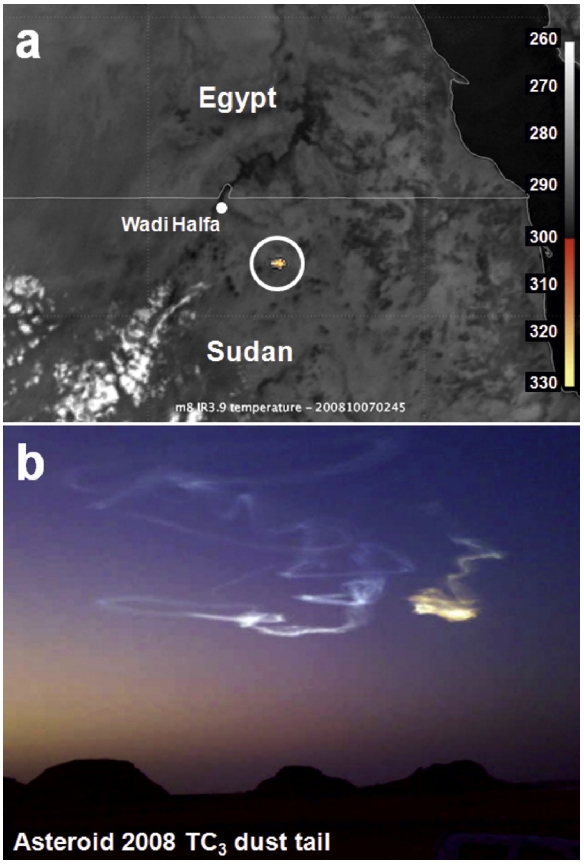

Fig. 4. (a) *Meteosat 8* thermal photograph of the impact location of asteroid 2008 TC_3 in the Nubian Desert, Sudan. The bright yellow spot (highlighted with circle) illustrates that the image was taken right at the time the asteroid detonated at an altitude of ~37 km. The spectrum on the right gives the picture's color-code with the temperature in Kelvin (Figure modified after http://asima.seti.org/2008TC3/images/Meteosat8impact.jpg, accessed 08/12/2013). (b) Photograph of the lingering trail/dust cloud of asteroid 2008 TC_3 over northern Sudan taken at early dawn October 7, 2008 (http://apod.nasa.gov/apod/ap081108.html, accessed 08/12/2013).

3. Recovery of fragments from Asteroid 2008 TC_3 (=Almahata Sitta samples)

Several systematic field campaigns in the strewn field along the calculated trajectory unexpectedly revealed numerous meteorite fragments that survived the explosion (Fig. 2). The strewn field searched has a size of about 30 km × 7 km (Jenniskens et al., 2009a; Shaddad et al., 2010). During the first of these campaigns (December 5–8th, 2008), 15 fresh-looking meteorites with a total mass of 563 g were found by a group of 45 students and staff from the University of Khartoum (Jenniskens et al., 2009b). After only 2 h search, student Mohammed Alameen discovered the first meteorite fragment on December 6, 2008. A second search (December 25–30th, 2008) with 72 participants revealed 32 additional fragments. The total of 47 meteorites had a weight of ~3.95 kg, with individual samples weighing between 1.5 and 283 g, spread along the approach path (Jenniskens et al., 2009b). In March 2009, a third field campaign raised the total number of meteorite fragments to about 250 (Zolensky et al., 2009). Later, official expeditions led to a total of more than 600 fragment finds, most of which are typically very small (0.2–379 g), totaling ~10.5 kg (Shaddad et al., 2010). The ~10 kg meteoritic material represent about 0.012% of the asteroids initial mass, given the mass of about 83 ± 25 t from Jenniskens et al. (2009b). Meteorite fragments from the Almahata Sitta strewn field were also found by independent search campaigns in July and October 2009 and later. Eighty-two of these fragments were investigated at the Institut für Planetologie in Münster (e.g., Bischoff et al., 2010a,b; Horstmann et al., 2012a; Horstmann, 2013).

All meteorite fragments are now designated as "Almahata Sitta" (Weisberg et al., 2009), which is the Arabic name for Station 6 (20°45.207′N; 32°32.946′E), a railway station between Wadi Halfa and Abu Hamad (Shaddad et al., 2010) and, thus, the closest named locality in the fall region in the Nubian Desert (Fig. 2).

4. Mineralogy and petrology of Almahata Sitta fragments

4.1. General overview

After the first sample of Almahata Sitta was studied petrologically and chemically (sample No.7 = AHS 7 in this study), the meteorite was classified as a fine-grained, anomalous polymict ureilitic breccia (Fig. 5, Jenniskens et al., 2009b). After additional samples were studied, it soon emerged that abundant fragments of typical coarse-grained ureilites and various types of different chondritic lithologies were also among the fragments collected in the strewn field (e.g., Bischoff et al., 2010a,b, 2012, 2013a,b; Zolensky et al., 2010a,b; Horstmann et al., 2010, 2012a; Horstmann and Bischoff, 2010a,b; Rumble et al., 2010a,b; Kohout et al., 2010a,b; Shaddad et al., 2010). Considering the physical, chemical, and mineralogical-textural properties of these samples, it was found that they are remarkably heterogeneous – as a collection of meteorites from a single asteroid impact. All samples, both chondritic and ureilitic recovered, showed a fresh and unweathered appearance. Furthermore, short-lived cosmogenic radionuclides of two chondritic fragments (MS-D and MS-CH) from the strewn field proved that these meteorites also belong to the Almahata Sitta meteorite shower (Bischoff et al., 2010a). This led Bischoff et al. (2010a) to call Almahata Sitta a polymict "breccia containing many different ureilitic and chondritic lithologies". The results of Bischoff et al. (2010a,b) were confirmed by other workers (e.g., Kohout et al., 2010b; Shaddad et al., 2010; Zolensky et al., 2010b; Welten et al., 2011; Meier et al., 2010, 2012). Kohout et al. (2010b) estimated that about 50% of their 60 samples studied could be of non-ureilitic origin, whereas, considering hand specimen properties, Shaddad et al. (2010) estimated ~20–30 mass% non-ureilitic samples among the collected rocks. They found that this percentage is similar among the large (~100 g) as well as among the small (~1 g) fragments. 30 chondrites (~36%) were found among the 82 samples examined at the University of Münster (e.g., Bischoff et al., 2010a,b, 2013a,b; Horstmann et al., 2010, 2012a).

Considering the main data sets on the mineralogical classifications (110 samples compiled in Table 2), which may not be totally representative (e.g., Bischoff et al., 2010b, 2013a,b; Zolensky et al., 2010b; Horstmann et al., 2010, 2012a), the different lithologies will be briefly described according to their abundances.

Most abundant are coarse-grained (compact) ureilitic lithologies (38 samples), followed by fine-grained, porous ureilitic rocks (19 samples). Eight of the fine-grained ureilites show variable grain sizes and often appear dark, similar to AHS 7. Another seven ureilite samples have unspecified textures. In two fragments described as "metal-sulfide assemblages with enclosed ureilitic portions", sulfide and metal are the dominating constituents (Bischoff et al., 2010b). One sample with ureilitic oxygen isotope characteristics is a plagioclase-rich rock, an andesite, most likely representing a crustal rock of the ureilite parent body (Bischoff et al., 2013a,b). Enstatite chondrites of both types (EH and EL of different petrologic type) and with highly variable textures are the most abundant chondritic samples (28 specimens; EL: 21;EH: 7; Table 2). Subordinate, several H, L, and LL group ordinary chondrites (5 samples)

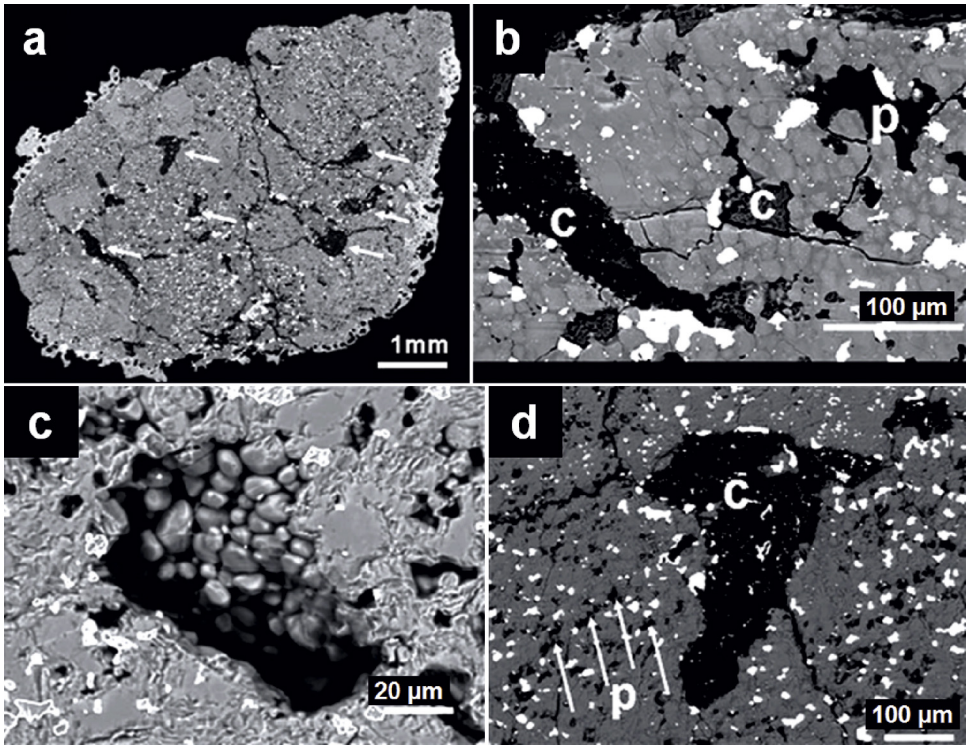

Fig. 5. Overview of the first fragment no.7 of Almahata Sitta (AHS 7) analyzed and characterized by Jenniskens et al. (2009b). (a) BSE image of the fragment showing high- and low-porosity lithologies, and large carbonaceous inclusions (white arrows). (b) Low-porosity area with rounded grains, carbonaceous areas (C) and pores (P). (c) Close-up of a pore containing euhedral to anhedral olivine and pyroxene grains that are presumably vapor-phase deposits. (d) Large carbonaceous aggregate (C) with small troilite and kamacite grains (bright spots) surrounded by high-porosity (P) silicates. Figure modified after Jenniskens et al. (2009b).

have been recognized, as well as one carbonaceous (CB_a) and one Rumuruti (R)-like chondrite (Table 2).

4.2. Mineralogy and petrology

4.2.1. Ureilitic fragments – textural aspects

Ureilites are typically coarse-grained asteroidal mantle restites dominated by olivine and pyroxene (e.g., Mittlefehldt et al., 1998). Almahata Sitta ureilites (Figs. 6 and 7) comprise a wealth of grain sizes, textures, and mineral compositions, and several distinct samples were examined (e.g., Zolensky et al., 2009, 2010a,b; Jenniskens et al., 2009b; Herrin et al., 2009, 2010a,b; Bischoff et al., 2010a,b; Horstmann and Bischoff, 2010a, Warren and Rubin, 2010; Mikouchi et al., 2010a,b; Horstmann et al., 2011a,b, 2012a; Table 2). Jenniskens et al. (2009b) described AHS 7 (Fig. 5) as an anomalous polymict ureilite, which served as a basis for the Almahata Sitta meteorite classification (Jenniskens et al., 2009b; Weisberg et al., 2009). In addition, Zolensky et al. (2009, 2010b) and Herrin et al. (2009) described "black" and "white" lithologies. The black lithology comprises porous and friable, fine-grained stones addressed as fragmental (polymict) breccias with subrounded mineral fragments, and olivine- and pyroxene-dominated clasts embedded in a cataclastic matrix (Zolensky et al., 2009), which will collectively be referred to as fine-grained here, following Bischoff et al. (2010a,b). The white lithology is more compact and coarse-grained and also described as coarse-grained by Bischoff et al. (2010a,b) and Horstmann et al. (2012a).

Zolensky et al. (2010a) reported initial ranges of silicate compositions from 19 different Almahata Sitta ureilites (Note that they were unspecified with respect to specimen number at that time, but later detailed in Zolensky et al., 2010b) and found a large range of chemical compositions, forming a single trend of near constant molar Mn/Fe-ratio at low Fe compared with other ureilites. Zolensky et al. (2010b) found that the abundance of pyroxene (mainly pigeonite) is generally larger than that of olivine and suggest to call Almahata Sitta a pigeonite-olivine ureilite.

The remaining paragraph will be further subdivided to separately describe (a) coarse-grained ureilites, (b) fine-grained ureilites, (c) dark ureilites and/or those with variable grain size, (d) ureilitic metal-sulfide assemblages, and (e) a ureilite-related andesite.

4.2.1.1. Coarse-grained ureilites. Coarse-grained ureilites in Almahata Sitta (Fig. 6) have been mineralogically examined by, e.g., Zolensky et al. (2009, 2010a,b), Herrin et al. (2009, 2010a,b), Bischoff et al. (2010a,b), Horstmann et al. (2012a), and Hutchins and Agee (2012). They were found with variable modal (olivine/pyroxene ratios) and chemical compositions (Table 2). Both olivine-rich (the majority of samples) and pyroxene-rich ureilitic fragments (e.g., MS-16, MS-169, MS-MU-004) were identified. [Please note that the apparent modal proportions may be significantly biased by limited sample size. Hence, they might not be entirely representative of the host lithology.] Olivine-rich coarse-grained ureilites (Fig. 6) show grain-sizes up to several millimeters, whereas pyroxene-rich samples typically have grain sizes significantly below 1 mm (Table 2). Similar to other ureilites, Almahata Sitta coarse-grained ureilites are often characterized by reduction rims around olivine (and sometimes pyroxene), sprinkled with numerous tiny Fe metal grains (Fig. 6e, f). Chemically, the coarse-grained Almahata Sitta ureilites cover much of the full compositional spectrum previously known from ureilites (e.g., Mittlefehldt et al., 1998; Goodrich et al., 2004) and range from Mg-rich (e.g., MS-16: Fa_{5-6}; MS-182: $Fs_{3-4.5}$) to much more Fe-rich silicate core compositions (e.g., MS-167: $Fa_{20.5-22}$; MS-170: Fs_{17-19}; Table 2).

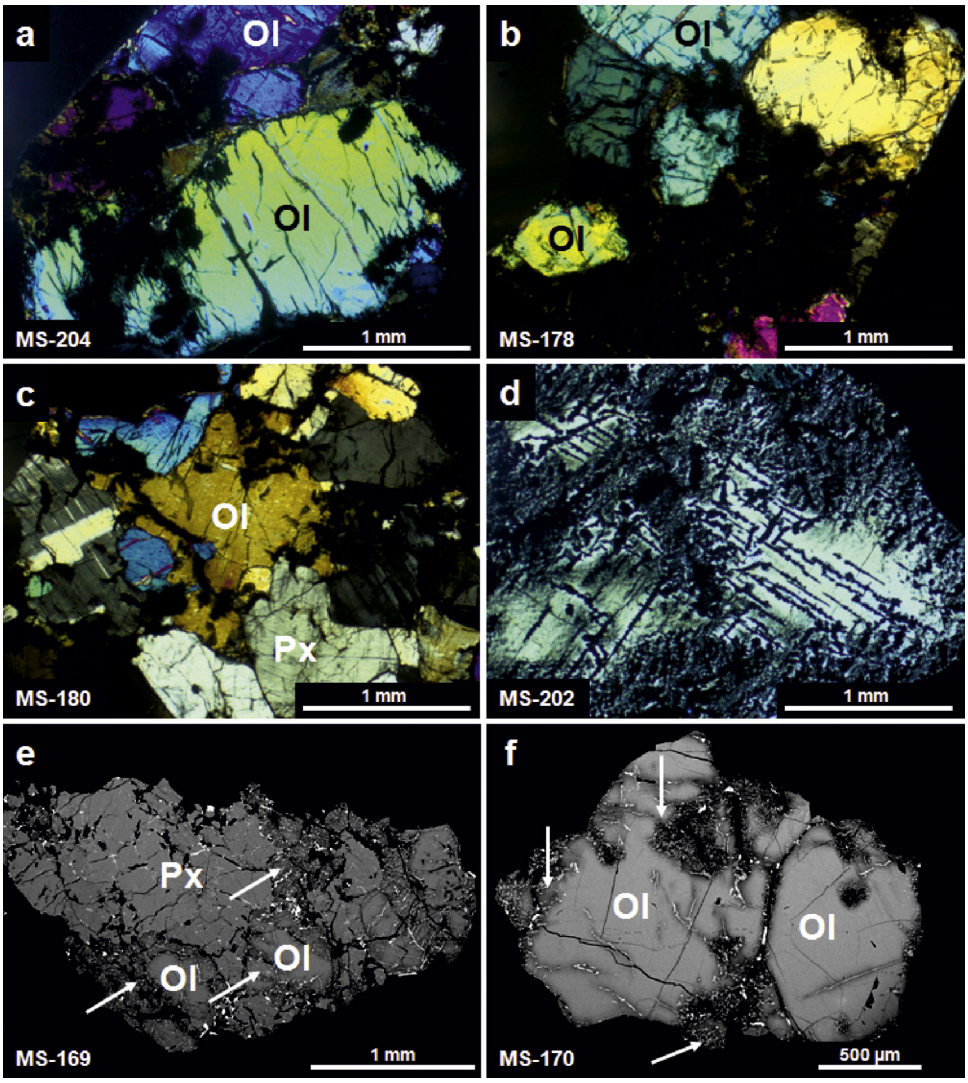

Fig. 6. Almahata Sitta coarse-grained ureilites. (a) MS-204, (b) MS-178, and (c) MS-180 have the typical coarse-grained ureilite texture of large olivine (and pyroxene) grains. Individual olivine grains can reach sizes up to several millimeters. (d) Ureilite MS-202 has an unusual internal texture with worm-like inclusions of metal and minor sulfide. Olivine is zoned from ~Fa_{20-21} to ~Fa_4 next to the metal inclusions. (a–d) Optical photomicrographs, crossed polarizer. (e) and (f) BSE images of coarse-grained ureilites MS-169 and MS-170 illustrating the reduction textures typical of ureilites. Olivine is commonly characterized by reduced, Fo-rich rims (arrows) sprinkled with numerous tiny metal grains originating from reduction of FeO from the silicate.

Among the coarse-grained rocks, several unique textures were found. MS-156 and MS-202, for example (Bischoff et al., 2010b; Horstmann et al., 2012a), show zoned olivine ($Fa_{\sim 8-19}$) hosting a complex network of sulfide and metal in the reduced portions (Fig. 6d). MS-171 (Bischoff et al., 2010b) exhibits a highly mosaicized texture, similar to textures in LaPaz Icefield (LAP) 03587 and Larkman Nunatak (LAR) 04315 (Warren and Rubin, 2010).

4.2.1.2. Fine-grained ureilites. Fine-grained ureilites from the Almahata Sitta collection (Fig. 7a–d) have been studied by, e.g., Jenniskens et al. (2009b), Bischoff et al. (2010a,b), Zolensky et al. (2009, 2010a,b), Herrin et al. (2009, 2010a,b), Mikouchi et al. (2010a,b), Warren and Rubin (2010), Horstmann and Bischoff (2010a), Ross et al. (2011a), Hutchins and Agee (2012), Horstmann (2013), and Horstmann et al. (2013b). This type of rock is characterized by strongly recrystallized (polycrystalline) and typically strongly reduced mineral assemblages for both olivine and pyroxene, and considerable porosity (up to ~40%). Some of the fine-grained, porous rocks are dominated by pyroxene (Zolensky et al., 2010a), others are rich in olivine (Bischoff et al., 2010b; Warren and Rubin, 2010). The textures were described as granoblastic and mosaicized (Zolensky et al., 2010a,b; Mikouchi et al., 2010b) with very small (10–20 µm) grains of olivine and pyroxene. In addition, pyroxene is present as an interstitial phase between euhedral olivine grains. In AS-H109, Warren and Rubin (2010) described texturally similar areas with an olivine microporphyritic melt texture in which individual, recrystallized olivine grains are typically <30 µm in size, and in many cases even <20 µm, showing an interstitial filling of Ca-rich pyroxene (Fig. 7d). Frequently, some relic grains of olivine and/or pyroxene can be found, with olivine showing the typical zoning known from coarse-grained ureilites. Mikouchi et al. (2010a,b) refer to other polycrystalline ureilites such as Haverö, Y-74154, and ALH81101 for similar textures. Chemically, the fine-grained ureilites comprise a range of silicate compositions, which are generally similar to those in coarse-grained ureilites (Table 2). However, the reduced compositions down to Fa_0 are prevailing. One ultra-fine-grained rock (MS-185: <10 µm grain size) was found with strongly reduced olivine giving maximum fayalite of 1.5 mol% (Table 2; Horstmann et al., 2012a).

Jenniskens et al. (2009b) described rare zoning in olivine, larger-sized carbonaceous aggregates, a fine-grained texture, high

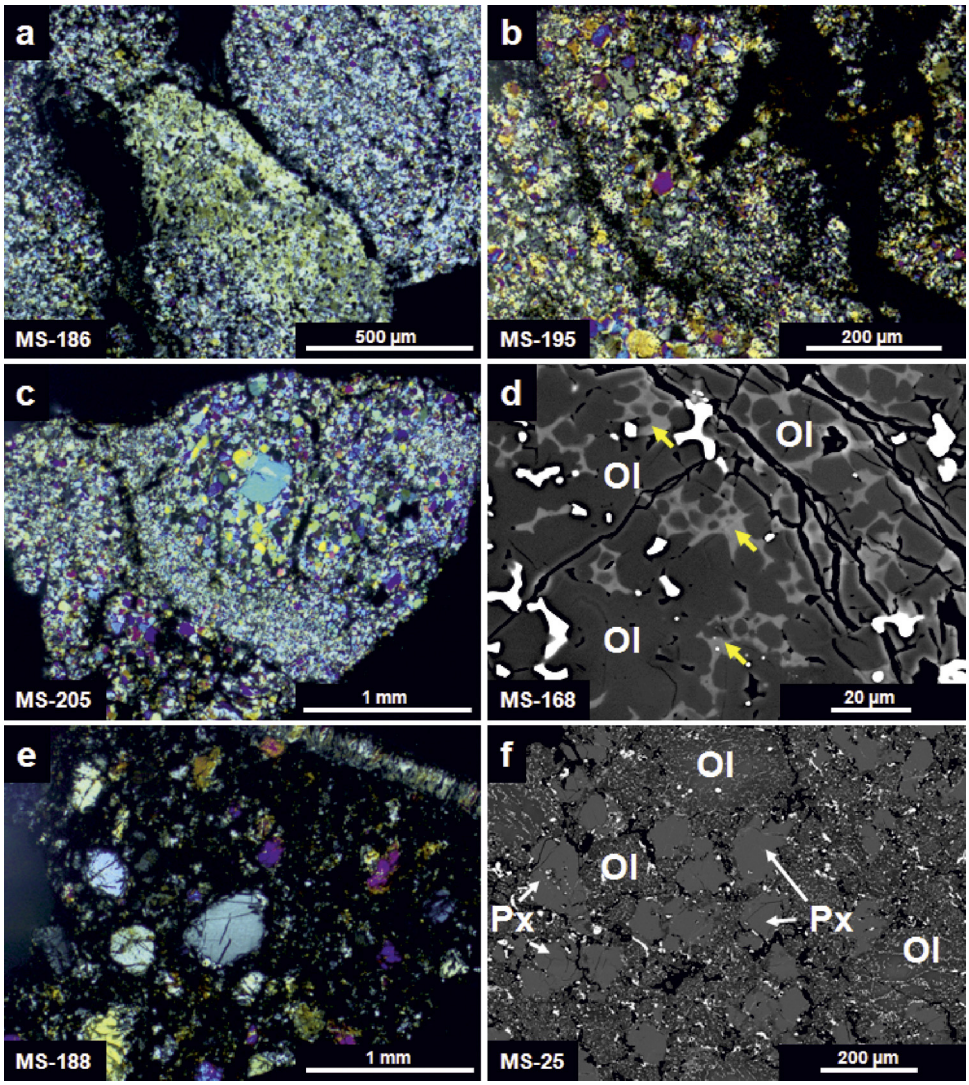

Fig. 7. Almahata Sitta fine-grained ureilites. (a) MS-186, (b) MS-195, and (c) MS-205 are typical examples of recrystallized fine-grained ureilites, which are believed to have formed via so-called impact smelting (Warren and Rubin, 2010). MS-186 and MS-195 are characterized by very small grain sizes (typically <30 µm), often showing an olivine microporphyritic texture as in (d): Rounded olivine grains with an interstitial Ca-rich pyroxene-like filling and opaques (metal and minor FeS, white) are common, replacing former coarse-grained olivine as shown in Fig. 6. MS-205 is a fine-grained ureilite showing variable grain sizes (<30–100 µm), resulting from different degrees of overprinting of the host rock (see text for details). (a-c) Optical photomicrographs, crossed polarizer; (d) BSE image. (e) Optical photomicrograph (crossed polarizer) of the MS-188 "dark" ureilite. Islands of relic silicate (mainly pyroxene) occur in a "matrix" of strongly reduced and recrystallized olivine. This is further illustrated in (f) showing the high abundances of numerous tiny metal grains dispersed in olivine and almost metal-free pyroxene in MS-25 of similar textural type.

metal content, and high porosity with possible vapor-phase mineral growth of olivine in the AHS 7 fine-grained ureilite (Fig. 5). Polycrystalline olivine has Fa_{8-15} and minor CaO (0.15–0.51 wt%) and Cr_2O_3 (0.03–1.58 wt%), low-Ca pyroxene (Fs_2Wo_5-$Fs_{17}Wo_4$) with 0.33–1.02 wt% Cr_2O_3, pigeonite ($Fs_{15}Wo_5$-$Fs_{18}Wo_{11}$; Cr_2O_3: 0.72–1.11 wt%), and kamacite ($Fe_{0.92}Ni_{0.08}$-$Fe_{0.96}Ni_{0.04}$). Further phases include troilite having up to 4.3 wt% Cr and rounded pyroxene grains containing an abundant Fe-rich nanophase (Jenniskens et al., 2009b; Zolensky et al., 2009, 2010a).

Zolensky et al. (2009, 2010a) and Herrin et al. (2009) described fine-grained ureilites (their black lithology) as consisting of mm-scale clasts or enclaves of fine-grained (10–40 µm) porous (up to 40%) olivine-dominated and pyroxene-dominated sublithologies. The former are more homogenous in their mineral compositions than the latter. Their boundaries are sometimes only poorly defined, but often separated by assemblages of metal, sulfide, and a carbon-phase and/or voids (Herrin et al., 2009). Zolensky et al. (2009) noted that although the range of silicate compositions is characteristic of ureilites, it is unusually broad for an individual ureilite. Furthermore, they reported that olivine does not exhibit prominent zoning (as in coarse-grained ureilites), whereas pyroxene shows reduced rims where it is in contact with silica (Herrin et al., 2009). The pores in, e.g., AHS 7, were found coated with anhedral to euhedral crystals of olivine (Fa_{12-15}), similar in composition to the remaining fragments (Fig. 5c; Zolensky et al., 2010a). Additionally, spherules of kamacite and botryoidal masses of troilite can occur in the pores. Tomographic analyses revealed that "the pores define thin, discontinuous 'sheets' connected in three dimensions" (Zolensky et al., 2009, 2010b). They probably outline grains that have been incompletely welded together with the crystals in the pores, possibly being vapor phase deposits. In consequence, Almahata Sitta could represent "an agglomeration of fine-grained, incompletely reduced pellets formed during impact, and subsequently welded together at high temperature" (Zolensky

et al., 2009). Zolensky et al. (2010a) found a foliation in AHS 7 based on a preferred orientation of metal and suggested that it is probably related to the genesis of this fragment.

Mikouchi et al. (2010a,b,c) performed FIB-TEM investigations of pyroxene (mg# = ~92) in the fine-grained ureilite AHS 7. They conclude that the fine-grained pyroxenes (10–20 μm), both low-Ca and high-Ca, showing a mosaicized texture must have crystallized at very high equilibration temperatures (1240–1280 °C). Additionally, some areas in the pyroxene show augite exsolution lamellae (10–15 nm wide) in pigeonite (see also below).

The fine-grained ureilites (e.g., AS-H109, MS-20, MS-165, MS-168) were also found to host large Si-bearing metal grains (up to ~4.5 wt% Si; Warren and Rubin, 2010; Horstmann et al., 2013b), in addition to low-Si Fe,Ni and Fe metal, and niningerite (Mg-rich sulfide), compositionally similar to those typical of E chondrites and enstatite achondrites (Bischoff et al., 2010a,b; Warren and Rubin, 2010; Horstmann et al., 2013b).

Herrin et al. (2009) concluded that the textures observed in Almahata Sitta fine-grained ureilites (e.g., Fig. 7a and b) result from reduction processing. Warren and Rubin (2010), in providing a detailed examination of fine-grained ureilites, concluded that this type of lithology with its variable but distinct texture and mineralogy formed via so-called impact smelting of a former coarse-grained ureilite along with the final catastrophic disruption of the ureilite parent body (UPB). Horstmann et al. (2013b) found evidence for metallic melt fractionation in fine-grained ureilites (see below) and concluded that niningerite was formed via sulfidation of silicates during impact smelting.

4.2.1.3. Dark ureilites and ureilites with variable grain sizes. Zolensky et al. (2009, 2010b) and Jenniskens et al. (2009b) described AHS 7 as a breccia having mafic silicate fragments of variable grain sizes. Also, Bischoff et al. (2010b) and Horstmann et al. (2012a) described several ureilites showing variable grain sizes (an example is shown in Fig. 7c): some domains are variably fine-grained (generally <50 μm). Some domains exhibit larger crystals (up to ~700 μm). Some of these rocks were also classified as breccias (MS-190, MS-191, and MS-205; Horstmann et al., 2012a), similar to the original classification routine (e.g., Zolensky et al., 2009, 2010a,b; Jenniskens et al., 2009b). However, these ureilites are more likely heterogeneously overprinted (impact-smelted?) former coarse-grained ureilites, resulting in variable grain size and relic (coarser-grained) minerals.

Some ureilites (e.g., MS-25 and MS-190) appear dark in transmitted light and mainly exhibit a strongly reduced mineralogy (e.g., MS-25: down to $Fa_{0.5}$; Fig. 7e and f) sprinkled with numerous tiny inclusions of mainly Fe metal and minor FeS (Horstmann et al., 2012a; Roggon, 2012). Only some pyroxene and olivine grains of variable size appear as relics in the reduced ground mass, often largely unaffected by reduction (highest Fa and Fs values). The reduced minerals also show smaller grain sizes (down to ~50 μm) than the relic grains (up to ~700 μm; Fig. 7e and f). However, we cannot completely exclude that some of the samples have a monomict fragmental character due to re-processing (e.g., fragmentation) upon impact.

4.2.1.4. Ureilitic sulfide-metal assemblages. Unusual sulfide-metal assemblages (Fig. 8) with fine-grained ureilite material (MS-158, MS-166, and AHS 33) have been described and analyzed (Bischoff et al., 2010a,b; Horstmann et al., 2011b; Ross et al., 2011a,b; Horstmann, 2013). These samples are dominated mainly by rounded metal grains several hundred microns across that often form clusters embedded in large masses of FeS (Fig. 8; Bischoff et al., 2010a,b). Hence, they are texturally generally similar to metal-sulfide objects in chondrites and sulfide-rich meteorites. Fine-grained ureilite material is typically enclosed in FeS and only

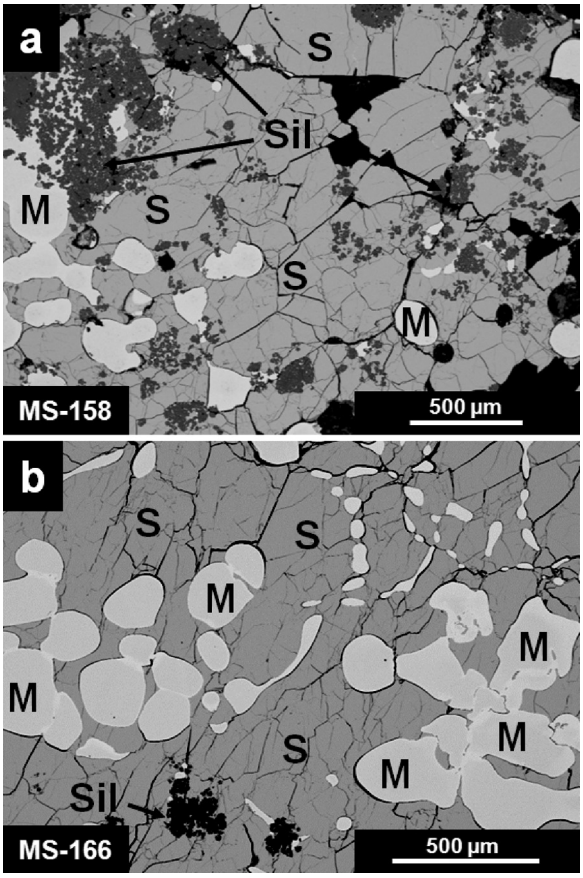

Fig. 8. Almahata Sitta sulfide-metal assemblages (a) MS-158 and (b) MS-166 shown in BSE images. Both samples are fully crusted individuals showing rounded (zoned) metal grains (M) sometimes forming clusters, embedded in large masses of troilite (S). Minor fine-grained silicate material (Sil) with ureilite composition can be found enclosed in predominantly troilite and subordinate in metal as shown in the upper left of (a).

rarely in metal (Fig. 8). The metal grains show Ni zoning: typically low-Ni cores (~8–10 wt% Ni) are surrounded by a sharply developed Ni-rich rim (up to ~39 wt%). Some grains, however, were found with somewhat continuous, though not ideal concentric zoning. Horstmann et al. (2011b) concluded that the zoned metal formed via fractional crystallization with the large masses of FeS representing the remaining metallic liquid. However, further detailed in situ siderophile trace element measurements of metal and FeS in combination with bulk chemical analyses of one fragment (MS-166) revealed a rather complex history for MS-158 and MS-166 (Horstmann, 2013). It appears that mainly residual metal (with some domains related to fractional crystallization) was invaded by a S-rich metallic melt and reacted with each other forming the Ni-rich rims via diffusion. Hence, MS-158 and MS-166 cannot represent the missing S-rich metallic melt thought to be involved in ureilite petrogenesis, although they might conceivably be matched with mixed metallic melt on the UPB or as successor body (Horstmann, 2013). However, atmospheric reprocessing affecting the texture of the sample during atmospheric passage cannot be excluded. Ross et al. (2011a,b) examined another sulfide-metal assemblage, AHS 33. The siderophile trace element systematics yield highly variable and grain-dependent results.

The fully crusted MS-166 fragment was found with an unusual, highly porous fusion crust rich in wüstite ($Fe_{1-x}O$) that formed by oxidation/desulfurization mainly of FeS during atmospheric passage (Horstmann et al., 2012b,c, 2013a). In situ siderophile trace element systematics revealed an imprint of elemental partitioning

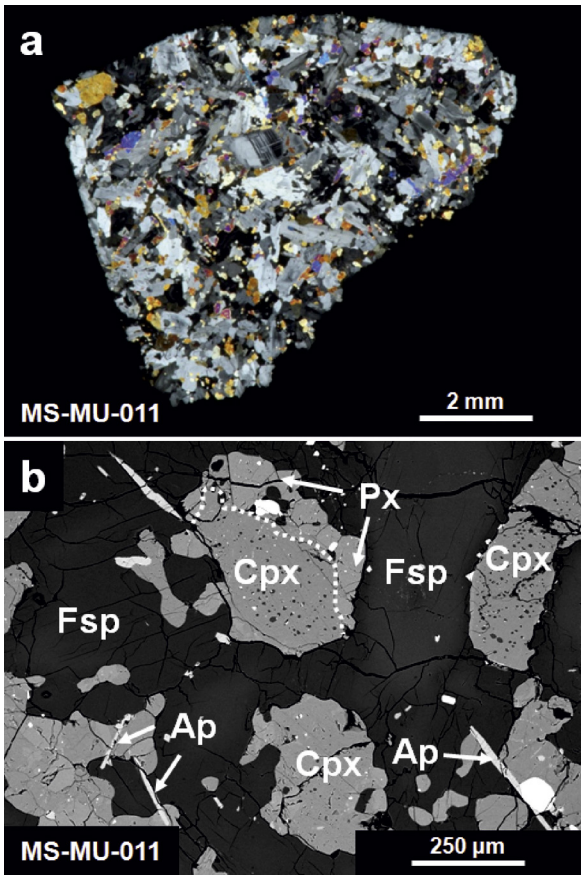

Fig. 9. Almahata Sitta MS-MU-011 andesite. (a) Optical photomicrograph of a thin section with crossed polarizer. The rock is dominated by feldspar (~70 vol%, mainly gray) and subordinate Ca- and low-Ca pyroxene (colored domains). Feldspar appears as large, often lath-shaped grains, but also more anhedral grains occur. (b) BSE image showing details of the typical texture of MS-MU-011. Feldspar (Fsp, frequently zoned) dominates with domains of Ca-pyroxene (Cpx) associated with low-Ca pyroxene (Px). Ca-rich pyroxene is typically characterized by many inclusions, whereas these are rare in low-Ca pyroxene. Nicely developed Cl-apatite laths (Ap) occur as one type of accessory phase. Among the remaining bright phases in (d) are mainly ilmenite and Fe, Cr, Ti-spinel.

influenced by oxygen in a metallic melt, previously undocumented by laser ablation-inductively coupled plasma-mass spectrometry (Horstmann et al., 2012b,c, 2013a).

4.2.1.5. Ureilite-related andesite. First results on the mineralogy, mineral chemistry, and oxygen isotope composition of a feldspar-rich fragment, MS-MU-011, Fig. 9) were presented by Bischoff et al. (2013a), describing the rock as a basalt based on its texture. However, the bulk chemistry revealed that it is an andesite (Bischoff et al., 2013b; submitted).

On the basis of its greenish color, this 24.2 g specimen was, although having a fusion crust, at first considered as a doubtful meteorite specimen. Thin section inspection (Fig. 9) revealed abundant feldspar (anorthoclase, plagioclase; ~70 vol%) including subhedral, zoned plagioclase laths (~An_{10-55}) embedding Cr-bearing Ca-pyroxene (~$Fs_{20-21}Wo_{36-37}$, Cr_2O_3: ~1 wt%), and Ca-poor pyroxene (~$Fs_{35-37}Wo_{7-10}$; Bischoff et al., 2013a). In most cases the molar Fe/Mn ratio of pyroxene was 15–20 (Bischoff et al., 2013a). As minor phases, euhedral laths of Cl-apatite, whitlockite, ilmenite, Ti, Cr, Fe-spinel, FeS, and metal were identified. The metal grains are basically Ni-free. Bischoff et al. (2013a) also described rare pockets of fine-grained FeS–Fe-metal intergrowths (up to ~30 μm). Due to fast cooling, SiO_2-normative melt inclusions (~4.5 wt% K_2O) were formed within large crystals (e.g., pyroxene; Fig. 9b). Fine-grained intergrowths of albitic plagioclase ($An_{<10}$), skeletal pyroxene, and a SiO_2-normative melt (with up to 4.5 wt% K_2O; perhaps glassy) occur in the interstices between the major minerals and can also be ascribed to fast cooling. Cohen et al. (2004) described feldspathic fragments in polymict ureilites which, based on texture, mineralogy, and mineral chemistry, are similar to MS-MU-011. Bischoff et al. (2013a) suggest that MS-MU-011 is the first large sample representing material from the crust of the ureilite parent body.

4.2.2. Ureilitic fragments – mineralogical and chemical aspects

4.2.2.1. Opaque phases. Ross et al. (2011a) performed 2D analyses of Almahata Sitta ureilite thin sections and 3D X-ray computed tomography scanning of probe blocks to study the modal abundance and appearance of metal, including grain boundary metal, metal inclusions in silicates, and secondary reduction metal. They found that metal shows a large variation in both modal abundance and textural appearance between different samples: AHS 22, for example, has ~1.8 vol% metal (grain boundary metal ≤35 μm in width), whereas AHS 44 has ~3.4 vol% metal of much larger grain size (>250 μm). Welten et al. (2010a) estimated 0–13.5 wt% metal in six ureilites (AHS 1, 4, 15, 36, 44, and 47) based on the correlation of bulk Fe and Ni.

Metal in ureilitic samples AHS 15 and 44 was investigated by Goodrich et al. (2010a). The textures suggest that metal was shock (s)melted in AHS 44, but not in AHS 15. Metal in AHS 44 is compositionally relatively homogeneous (Ni: 4.9 ± 0.3, Co: 0.38 ± 0.03, P: 0.35 ± 0.09, Si: 1.5 ± 0.4, in wt%) and in the range of other ureilites. AHS 44 reveals internal crystalline textures: Schreibersite occurs as μm to sub-μm grains on the edges of metal that itself is depleted in P (by ~0.2%) near these gains. Metal also contains many rounded pits. Electron backscatter diffraction (EBSD) of one metal area shows elongated laths of kamacite with an unidentified interstitial phase. In the olivine-augite-orthopyroxene assemblage of AHS 15, metal (1.6 wt% Ni, 0.12 wt% Co, 0.8 wt% P, 0.03 wt% Si) contains many large (~10–60 μm) schreibersite grains (~2.5 wt% Ni). Calculation of equilibrium temperatures in the Fe–Ni–P system from coexisting metal and schreibersite suggest ~700 °C from Ni and P in AHS 15 and ~550 °C from P in AHS 44, but Ni contents in the latter were not on equilibrium tie lines (Goodrich et al., 2010a). Siderophile trace element patterns are similar to those in other ureilites.

Mikouchi et al. (2011, 2013) analyzed metal in AHS 1, AHS 7, and AHS 44 by means of EBSD and TEM. In AHS 1 and AHS 7, large vein and small scattered Fe-metal grains were studied and revealed that almost all metal is *bbc* kamacite (α-Fe) of variable grain size (5–100 μm). Vein metal along silicate grain boundaries (~500 μm long) in AHS 44 shows a large diversity of textures and phase assemblages (see above). Some intergrowths for example show elongated laths (up to 30 μm long) of cohenite, confirmed via EPMA and EBSD. Fe-metal in this type of intergrowth shows small amounts of γ-Fe (*fcc*) in addition to kamacite, not resolvable by SEM-BSE. Mikouchi et al. (2011) attribute the small amount of γ-Fe in AHS 44 either to fast cooling by shock melting or shock re-melting of pre-existing metal and graphite forming eutectic-looking textures. Mikouchi et al. (2013) performed TEM studies on one grain boundary metal from AHS 44 and found laths of α-Fe (with a tweed-like texture), whereas interstitial areas are γ-Fe, suggesting the formation of two iron phases by the martensite transformation. In contrast, metals in AHS 1 and AHS 7 show no cohenite and γ-Fe; these might have experienced different thermal histories (Mikouchi et al., 2011). Additionally, Aoyagi et al. (2013a,b) studied metal grains in AHS 44, AHS S138, and AHS H1 and observed the parageneses of α-Fe and γ-Fe (+ schreibersite) as well as the assemblage of α-Fe, γ-Fe, and cohenite (+ schreibersite). So far, cohenite has never been observed

in grain boundary metal in typical coarse-grained ureilites and, therefore, Aoyagi et al. (2013a) suggest that local re-melting of different amounts of primary metal + graphite + Fe phosphide (+ Fe sulfide) would be responsible for the observed assemblages in AHS 44 and AHS S138. The large metal studied in AHS H1 has a core of pure α-iron and a periphery consisting of a complex combination of multiple phases (Aoyagi et al., 2013b).

Ross et al. (2011b) studied different types of metal in ureilites AHS 7, 15, 22, 27, 36, and 44 with respect to petrography and geochemistry. They also examined one H5 chondrite (AHS 25) and one sulfide-metal assemblage (AHS 33). Texturally, EBSD mapping revealed that metal in AHS 7, 22, and 44 is made up of different sub-grains, some of which show internal deformation. In situ siderophile trace element systematics in AHS 7, 36, and 44 are in accordance with high degrees of metallic melt extraction (60–80%), similar to other ureilites. AHS 15, 22, and 27 metal differs from other ureilites by indicating lower degrees of metallic melt extraction. AHS 27 metal additionally has unusually high Ni (up to 11.3 wt%) and almost chondritic highly siderophile element ratios, distinguishing it from any other previously measured ureilite.

Warren and Rubin (2010) described and analyzed large Si-bearing metal grains in AS-H109 (up to ~4 wt% Si), and Horstmann et al. (2013b) studied in detail large Si-bearing metal grains in fine-grained ureilites MS-20, MS-165, and MS-168. Following Warren and Rubin (2010), they concluded that the metal largely formed along with impact smelting of the parent lithologies. In situ siderophile trace element analyses revealed two distinct metal populations in MS-20 and MS-168: residual metal as observed in many other coarse-grained ureilites (MS-168), and metal with a partial melt signature previously unknown from any ureilite (MS-20). Horstmann et al. (2013b) concluded that this most likely indicates solid metal–liquid metal fractionation along with the final catastrophic disruption of the ureilite parent body, but they cannot rule out that this is a primary feature from ureilite petrogenesis.

Hochleitner et al. (2010) examined the mineralogy of opaque phases in AHS 39 and found up to five metal phases of different compositions, mainly showing variations in Fe, Ni, Si, and Co. Hoffmann et al. (2011a) reported four different types of kamacite in AHS 39 (Fe: 90.95–95.24 wt%, Ni: 1.22–4.31 wt%, Si: 0.22–3.86 wt%, Cr: 0.13–0.18 wt%, P: 0.37–0.52 wt%). One type of kamacite (kamacite I; Fe: 90.95 wt%, Ni: 4.31 wt%, Si: 3.86 wt%, Co: 0.20 wt%, minor P and Cr), "builds up the large sheets between silicate grains" (Hochleitner et al., 2010; Hoffmann et al., 2011a). They conclude that the high Co in this type of kamacite distinguishes it from all other metal phases they analyzed, having Co below detection limit; it might be of extraneous origin and was probably introduced by a Ni-poor iron meteorite impactor. Troilite (Cr: 1.20 wt%, Si: 0.86 wt%, Mn: 0.22 wt%, Ni: 0.04 wt%) and Cr-rich troilite (up to 6.8 wt% Cr, 0.39 wt% V) have been indentified in AHS 39 carbon-rich veins, and daubreelite (2.27 wt% Mn, 0.42 wt% V) was also found in the carbon-rich veins intergrown with troilite and some tiny troilite grains occur within olivine.

4.2.2.2. Diamonds and other C-rich phases. Diamond and aliphatic carbon were found in AHS 7 (Jenniskens et al., 2009b). Miyahara et al. (2013) described a huge single diamond crystal (~100 μm) intergrown with graphite based on SEM-EBSD studies. Also, diamonds and related phases were further investigated by Ross et al. (2010, 2011c) using microRaman map images and single spectra. They compared the change in peak center wave number and full-width at half-maximum to terrestrial diamond to infer the formation style and history of diamond in Almahata Sitta. The presence of lonsdalite (hexagonal diamond) might be indicated by the larger peak shift away from terrestrial kimberlite diamond. Raman spectra of diamond in brecciated and unbrecciated ureilites are undistinguishable. However, diamond in Almahata Sitta is different from other, both brecciated and unbrecciated ureilites. Ross et al. (2011c) found that diamond in AHS 7 shows a peak center range of 1318.5–1330.2 cm^{-1} and a full width at half maximum (FWHM) range of 6.6–17.4 cm^{-1}, which would represent a shock pressure of at least 60 kbar. Shock processes have been discussed as the most likely origin of ureilite diamond formation (e.g., Vdovykin, 1972; Bischoff et al., 1999; Grund and Bischoff, 1999). Ross et al. (2011c) also found amorphous carbon in Almahata Sitta and graphite that shows a G-band peak center range of 1569.1–1577.1 cm^{-1} and a G-band FWHM range of 24.3–41.6 cm^{-1}. They suggest that these data would represent formation temperatures of 990 ± 120 °C.

4.2.3. Chondritic fragments – textures and mineral characteristics

A highly variable collection of chondritic meteorites covering various chondrite classes was identified among the finds in the asteroid 2008 TC_3-Almahata Sitta strewn field (Figs. 10–12). Overall 35 rocks were described in more detail regarding mineralogy and chemistry (Bischoff et al., 2010a,b; Horstmann et al., 2010, 2011a, 2012a; Horstmann and Bischoff, 2010a,b; Zolensky et al., 2010b; Warren and Rubin, 2010; El Goresy et al., 2011, 2012). The results are compiled in Table 2.

4.2.3.1. Enstatite chondrites. A wealth of different enstatite (E) chondrites was found among the Almahata Sitta samples representing distinct lithologies (Fig. 10). Both EL and EH chondrites were identified; petrologic types range from primitive type 3 (e.g., MS-14 EH3) to highly metamorphosed rocks (e.g., MS-D EL6) (Table 2).

Bischoff et al. (2010a,b) and Horstmann et al. (2012a) described various E chondrites covering almost all petrologic types (types 3, 3/4, 6, impact melt rocks and breccias), showing diverse textures of their silicate and especially opaque constituents (Fig. 10). Several rocks were found with metal nodules (described previously from other E chondrites) that are either complex intergrowths of metal and minor sulfide, perryite/schreibersite, and/or silicates, or metal-silicate assemblages in which euhedral enstatite and/or sinoite laths are intergrown with metal (Si-bearing kamacite; Bischoff et al., 2010a,b; Horstmann, 2013; Fig. 10b and d). Numerous sulfide (e.g., niningerite, alabandite, keilite, oldhamite, troilite) and metal chemistries in various E chondrites are listed in Horstmann (2010, 2013). Zolensky et al. (2010b) also briefly mentioned one EL6 and one EH5/6 chondrite among their samples examined.

El Goresy et al. (2011, 2012) and Lin et al. (2011) performed a detailed mineralogical and chemical study of EL3 chondrites MS-17 and MS-177. [Note that these works listed the classification of MS-17 more precisely as EL3, compared to EL3/4 in Bischoff et al. (2010b).] Two distinct oldhamite populations were identified in MS-17: (a) matrix oldhamite with schreibersite inclusions and (b) amoeboid grains in chondrules. Oldhamite rare earth element patterns have a negative Eu anomaly and are distinct from EH3 oldhamite. El Goresy et al. (2011) conclude that the different settings and appearances of oldhamite (with and without inclusions) indicate different fO_2 at their formation via condensation reactions. Lin et al. (2011) explained the paragenesis of oldhamite, sinoite, and graphite in MS-17 as the earliest solid condensate. El Goresy et al. (2012) studied similar assemblages of sinoite, graphite, and oldhamite associated with metal nodules in MS-17 and MS-177. Based on C and N isotopic compositions, and rare earth element systematics of oldhamite, they concluded that these assemblages formed via condensation (sequence: oldhamite → sinoite → graphite) and are clearly not products of impact melting. This conclusion was challenged by Horstmann (2013) who showed that the metal in primitive EL3 MS-17 is of melt origin (see below).

Horstmann et al. (2011a) and Horstmann (2013) reported on rare earth element abundances in oldhamite and keilite from E chondrites MS-14, MS-17, MS-52, MS-155, MS-159, MS-164, and MS-D. Oldhamite in MS-14 (EH3) is similar to that in other EH3

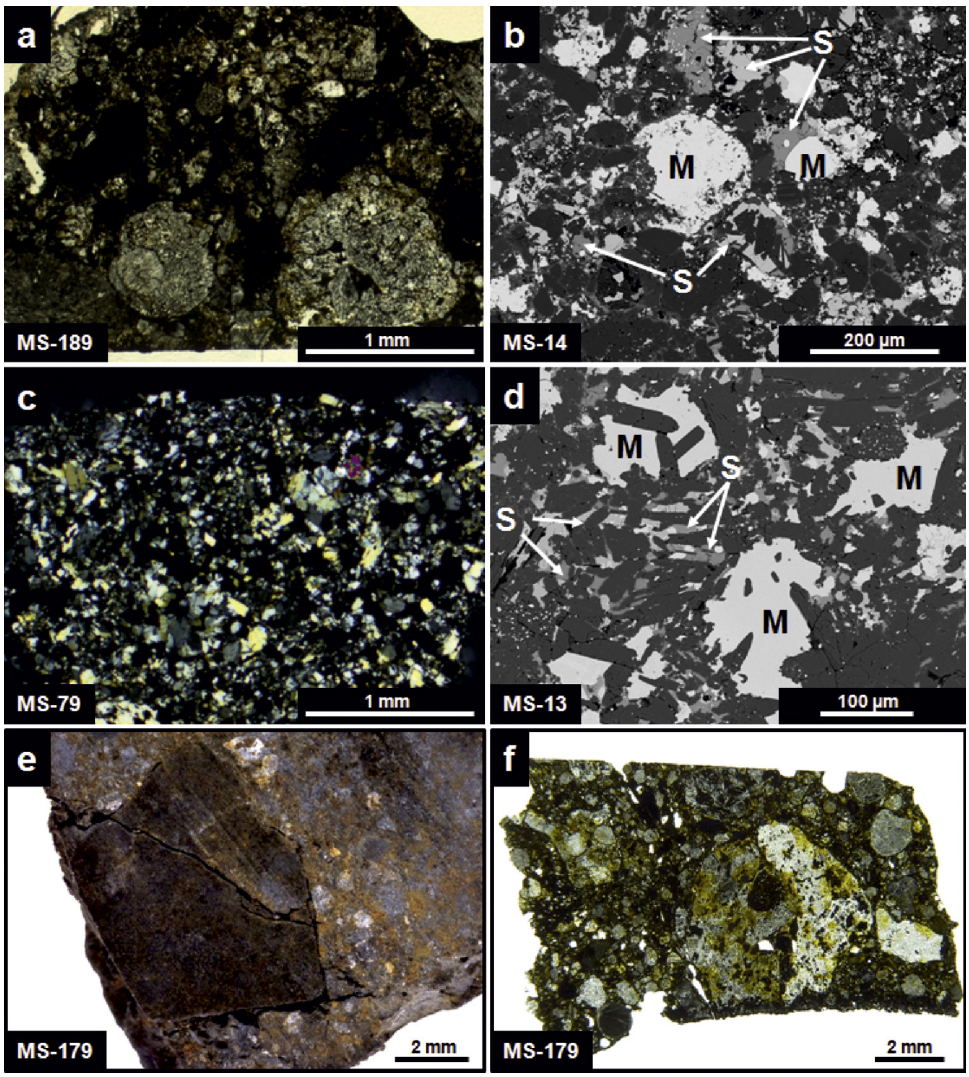

Fig. 10. Almahata Sitta enstatite chondrites. (a) Optical photomicrograph of the MS-189 EL3 chondrite showing the primitive, chondritic texture. (b) BSE image of MS-14 (EH3) showing the high abundance of opaque phases and its complex texture. Various sulfides (S, medium gray phases) such as troilite, oldhamite, niningerite, and daubreelite occur in addition to metal nodules (M, white). The nodules show complex internal textures with inclusions of, e.g., perryite, schreibersite, and/or troilite. (c) Overview of the MS-79 EL 6 chondrite (optical photomicrograph, crossed polarizer). The rock is metamorphosed and recrystallized blurring the chondritic fabric. (d) BSE image of the MS-13 EH IMR. Similar to MS-14, various sulfides (S) occur. Metal (M) typically occurrs as compact objects of kamacite with lath-shaped enstatite enclosed or apparently growing into the metal from the matrix, forming so-called metal-silicate intergrowths. (e) Detailed image of one fragment in the MS-179 EL3-5 breccia (optical photograph). (f) Overview (optical photomicrograph) of one MS-179 thin section illustrating the various lithologies/fragments in this rock. Some fragments appear recrystallized (e.g., white areas), other domains show a chondritic fabric.

chondrites and has positive Eu and Yb anomalies or rather flat patterns. MS-17 (EL3/4), MS-164 (EL3/4), MS-52 (EL6), MS-D (EL6), and MS-159 (EL IMR) all show negative Eu anomalies in oldhamite, with the difference of an overall flat pattern in the case of EL3/4 s and a convex-upward pattern for EL6 and EL IMR samples. Enrichments of REE in oldhamite range from ~30 to 200 × CI, but are typically around 100 × CI. Oldhamite in MS-155 (EH IMR) has a flat REE pattern without any anomalies. Keilite in MS-159 (EL IMR) and MS-D (EL6) exhibits a fractionated pattern (heavy REE enriched to ~15–20 × CI) with negative Eu anomaly (≤1.5 × CI) and light REE depletion (≤4 × CI). Horstmann (2013) analyzed metal grains of different textural appearance in nine E chondrites by means of laser ablation-inductively coupled plasma-mass spectrometry. He found that with progressive metamorphism, metal compositional variability generally approaches the average bulk E chondrite metal compositions of Kong et al. (1997). Several, samples (e.g., MS-14, MS-155, and MS-164) were found with clear indications for a partial melt origin. Particularly for MS-14 (EH3) and MS-164 (EL3/4), this is an interesting observation because it argues against the condensation origin of metal in primitive E chondrites, as suggested by El Goresy et al. (2012) and Weisberg et al. (1997, 2013). Basically, Horstmann (2013) showed, based on Almahata Sitta E chondrites, that metal nodules in E chondrites, irrespective of its textural appearance and petrologic type of the host rock, are distinct from metal condensate signatures. Furthermore, textural and mineral chemical constraints also argue against the preferred in situ impact melt origin of metal-silicate assemblages found in many primitive EL chondrites (e.g., Van Niekerk and Keil, 2011, and references therein), but argues in favor of a pre-accretionary melt origin of these objects. This suggests that at least some Almahata Sitta fragments earlier described as impact melt rocks (IMR; Bischoff et al., 2010b) might be re-classified as unmelted rocks.

4.2.3.2. Ordinary chondrites. Several ordinary chondrites were recovered from the Almahata Sitta strewn field (Fig. 11a and b), which some authors originally considered to be unrelated to

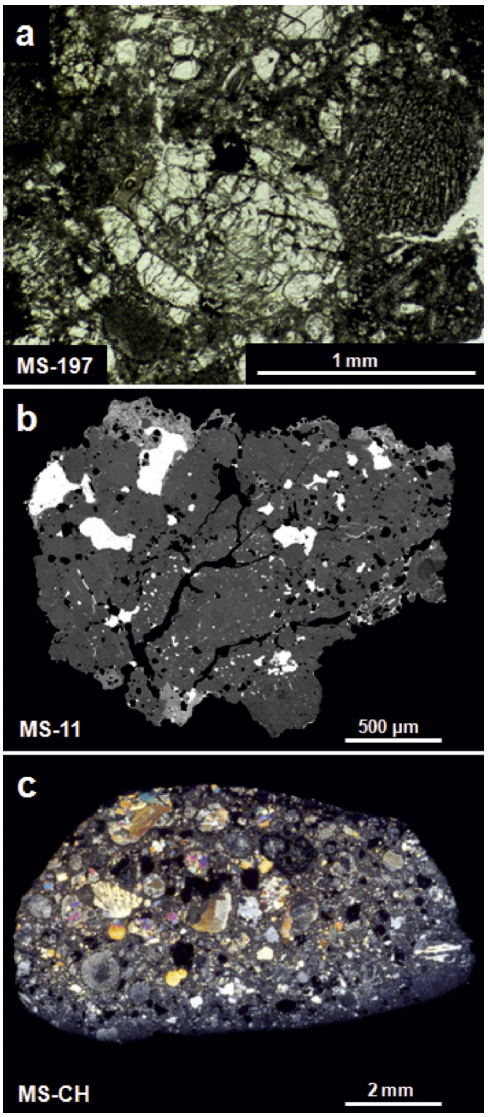

Fig. 11. Almahata Sitta ordinary and Rumuruti-like chondrites. (a) MS-197 LL4/5 chondrite (optical photomicrograph, crossed polarizer). (b) BSE image of the MS-11 H5/6 chondrite containing large metal grains (white). (c) Unique Rumuruti-like chondrite MS-CH (type 3.8), showing abundant chondrules and high matrix abundance (~45 vol%). Optical photomicrograph of a thin section.

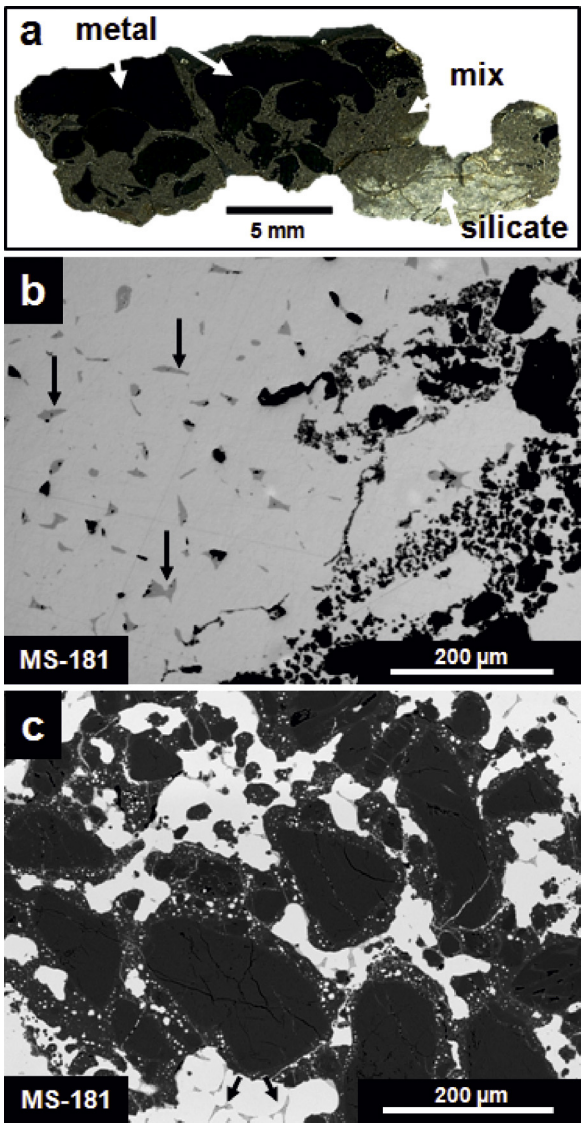

Fig. 12. Almahata Sitta Bencubbin-like chondrite MS-181 (CB_a). (a) Overview of a MS-181 slice illustrating the high abundances of metal (total metal ~60 vol%). Interstitial portions (mix) show silicates in complex intergrowths with smaller metal grains [see (c) for details]. Silicates also occur as larger polymineralic grains of different textural type (total silicates ~40 vol%). (b) Reflected light image showing a typical close-up of the metal-rich portion of MS-181. Metal commonly appears with interstitial FeS containing variable amounts of Cr (arrows). Dark areas are silicates. (c) BSE image of a typical portion of the material interstitial to the large metal globules and the silicate portions. Silicate fragments and chondrules are mainly surrounded by a silicate-rich rim dispersed with numerous metal spherules. Metal shows again interstitial FeS (arrows).

Almahata Sitta (e.g., Rumble et al., 2010a). Bischoff et al. (2010b) reported mineral compositions of one shock-darkened H5 (MS-151) and one H5/6 chondrite (MS-11, Fig. 11b) containing shock-melted areas. AHS 25 was identified as another H5 chondrite showing metal with martensite composition (~14 wt% Ni; Zolensky et al., 2010b; Warren and Rubin, 2010). MS-197 is an LL4/5 chondrite (~Fa_{30}, ~Fs_{23}; Fig. 11a, Table 2), but note that the MS-197 sample was mislabeled in Horstmann et al. (2012a) as L4/5. Fragment AHS A100 was classified as L4 (~Fa_{24}, ~Fs_{16}; Zolensky et al., 2010b).

4.2.3.3. Rumuruti-like chondrite fragment. A unique fragment (MS-CH; Fig. 11c; Table 2, Horstmann et al., 2010; Horstmann and Bischoff, 2010a) was discovered showing many characteristics typical of Rumuruti (R) chondrites (Bischoff et al., 1994, 2011). It is an olivine-rich rock (Fa_{35-37}) of petrologic type 3.8 ± 0.1, weighing 5.68 g. The average oxygen isotope composition is close to the range of R chondrites (see below; Horstmann et al., 2010). The matrix abundance is ~45 vol% and the mean chondrule size is ~450 µm. Several altered spinel-rich Ca,Al-rich inclusions were identified. The equilibrated R chondrites are characterized by a lack of metal and high FeO-concentrations in silicates (e.g., olivine with Fa_{38-40}; Bischoff et al., 2011). Several characteristics, however, distinguish MS-CH from this class of highly oxidized chondrites, e.g., the higher abundances of metal (~2.5 vol%) or the absence of magnetite and platinum-group element-rich phases such as sulfides, tellurides, and arsenides, making it a unique chondrite with affinities to R chondrites.

4.2.3.4. Carbonaceous chondrite. The CB_a chondrite MS-181 weighing 58.6 g is a metal-rich rock (~60 vol%) and contains silicates (~40 vol%; Bischoff et al., 2012; Fig. 12) of various textures similar to those described by Krot et al. (2007) and Rubin et al. (2003) for

CB-chondrites. Large kamacite globules (up to ~8 mm) have highly variable abundances of Cr-bearing FeS-inclusions (0.6–10.8 wt% Cr) of different morphologies (Fig. 12a and b). The sub-textures in metal are similar to those in Gujba (Krot et al., 2007). Kamacite has mainly 6–8 wt% Ni, ~0.5–0.9 wt% Co, and traces of P (~0.4 wt%), and Cr (≤0.4 wt%); rarely, tiny metal grains contain up to ~31 wt% Ni. Silicates also occur as spheroidal or ellipsoidal globules in complex intergrowths with smaller metal grains interstitial to the large ones. The silicates occur as chondrules of different textural type (e.g., cryptocrystalline, barred, and porphyritic) and fragments that are mainly surrounded by a silicate-rich rim dispersed with numerous metal spherules (Fig. 12c). MS-181 pyroxene is $Fs_{2.7\pm1.1}Wo_{3.1\pm2.9}$ on average with a total range of $Fs_{0.9-5.9}Wo_{0.7-10.8}$, olivine has Fa_{3-4}, and Ca-pyroxene gives $Fs_{1.1-3.5}Wo_{35.0-46.8}$. Ca-pyroxene shows variable Al contents (7.6–12.8 wt% Al_2O_3).

5. Bulk chemical and isotopic compositions of Almahata Sitta subsamples

5.1. Bulk composition

Based on the occurrence of different types of chondritic and achondritic fragments and their variety of lithologies, a reliable bulk composition of asteroid 2008 TC_3 and of the Almahata Sitta meteorite cannot be obtained. Instead, only the bulk compositions of individual fragments can be determined. So far, only a few fragments have been analyzed (Jenniskens et al., 2009b; Friedrich et al., 2010; Meadni and Taha, 2011; Table 3). Jenniskens et al. (2009b) found that AHS 7 has bulk trace element compositions similar to those of many ureilites, with REE patterns possessing a distinct negative Eu anomaly and general abundances between 0.1 and 0.6 × CI. Fragment AHS 7 is one of four samples analyzed (AHS 4, 7, 15, 47), all of which have ureilitic compositions (Friedrich et al., 2010): The highly refractory siderophile elements are similarly enriched in the four samples, whereas the more volatile elements indicate larger variability (Table 3). In fragment AHS 15, the heavy REE concentrations reach ~CI-values. In all patterns which show a negative Eu anomaly, the light REE are depleted relative to the heavy REE and the abundances are typically between 0.01 and 0.3 × CI. Furthermore, the CI-normalized siderophiles and moderately siderophile elements typically fall in the same range as those of ureilites previously analyzed, with a greater variability of the more volatile siderophile elements. Considering other trace elements, the mean CI-normalized concentrations of the four highly volatile elements Bi, Te, Se, and Cd show a relatively flat trend with a mean value of 0.050 ± 0.002 × CI, and that Zn is significantly enriched relative to the other volatile elements, approaching CI concentrations in fragment AHS 47 (mean CI-normalized Zn of all four fragments: 0.53 ± 0.32). The analysis of AHS 27 by Meadni and Taha (2011) revealed a very high Fe concentration of 44.6 wt%, which certainly is not consistent with the characterization of AHS 27 being an ureilitic rock (Shaddad et al., 2010).

Table 3
Bulk composition of four fragments of Almahata Sitta ureilite meteorites. Data from Friedrich et al. (2010).

Element	Unit	AHS 7[a]	AHS 4	AHS 15	AHS 47
Li	$\mu g\,g^{-1}$	1.7	1.0	0.95	1.3
Na	$mg\,g^{-1}$	NA	0.26	0.76	0.26
Mg	wt%	NA	24.5	20.9	21.1
Al	wt%	NA	0.262	0.477	0.148
P	$mg\,g^{-1}$	NA	0.74	1.6	0.49
K	$mg\,g^{-1}$	NA	<0.03	<0.03	<0.03
Ca	wt%	NA	1.05	4.23	0.87
Sc	$\mu g\,g^{-1}$	9.0	9.2	20.2	7.8
Ti	$\mu g\,g^{-1}$	274	175	676	126
V	$\mu g\,g^{-1}$	84	87	118	88
Cr	$mg\,g^{-1}$	NA	4.18	3.34	5.02
Mn	$mg\,g^{-1}$	3.06	3.72	3.66	2.7
Fe	wt%	NA	10.7	9.99	16.3
Co	$\mu g\,g^{-1}$	240	35	55	150
Ni	$\mu g\,g^{-1}$	NA	604	828	1890
Cu	$\mu g\,g^{-1}$	12	11	8.2	8.2
Zn	$\mu g\,g^{-1}$	105	154	88	307
Ga	$\mu g\,g^{-1}$	4.2	1.9	3.5	3
As	$\mu g\,g^{-1}$	1.0	1.0	≤0.3	1.1
Se	$\mu g\,g^{-1}$	1.0	1.5	0.9	0.8
Rb	$ng\,g^{-1}$	255	19	≤15	37
Sr	$ng\,g^{-1}$	551	613	1900	104
Y	$ng\,g^{-1}$	610	380	2600	180
Zr	$ng\,g^{-1}$	470	100 ± 20	1500	100
Nb	$ng\,g^{-1}$	180	20	30	30
Mo	$ng\,g^{-1}$	1600	110	300	300
Ru	$ng\,g^{-1}$	300	≤1340	380	NA
Ag	*$ng\,g^{-1}$*	*30*	*40 ± 10*	*20*	*30*
Cd	$ng\,g^{-1}$	NA	35	NA	NA
In	$ng\,g^{-1}$	NA	≤3	NA	NA
Pd	$ng\,g^{-1}$	140	30	60	60
Sn	$ng\,g^{-1}$	210	30 ± 10	20	60
Sb	$ng\,g^{-1}$	100	≤25	20	≤18
Te	$ng\,g^{-1}$	120	140	70	120
Cs	$ng\,g^{-1}$	19.2	0.4	2	2.5
Ba	$ng\,g^{-1}$	247	43 ± 12	421	273
La	$ng\,g^{-1}$	27	5.1	50	4.2
Ce	$ng\,g^{-1}$	58	17	130	10
Pr	$ng\,g^{-1}$	9.5	3.9	35	1.5
Nd	$ng\,g^{-1}$	48	27	254	6.7
Sm	$ng\,g^{-1}$	24	16	160	4
Eu	$ng\,g^{-1}$	5.6	5.1	22	0.8
Gd	$ng\,g^{-1}$	43	29	270	8.6
Tb	$ng\,g^{-1}$	10	7.1	62	2.5
Dy	$ng\,g^{-1}$	66	50	347	17.9
Ho	$ng\,g^{-1}$	19	13	90	5.8
Er	$ng\,g^{-1}$	65	42	259	21
Tm	$ng\,g^{-1}$	13	8.1	42	4.7
Yb	$ng\,g^{-1}$	81	54	256	35
Lu	$ng\,g^{-1}$	18	12	47	8.1
Hf	$ng\,g^{-1}$	14	5	53	3
Ta	$ng\,g^{-1}$	0.5	0.08	0.6	0.1
W	$ng\,g^{-1}$	300	11 ± 5	35	24
Re	$ng\,g^{-1}$	65	5	7	48
Ir	$ng\,g^{-1}$	700	50	90	340
Pt	$ng\,g^{-1}$	1000	70	100	500
Tl	$ng\,g^{-1}$	NA	≤9	NA	NA
Bi	$ng\,g^{-1}$	≤2	≤8	6	NA
Th	$ng\,g^{-1}$	2.5	0.3	8.2	1.2
U	$ng\,g^{-1}$	0.9	0.2	8.4	0.6

[a] Trace element results reproduced from Jenniskens et al. (2009b) for comparison. NA = not analyzed.

5.2. Oxygen isotopes

Oxygen isotope compositions of 35 different Almahata Sitta fragments and mineral phases in several samples were determined by Jenniskens et al. (2009b), Bischoff et al. (2010b, 2012, 2013a,b), Rumble et al. (2010a,b), Horstmann et al. (2010, 2012a), and Kita et al. (2011). The results of the bulk samples are listed in Table 4 and illustrated in Fig. 13. Many of the samples analyzed clearly fall along the same trend as known ureilites (parallel to the CCAM line, Fig. 13), but others have oxygen isotope compositions more similar to those of E chondrites. As shown above, these data mirror the EL and EH groups. Some oxygen isotope analyses clearly fall in the fields of ordinary H and L chondrites (Fig. 13). One fragment revealed oxygen isotope compositions similar to those of the highly oxidized R chondrite group (sample MS-CH; Horstmann et al., 2010); another can be attributed to the reduced carbonaceous chondrite group CB (MS-181; Bischoff et al., 2012). The oxygen isotope compositions of two aliquots from the andesite MS-MU-011 give $\delta'^{18}O = 8.08‰$, $\delta'^{17}O = 3.23‰$, $\Delta^{17}O = -1.061‰$ and $\delta'^{18}O = 7.96‰$, $\delta'^{17}O = 3.19‰$, $\Delta^{17}O = -1.040‰$, clearly consistent with a ureilitic origin. The data plot on the CCAM line with

Table 4
Oxygen isotope compositions [in ‰] of all Almahata Sitta fragments analyzed to date. In case of multiple analyses from one fragment, the average was calculated.

Sample	$\Delta^{17}O$	$\delta^{17}O$	$\delta^{18}O$	Ref.
AHS 4	−1.02	2.63	6.95	2
AHS 7	−0.40	3.52	7.44	1,2
AHS 15	−0.95	2.63	6.80	2
AHS 25	0.92	3.14	4.22	2
AHS 27	−1.28	1.82	5.88	2
AHS 36	−1.53	1.31	5.40	2
AHS 44	−1.04	2.74	7.18	2
AHS 47	−0.94	3.27	8.00	2
AHS 49	−0.99	2.63	6.89	2
AHS 51	−1.87	0.93	5.32	2
AHS 54	−2.26	0.43	5.10	2
MS-D	−0.01	3.06	5.85	3
MS-CH	1.76	4.35	4.94	3
MS-11	0.80	3.08	4.35	3
MS-16	−1.05	2.28	6.28	3
MS-20	−0.23	3.99	7.99	3
MS-52	0.02	3.31	6.27	3
MS-61	−0.60	3.57	7.94	3
MS-79	0.07	3.31	6.17	3
MS-124	−0.59	3.42	7.59	3
MS-151	0.75	2.98	4.26	3
MS-168	−0.48	3.80	8.10	3
MS-169	−1.69	1.55	6.16	3
MS-170	−0.82	3.40	7.97	3
MS-175	−0.89	2.97	7.30	3
MS-181	−2.18	−1.57	1.15	4,5
MS-183	−1.33	1.94	6.21	5
MS-184	−0.91	3.17	7.77	5
MS-188	−0.94	2.97	7.44	5
MS-189	−0.04	3.08	5.95	5
MS-190	−0.75	3.59	8.25	5
MS-197	1.23	3.96	5.19	5
MS-200	0.13	3.37	6.18	5
MS-201	0.31	3.50	6.08	5
MS-MU-011	−1.05	3.21	8.02	6

1: Jenniskens et al. (2009b); 2: Rumble et al. (2010b); 3: Bischoff et al. (2010b); 4: Bischoff et al. (2012); 5: Horstmann et al. (2012a); 6: Bischoff et al. (2013a).

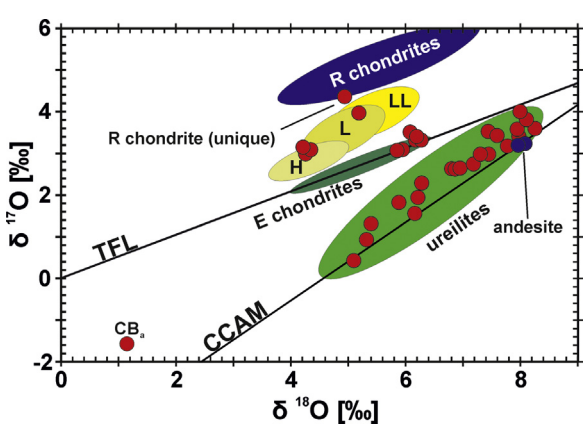

Fig. 13. Three oxygen isotope diagram ($\delta^{18}O$ vs. $\delta^{17}O$) showing the oxygen isotope compositions of all Almahata Sitta fragments analyzed to date (35 samples). The blue points represent two analyses of a ureilitic andesite (Bischoff et al., 2013a,b). Data are compiled from Jenniskens et al. (2009b), Bischoff et al. (2010b, 2012, 2013a,b), Rumble et al. (2010b), and Horstmann et al. (2010, 2012). In case of multiple analyses from one fragment, the average was calculated. CCAM = carbonaceous chondrite anhydrous mineral mixing line; TFL = terrestrial fractionation line.

$\delta'^{17}O = 0.94 \times \delta'^{18}O - 4.3‰$ (Fig. 13) (Bischoff et al., 2013a,b) and are similar to several feldspathic fragments in ureilitic breccias (Cohen et al., 2004; Goodrich et al., 2004; Kita et al., 2004).

Kita et al. (2011) studied the oxygen isotopes of mineral phases (olivine and pyroxene) from ureilitic lithologies AHS 15, 36, 44, 51, 54, and one H chondrite (AHS 25). The data from the five ureilites are generally consistent with the bulk rock data obtained earlier by Rumble et al. (2010a,b), and the analyses of olivine and pyroxene from various constituents of the H chondrite show resolvable variations. Based on the compositional range determined, Rumble et al. (2010b) concluded that the oxygen isotope compositions of the ureilites in Almahata Sitta are representative of all known monomict and polymict ureilites.

5.3. Light noble gases (and Ar–Ar)

The noble gases were analyzed in fragments AHS 1, 4, 36, 44, 47 (Welten et al., 2010a; Murty et al., 2010a; Ott et al., 2010) and in two chondritic fragments, AHS 25 and AHS A100 (Meier et al., 2012). Some selected data are summarized in Table 5. Preliminary data had been published in Meier et al. (2010), Murty et al. (2010b), and Welten et al. (2010b, 2011).

Welten et al. (2010a) determined the concentrations and isotopic compositions of noble gases in ureilitic samples AHS 4, 36, 44, and 47. They found He and Ar to be a mixture of cosmogenic, trapped, and radiogenic components, whereas Ne only consists of cosmogenic and trapped components. In addition, Meier et al. (2012) also studied the noble gases of the H (AHS 25) and L chondritic (AHS A100) samples and assumed that ^{3}He is entirely cosmogenic, while ^{4}He is mostly radiogenic with a small cosmogenic component. Based on the analyzed $^{20}Ne/^{22}Ne$ ratios of 0.84–0.86, these authors further suggest that Ne is also almost entirely cosmogenic, whereas the $^{36}Ar/^{38}Ar$ ratios of 3.3–4.3 would indicate significant amounts of trapped Ar. Interestingly, they concluded that this component is probably ureilitic Ar, suggesting that some transfer of noble gases occurred from the ureilite host to the chondritic lithologies. Contrary to the AHS ureilites, which have very low ^{40}Ar, the measured ^{40}Ar concentrations in AHS 25 and A100 are entirely radiogenic, indicating old K-Ar ages of ~4.6 Ga. Based on the lower $^{22}Ne/^{21}Ne$ ratios and lower radionuclide concentrations in the metal phase, Meier et al. (2012) concluded that AHS 25 experienced higher shielding than AHS A100 (80–150 g cm^{-2} vs. 30–50 g cm^{-2}).

Murty et al. (2010a) analyzed trapped nitrogen and noble gases in two ureilite samples [AHS 36 (a bulk sample) and 44 (a residue); see classification in Table 2]. Some data on noble gases are given in Table 6. The He and Ne isotopic ratios of the bulk samples clearly show that they are a mixture of trapped and cosmogenic components and that the temperature steps fall along the mixing line between cosmogenic and a trapped component (Ne-U) in the Ne three isotope plot. Ar, Kr, and Xe in both the bulk and the residue are dominated by a trapped component and the isotopic compositions of Kr and Xe are similar in all temperature steps for both samples. The isotopic signatures of N and Ar show a clear distinction between two fractions: a low temperature fraction (up to 500 °C) showed normal $^{38}Ar/^{36}Ar$ and heavy $\delta^{15}N$ that may have been hosted by amorphous C, and a high temperature fraction (>500 °C) with higher $^{38}Ar/^{36}Ar$ and lighter $\delta^{15}N$. The latter was presumably carried by diamond. Obviously, two populations of diamonds exist, which is indicated by different combustion temperatures: a sub-μm sized fraction combusts at ~700 °C, and a coarser-grained population with grain sizes of several μm is combusting at ~900 °C.

Ott et al. (2010) showed that the ^{3}He and Ne isotopes for AHS 1 and AHS 47 are essentially of pure cosmogenic origin and that no evidence for the presence of solar wind-implanted noble gases could be found. Both samples contain abundant trapped heavy noble gases (^{36}Ar, ^{84}Kr, and ^{132}Xe).

Beard et al. (2013) and Turrin et al. (2013) performed Ar–Ar analyses for the AHS 25 and A100 ordinary chondrite fragments. Based on their preliminary results, Beard et al. (2013) suggest that no hint of any strong thermal event on the Almahata Sitta parent body more recently than 4100 Ma ago could be found. In detail, the

Table 5
Concentrations (in 10^{-8} cm^3 STP g^{-1}) and isotopic ratios of light noble gases in Almahata Sitta (AHS) ureilites. For details see Welten et al. (2010b) and *Ott et al. (2010).

Sample	Mass (mg)	^{3}He	^{4}He	^{21}Ne	^{22}Ne	^{20}Ne/^{22}Ne	^{36}Ar	^{40}Ar	^{4}He	^{20}Ne$_{tr}$
AHS 1*	~15	14.3 ± 0.4	118 ± 3		5.20 ± 0.07	0.8572 ± 0.0041	23.8 ± 0.6			
AHS 4a	29.0	22.0	144	6.93	7.37	0.870	32.4	139.0	12	0.3
AHS 4b	52.2	22.0	144	7.09	7.53	0.872	29.0	84.0	11	0.3
AHS 36	47.0	24.2	171	7.25	7.73	0.870	13.1	97.7	25	0.3
AHS 44	71.4	27.0	315	5.80	7.08	1.752	1390	84.1	152	7.1
AHS 47*	~15	25.2 ± 0.5	230 ± 5		7.40 ± 0.11	1.0041 ± 0.0045	115.4 ± 2.8			
AHS 47a	32.0	27.6	251	7.66	8.26	1.041	108	154.0	85	1.9
AHS 47b	147.7	28.1	222	8.01	8.42	0.964	84	126.0	53	1.1

Table 6
Noble gas data for Almahata Sitta AHS A100 (L4) and AHS 25 (H5) chondrites. Table modified after Meier et al. (2012).

	AHS A100 L4		AHS 25 H5	
	#A100-1	#A100-2	#25-1	#25-2
Mass (mg)	162.3	65.84	183.2	67.80
Measured concentrations (10^{-8} cm^3 STP g^{-1})				
^{4}He	1821	1671	1494	1663
^{22}Ne	7.98	9.03	6.90	7.14
^{36}Ar	23.1	21.6	6.01	8.48
Measured isotopic ratios				
^{3}He/^{4}He	0.0155	0.0188	0.0152	0.0141
^{20}Ne/^{22}Ne	0.856	0.863	0.842	0.845
^{21}Ne/^{22}Ne	0.907	0.911	0.924	0.928
^{36}Ar/^{38}Ar	4.26	4.22	2.99	3.18
^{40}Ar/^{36}Ar	350	332	1250	896
Cosmogenic concentrations (10^{-8} cm^3 STP g^{-1})				
^{3}He$_{cos}$	27.4	30.7	22.0	22.8
^{21}Ne$_{cos}$	7.24	8.22	6.38	6.63
^{38}Ar$_{cos}$	1.26	1.22	1.02	1.24
Radiogenic concentrations (10^{-8} cm^3 STP g^{-1})				
^{4}He$_{rad}$	1650	1480	1360	1520
^{40}Ar$_{rad}$ = ^{40}Ar$_{meas}$	8094	7167	7480	7593

Ion counting errors, uncertainties of the blanks and of sample mass are about 0.1%. The uncertainty of the mass spectrometer sensitivity is <1% for ratios and <5% for concentrations.

AHS A100 L4 chondrite does not record any thermal event after its formation and early metamorphism on the parent body (Beard et al., 2013). These results are generally confirmed by Turrin et al. (2013).

Murty et al. (2010a) found that the N (and δ^{15}N) in the AHS 36 bulk sample and the AHS 44 acid residue are 21.1 ppm (−36.8‰) and 249.5 ppm (−74.3‰), respectively. They concluded that AHS 36 and 44 do not contain either an amorphous C phase with δ^{15}N ≥ 50‰ carrying noble gas, or a C phase carrying noble gases and N with δ^{15}N ≥ 153‰ combusting at <700 °C, both of which are observed in some other polymict ureilites. Feng et al. (2012) measured δ^{15}N = −24.9 ± 15‰ in sinoites from the EL3 fragment MS-17, which is similar to sinoite from an EL6 chondrite. They infer that this indicates no significant fractionation of N isotopes during thermal metamorphism.

5.4. Cosmic ray exposure ages

Cosmic ray exposure (CRE) ages were obtained for several ureilitic samples: AHS 36 (Murty et al., 2010a); AHS 4, 36, 44, and 47 (Welten et al., 2010a); AHS 1 and 47 (Ott et al., 2010), and two chondritic samples, AHS 25 and A100 (Meier et al., 2012; Table 7). For the ureilitic fragment AHS 36, Murty et al. (2010a) determined CRE ages of 13.8 and 16.0 Ma, based on ^{3}He and ^{21}Ne, respectively. Ott et al. (2010) came to a similar result and reported ^{21}Ne CRE ages of 13.2 and 14.2 Ma for the ureilitic samples AHS 1 and 47, respectively. Welten et al. (2010a) determined an average ^{21}Ne CRE age of 14.5 ± 0.9 Ma for four ureilite fragments, but they concluded that the ^{22}Ne/^{21}Ne ratio is not a reliable shielding indicator for large objects such as asteroid 2008 TC$_3$, so they also determined shielding-corrected CRE ages based on the ^{21}Ne/^{26}Al method. This

Table 7
Cosmic ray exposure ages [in Ma] of Almahata Sitta (AHS) samples.

Sample	T^{3}He	T^{21}Ne	T(^{21}Ne-^{26}Al)	T(^{38}Ar)$_{pre-exp}$	Class	Ref.
AHS 1		13.2			Ureilite	1
AHS 4a	12.9	13.9	19.3 ± 1.9		Ureilite	2
AHS 4b	12.9	14.0			Ureilite	2
ASH 25			21 ± 3	>16 ± 3	H5	3
AHS 36	14.1	13.3	18.0 ± 1.8		Ureilite	2
AHS 36	13.8	16.0			Ureilite	4
AHS 44	16.3	15.0	19.6 ± 2.0		Ureilite	2
AHS 47		14.2			Ureilite	1
AHS 47a	16.5	15.6			Ureilite	2
AHS 47b	16.7	15.1	21.1 ± 2.1		Ureilite	2
AHS A100			22 ± 4	>8 ± 2	L4	3

For details see [1]Ott et al. (2010), [2]Welten et al. (2010a,b), [3]Meier et al. (2012), and [4]Murty et al. (2010a,b).

Table 8
Data summary for cosmogenic radionuclides in three Almahata Sitta samples. For details see Bischoff et al. (2010b) and Taricco et al. (2010).

Radionuclide	Half-life	Activity concentrations in [dpm kg^{-1}]		
		MS-CH (5.1 g)	MS-D (8.65 g)	AHS 15
^{26}Al	717,000 years	57 (12)	75 (8)	62.1 ± 0.8
^{60}Co	5.2710 years	22 (5)	84 (6)	27.7 ± 0.8
^{54}Mn	312.13 days	114 (19)	134 (14)	83.5 ± 0.9
^{22}Na	2.6027 years	78 (15)	104 (12)	105.4 ± 1.0
^{46}Sc	83.788 days	19 (8)	<22	7.1 ± 1.0
^{57}Co	271.8 days	22 (10)	16 (3)	3.4 ± 0.5

approach yielded an average CRE age of 19.5 ± 2.5 Ma for the four ureilite fragments.

Meier et al. (2012) calculated ^{21}Ne/^{26}Al ages of 21–22 Ma for two chondritic fragments, AHS 25 and AHS A100. These ages overlap with the average CRE age of 19.5 ± 2.5 Ma for the ureilites obtained by Welten et al. (2010a). The ages of chondrites and ureilites are all within the same range and represent the transfer time of asteroid 2008 TC$_3$ from its parent body in the asteroid belt to Earth (~20 Ma). The CRE ages of the non-ureilite samples AHS A100 and 25 confirm the conclusions of Bischoff et al. (2010a) that the chondritic samples are "likely derived from the same parent body [asteroid 2008 TC$_3$] as the other AS [Almahata Sitta] meteorites, not representing a separate fall" (see also Section 5.5.2).

Meier et al. (2012) also report ^{38}Ar CRE ages for AHS 25 and 100 and find these to be higher than the ^{21}Ne/^{26}Al CRE ages. They conclude that both chondrites were pre-irradiated, prior to their last exposure to galactic cosmic rays as parts of asteroid 2008 TC$_3$. This scenario requires that they suffered cosmogenic He and Ne loss before (or during) incorporation into the ureilite host and were then shielded deep enough to avoid cosmic-ray exposure until the ejection of asteroid 2008 TC$_3$ from its parent asteroid ~20 Ma ago. Minimum pre-irradiation CRE ages were given as 16 ± 3 and 8 ± 2 Ma for AHS 100 and 25, respectively.

5.5. Terrestrial ages and cosmogenic radioisotopes

5.5.1. Terrestrial ages

The short-lived cosmogenic radioisotopes of two chondritic fragments (MS-CH, MS-D) were analyzed by means of γ-ray spectroscopy. The measured activity concentrations for the detected cosmogenic radionuclides (^{22}Na, ^{54}Mn, ^{46}Sc, ^{26}Al, ^{57}Co, ^{60}Co) are given in Table 8 (Bischoff et al., 2010a,b). These authors could show that the detection of ^{46}Sc (half life: 83.8 days [d]) in MS-CH, and ^{54}Mn (half life: 312.2 d) and ^{57}Co (half life: 271.8 d) in both samples clearly indicates that these fragments result from a very recent meteorite fall consistent with the Almahata Sitta event. In particular, the value for ^{46}Sc in MS-CH (see also Horstmann et al., 2010) clearly indicates that this fragment results from a very recent meteorite fall, about 335–420 d prior to the measurement. Bischoff et al. (2010b) state that for the sample MS-D one can give only a much weaker estimate of the date of fall, using the ^{57}Co and the ^{54}Mn data, resulting in a range of 300–600 d. Taricco et al. (2010) studied the radioisotopes of the ureilite AHS 15 (Shaddad et al., 2010), and measured the activities of the short-lived nuclides ^{22}Na, ^{54}Mn, ^{46}Sc, ^{26}Al, ^{57}Co, ^{60}Co (Table 8). The cosmogenic nuclides of a 37 g piece of MS-181 were also determined by Bischoff et al. (2012) and the detection of ^{54}Mn (halflife: 312.14 d), ^{22}Na (2.602 years), and ^{60}Co (5.27 years) is also characterizing this carbonaceous sample as a fresh meteorite fall consistent with the asteroid 2008 TC$_3$-Almahata-Sitta event from October 2008.

These data convincingly demonstrate that the ureilitic and the various different groups of chondritic samples all belong to the same meteoroid impacting Earth over Sudan, which was also inferred from the cosmogenic noble gases and radionuclides (Section 5.4).

Table 9
Concentrations of cosmogenic ^{10}Be, ^{26}Al, and ^{36}Cl (in dpm kg^{-1}) in Almahata Sitta (AHS) ureilites (Welten et al., 2010a) and chondrites (#, Meier et al., 2012). The last column shows normalized ^{36}Cl concentrations (in dpm kg^{-1} [Fe*]), in which Fe* = Fe + 12Ca. For details see Welten et al. (2010a).

Sample	^{10}Be	^{26}Al	^{36}Cl	Fe*	^{36}Cl*
AHS 1	19.0 ± 0.4	43.8 ± 0.9	5.9 ± 0.2	31.8	18.6 ± 0.6
AHS 4	22.5 ± 0.9	56.6 ± 1.9	5.4 ± 0.1	30.3	17.8 ± 0.4
AHS 15	19.6 ± 0.4	60.0 ± 2.0	15.3 ± 0.5	84.2	18.2 ± 0.6
AHS 25#	17.1 ± 0.5	55.0 ± 2.4	9.2 ± 0.2		
AHS 36	21.9 ± 0.4	55.1 ± 2.3	3.6 ± 0.1	21.0	17.3 ± 0.5
AHS 44	21.4 ± 0.4	49.0 ± 1.9	6.1 ± 0.1	35.4	17.2 ± 0.4
AHS 47	24.1 ± 0.9	55.8 ± 1.6	5.6 ± 0.1	27.7	20.1 ± 0.5
AHS 100#	20.5 ± 0.6	63.7 ± 2.4	11.2 ± 0.2		

5.5.2. Radionuclides

Welten et al. (2010a,b) measured the ^{10}Be, ^{26}Al, and ^{36}Cl concentrations in six ureilite fragments from Almahata Sitta (Table 9). They found ^{10}Be concentrations of 19–24 dpm kg^{-1}, and concluded that these variations are due to variations in shielding as well as in bulk carbon, which is a major target element for ^{10}Be production. The ^{36}Cl concentrations, which vary from 3.6 to 15.3 dpm kg^{-1}, show a strong correlation with the bulk concentrations of Fe and Ca, the two major target elements for ^{36}Cl production. After normalizing for variations in bulk Fe and Ca, the six samples show a relatively constant ^{36}Cl concentration of 18.2 ± 1.1 dpm kg[Fe + 12Ca]$^{-1}$. The ^{26}Al concentrations vary from 44 to 60 dpm kg^{-1} and are negatively correlated with the ^{22}Ne/^{21}Ne shielding parameter, indicating that AHS 1 and AHS 44 represent samples from near the pre-atmospheric surface, while AHS 4, 15, 36, and 47 represent samples from greater shielding depth. The combined radionuclide data are best explained by irradiation in an object with an effective radius of approximately 300 g cm^{-2}. Assuming an absolute pre-atmospheric radius of 180 cm for asteroid 2008 TC$_3$ (Scheirich et al., 2010), this radius corresponds to a density of 1.66 g cm^{-2}. This is also concluded by Meier et al. (2012) when analyzing AHS 25 and A100, reporting similar results as Welten et al. (2011). Meier et al. (2012) report ^{10}Be, ^{26}Al, and ^{36}Cl activities near equilibrium values for moderately shielded ordinary chondrites (Table 9). Hence, this also confirms the suggestion of Bischoff et al. (2010a,b) that the chondritic lithologies represent xenolithic clasts of the asteroid 2008 TC$_3$. Note, however, that there is still a chance that some of the collected non-ureilitic fragments for which no terrestrial or cosmic ray exposure ages exist may derive from earlier (though still recent) falls.

Based on the activities of ^{60}Co and ^{26}Al in AHS 15, Taricco et al. (2010) calculated that the sample was located at a depth of 41 ± 14 cm inside the asteroid with a 1.5–2 m radius.

Table 10
Cr isotopic compositions of Almahata Sitta (AHS) fragments. For details see Qin et al. (2010b).

Sample	ε^{53}Cr	ε^{54}Cr	^{55}Mn/^{52}Cr
AHS 4	0.22 ± 0.06	−0.72 ± 0.11	0.729
AHS 4 Magnetic	0.41 ± 0.08	−1.86 ± 0.20	1.41
AHS 15	0.26 ± 0.05	−0.76 ± 0.14	0.591
AHS 27	0.18 ± 0.04	−0.81 ± 0.18	0.572
AHS 27 Magnetic	0.20 ± 0.09	−0.80 ± 0.19	0.811
AHS 36	0.31 ± 0.04	−0.69 ± 0.07	0.847
AHS 36 Magnetic	0.33 ± 0.07	−0.80 ± 0.20	1.23
AHS 44	0.15 ± 0.03	−0.80 ± 0.10	0.561
AHS 47	0.18 ± 0.05	−0.78 ± 0.08	0.548
AHS 47 Magnetic	0.21 ± 0.07	−0.75 ± 0.26	0.725
AHS 49	0.19 ± 0.05	−0.79 ± 0.13	0.591
AHS 51 Magnetic	0.23 ± 0.06	−0.85 ± 0.20	1.06
AHS 54	0.34 ± 0.04	−0.67 ± 0.12	1.20
Average		−0.77 ± 0.10	

5.6. Other isotopes

Nine ureilitic fragments were studied for their Cr isotope compositions (Qin et al., 2010a,b; Table 10). Qin et al. (2010b) found that all samples essentially show the same ε^{54}Cr deficit relative to the terrestrial Cr standard, which contrasts with the positive ^{54}Cr anomalies observed for carbonaceous chondrites. A positive correlation between the oxygen isotope composition (Δ^{17}O) and the ε^{54}Cr has been proposed for carbonaceous chondrites (e.g., Trinquier et al., 2007; Yin et al., 2009). Carbonaceous chondrites have been suggested as ureilite precursor material, but Qin et al. (2010a,b) proposed that the Cr isotope compositions of Almahata Sitta samples indicate that the ureilite precursor material was distinct from known carbonaceous chondrites. Instead, the ε^{54}Cr value is similar to that of the HED parent body, suggesting that their precursors may have accreted in a similar nebula region/environment. Additionally, these authors propose that variations of ε^{53}Cr presumably reflect live ^{53}Mn at the time of last isotopic equilibration.

Qin et al. (2010b) also studied the Mn/Cr-systematics and found that the samples are showing resolvable variations in ε^{53}Cr correlated with Mn/Cr ratios which suggest that ^{53}Mn was still alive at the time of the formation of Almahata Sitta constituents. They report an initial ^{53}Mn/^{55}Mn value of 3.1 (±1.1) × 10^{-6}, corresponding to an age of 4563.6 ± (2.2) Ma. Similar ages were obtained for fragments in polymict ureilites (Goodrich et al., 2010b).

Within the EL3 fragment MS-17, Lin et al. (2011) report the identification of several lawrencite grains with significant excesses of ^{36}S having large inferred ^{36}Cl/^{35}Cl ratios of 0.92×10^{-4}–1.42×10^{-4}. Further data are presented by Feng et al. (2012), who noted that "the higher the Cl/S ratios of lawrencite, the lower inferred ^{36}Cl/^{35}Cl ratios".

5.7. Organic components

Glavin et al. (2010a,b) carried out analyses of extraterrestrial amino acids in fragment AHS 4 (Table 11). These revealed a complex distribution of two- to seven-carbon aliphatic amino acids and one- to three-carbon amines with abundances ranging from 0.5 to 149 ppb. Glavin et al. (2010b) clearly found that "the enantiometric ratios of the amino acids alanine, β-amino-*n*-butyric acid, 2-amino-2-methylbutanoic acid (isovaline), and 2-aminopentanoic acid (norvaline) in the meteorite were racemic (D/L ~1), indicating that these amino acids are indigenous to the meteorite and not terrestrial contaminants".

Burton et al. (2011a,b) determined the amino acids of fragments AHS 25 and 27 (Table 11). While AHS 27 is a ureilitic sample, AHS 25 is a H5 chondrite. All samples contain amino acids. They found the 4-carbon (C_4) amino acids β-aminobutyric acid (β-ABA) and α-aminoisobutyric acid to be present in 1.5-fold or greater abundances in the meteorite samples compared to the sand sample of the strewn field. They also identified other indigenous 5-carbon (C_5) amino acids including isovaline, 3-aminopentanoic acid, 3-amino-2,2-dimethylpropanoic acid, 4-amino-2-methylbutanoic acid, and 4-amino-3methylbutanoic acid. An interesting point concerning the C_5 amino acid data is the distribution of amine positions among the different meteorites (i.e., α, β, γ or δ) leading to the conclusion that the variable acid compositions between the ureilitic fragments may argue for the presence of more than one parent ureilite in asteroid 2008 TC_3 (Burton et al., 2011a). Burton et al. (2011b) summarized that despite the genetic (?) differences of fragments AHS 25 (H5) and AHS 27 (ureilite), similar amino acid compositions were obtained; on the other hand, in the two ureilitic samples AHS 4 and AHS 27 the distribution of amino acids was distinct. For Burton et al. (2011b) the discovery of this concentration of amino acids in fragment AHS 4 was unexpected, because "the high temperatures experienced by the ureilites were more than sufficient to destroy any amino acids that were present".

Polycyclic aromatic hydrocarbons (PAHs) were studied in ureilitic fragments AHS 1, 4, 7, 15, 27, and 47 and chondritic fragments AHS 25 (H5), 16 (EL6), and 41 (EH5 or 6) (Sabbah et al., 2010). They detected numerous organic compounds with a PAH signature (Fig. 14). Interestingly, the chondritic samples show similar distributions of PAHs compared with the ureilitic fragments. Therefore, they concluded that the chondritic and ureilitic fragments derived from the same asteroid (2008 TC_3) and that the organic compounds, originally contained within the ureilite portions, could have spread out into other (foreign) constituents of the parent body. This conclusion is very similar to that of Meier et al. (2012) that the ureilitic Ar component was incorporated into the xenolithic chondrite samples.

6. Physical properties of individual samples

6.1. Spectroscopic features

Comparison of the reflectance spectra of Almahata Sitta samples and asteroid 2008 TC_3 indicate that they both classify as F-class (Jenniskens et al., 2009b; note that only one spectrum of poor quality was obtained). However, based on the classification scheme of Tholen (1989), ureilites were thought to derive from S-type asteroids (Gaffey et al., 1993). According to Jenniskens et al. (2009b), F-type asteroids, constituting only ~1.3% of the asteroid population, can now firmly be linked to anomalous ureilitic material due to the present results. Cloutis et al. (2010) mentioned a major spectral difference between asteroid 2008 TC_3/Almahata Sitta and typical ureilite spectra they obtained. They found a reflectance downturn short of approximately 0.5 μm, which was not seen in the spectrum of 2008 TC_3 and in the published spectrum of sample AHS 7 (Jenniskens et al., 2009b).

Sandford et al. (2010a,b,c) performed infrared spectroscopy of samples of multiple rocks from Almahata Sitta and identified substantial variation of olivine and pyroxene abundances among these samples (Fig. 15). Based on the analyses of 26 ureilitic samples an olivine:pyroxene ratio of 74:26 was found. This is in the middle of the range of other ureilites, which generally are heterogeneous concerning the modal abundances of olivine and pyroxene. They also found, despite the ureilitic spectra showing features characteristic of olivine and pyroxene, one unique spectrum belonging to sample AHS 15 (subsample 15#2; Fig. 15d). It yielded a pyroxene spectrum most consistent with assignment to enstatite. However, AHS 15 is a ureilite (Table 2), the pyroxene has ~$Fs_{16}Wo_5$ (different from pure enstatite and typical E chondrite pyroxene) and, consequently, the spectrum does not indicate enstatite chondritic material.

Table 11
Concentrations of amine components in Almahata Sitta (AHS) ureilites (AHS 4, AHS 27) and the H5 chondrite AHS 25. For details see Glavin et al. (2010b) and Burton et al. (2011b).

Amine compound	AHS 4 ureilite		AHS 25 H5		AHS 27 ureilite	
	Free (ppb)	Total (ppb)	Free (ppb)	Total (ppb)	Free (ppb)	Total (ppb)
Amino acids						
D-Aspartic acid	1.2 ± 0.2	3.0 ± 0.2	<1	<3	0.4 ± 0.2	<3
L-Aspartic acid	1.4 ± 0.3	5.0 ± 1.5	<1	<9	2.0 ± 1.8	3.8 ± 1
D-Glutamic acid	0.5 ± 0.1	3.5 ± 0.4	<0.1	2.3 ± 0.6	n.d.	1.9 ± 0.6
L-Glutamic acid	0.9 ± 0.2	7.7 ± 0.7	1.2 ± 0.4	13 ± 3	1.0 ± 0.4	7.8 ± 0.9
D-Serine	<0.5	<1.3	0.7 ± 0.2	2.7 ± 0.3	0.4 ± 0.1	1.3 ± 0.1
L-Serine	<1.6	<1.4	0.7 ± 0.3	12 ± 1.3	2.7 ± 0.5	6.7 ± 0.8
D-theorine	<0.8	<1.3	<0.1	<0.1	<0.1	<0.1
D-theorine	<0.8	<1.5	<0.1	<0.1	<0.1	<0.1
Glycine	21 ± 1	69 ± 24	65 ± 7	83 ± 10	64 ± 3	64 ± 10
BALA	4.2 ± 0.7	17 ± 7				
GABA	1.8 ± 0.3	12 ± 1	0.9 ± 0.7	18 ± 2	5.9 ± 3.6	9.2 ± 1.4
D-Alanine	5.0 ± 0.2	11 ± 3	10 ± 1	13 ± 2	13 ± 1	13 ± 2
L-Alanine	5.1 ± 0.2	11 ± 2	16 ± 2	20 ± 2	22 ± 8	19 ± 2
D-β-ABA	1.2 ± 0.2	4.5 ± 1.4	<1	1.0 ± 0.1	0.5 ± 0.1	1.0 ± 0.2
L-β-ABA	1.2 ± 0.8	4.7 ± 1.3	0.2 ± 0.1	0.8 ± 0.2	0.5 ± 0.1	0.9 ± 0.3
α-AIB	3.6 ± 1.0	7.1 ± 5.8	5.7 ± 0.5	2.9 ± 0.3	4.5 ± 0.7	1.8 ± 0.6
D,L-α-ABA	1.7 ± 0.1	5.0 ± 0.5	0.8 ± 0.1	1.9 ± 0.4	0.8 ± 0.2	1.1 ± 0.2
EACA	3.6 ± 1.8	<4	2.8 ± 0.9	30 ± 5	6.5 ± 2.7	35 ± 4
C_5 amino acid detected						
α						
D-norvaline (D-2-apa)	<0.3	0.7 ± 0.1	<0.1	<0.8	<0.1	<0.7
L-norvaline (L-2-apa)	<0.2	0.7 ± 0.1	<0.1	<0.9	<0.1	<0.7
D-isovaline (D-2-a-2-mba)	0.6 ± 0.1	1.3 ± 0.1	0.4	1.2 ± 0.1	0.5 ± 0.4	0.5 ± 0.2
L-isovaline (L-2-a-2-mba)	0.7 ± 0.1	1.4 ± 0.1	<0.1	1.5 ± 0.1	1.2 ± 0.7	1.2 ± 0.2
D-valine (D-2-a-3-mba)	0.3 ± 0.1	0.5 ± 0.1	<0.1	0.3 ± 0.1	0.2 ± 0.1	0.3 ± 0.2
L-valine (L-2-a-3-mba)	1.4 ± 0.3	1.3 ± 0.5	6.3 ± 1.0	12 ± 2	5.7 ± 1.0	11 ± 4
β						
D,L-3-apa	0.4 ± 0.1	1.1 ± 0.2	<0.1	<0.1	0.5 ± 0.4	0.5 ± 0.2
D,L- and allo-3-a-2-mba	<0.1	<0.1	<0.1	0.3 ± 0.1	<0.1	0.2 ± 0.1
3-a-3-mba	<0.4	<3	<0.1	<0.1	<0.1	<0.1
3-a-2,2-dmpa	0.8 ± 0.1	1.8 ± 0.2	<3	5.0 ± 0.4	<3	3.4 ± 0.2
D,L-3-a-2-epa	<0.8	<2	<0.1	<0.1	<0.1	<0.1
γ						
D,L-4-apa	0.8 ± 0.1	15 ± 2	<0.1	<0.6	<0.2	<0.6
D,L-4-a-2-mba	2.6 ± 0.2	65 ± 8	<0.1	0.7 ± 0.3	<0.1	1.2 ± 0.6
D,L-4-a-3-mba	1.5 ± 0.2	18 ± 3	<0.7	3.1 ± 0.1	<0.7	3.1 ± 0.1
δ						
5-apa	0.9 ± 0.1	6.3 ± 2.1	<0.2	2.1 ± 0.1	<0.2	2.1 ± 0.1
Total C_5 amino acids	10 ± 2	113 ± 17	10 ± 1	25 ± 4	11 ± 2	25 ± 5
Total amino acids	62 ± 9	274 ± 66	127 ± 8	262 ± 12	146 ± 10	215 ± 12
Amines						
Ethanolamine	19 ± 1	21 ± 1				
Methylamine	11 ± 1	13 ± 1				
Ethylamine	76 ± 5	105 ± 8				
Isopropylamine	84 ± 10	149 ± 17				
Total amines	190 ± 17	288 ± 27				

Hiroi et al. (2010a,b) performed reflectance spectroscopy of eleven Almahata Sitta meteorite samples in order to investigate possible compositional variations among the samples as well as the degrees of terrestrial weathering. They found, like Sandford et al. (2010a,b,c), differences in olivine and pyroxene contents among the samples overall indicating ureilitic compositions. Hiroi et al. (2010a) could clearly show that the spectrum of sample AHS 25 is similar to that of the H chondrite Ochansk (Fig. 16). One ureilitic sample (AHS 51) shows relatively narrow absorption bands at ~0.5 and 1.9 μm in bidirectional visible-near infrared spectra. Also, considering the strong 3 μm hydroxyl band in the Fourier transform infrared reflectance spectrum, Hiroi et al. (2010a) suggest that these features would result from terrestrial weathering. Taking results from analyzing asteroid 2008 TC_3 into account, Hiroi et al. (2010b) suggest that most Almahata Sitta samples recovered would be similar in textures and albedo to the studied samples AHS 27, AHS 4, and AHS 47. Their conclusion is based on the results of linear least-square fits of the asteroid 2008 TC_3 spectrum with two sets of the meteorite spectra: the asteroid must have had an albedo of 0.10–0.12 and no fine regolith on its surface. Note that the average albedo of asteroid 2008 TC_3 is an important parameter, since both the absolute size, as well as the density and porosity are based on it (see Section 6.3).

6.2. Raman spectroscopic features

Kaliwoda et al. (2011a,b, 2013) used Raman spectroscopy to identify minerals in unspecified Almahata Sitta samples. They found graphite, diamond, graphene, suessite, schreibersite, cohenite, kamacite, (Cr-bearing) troilite, pyroxene, plagioclase, and olivine. Based on the finding of diamond we suggest that these authors studied (mainly) ureilitic fragments.

6.3. Density of meteorite fragments and asteroid 2008 TC_3

Densities of several individual Almahata Sitta stones were determined to constrain physical properties (mass, porosity) and, hence, the internal structure of asteroid 2008 TC_3. A bulk density of about 3 g/cm^3 for individual meteorite fragments and a grain density of about 3.9 g/cm^3 were determined by Kohout et al. (2010a,b), which

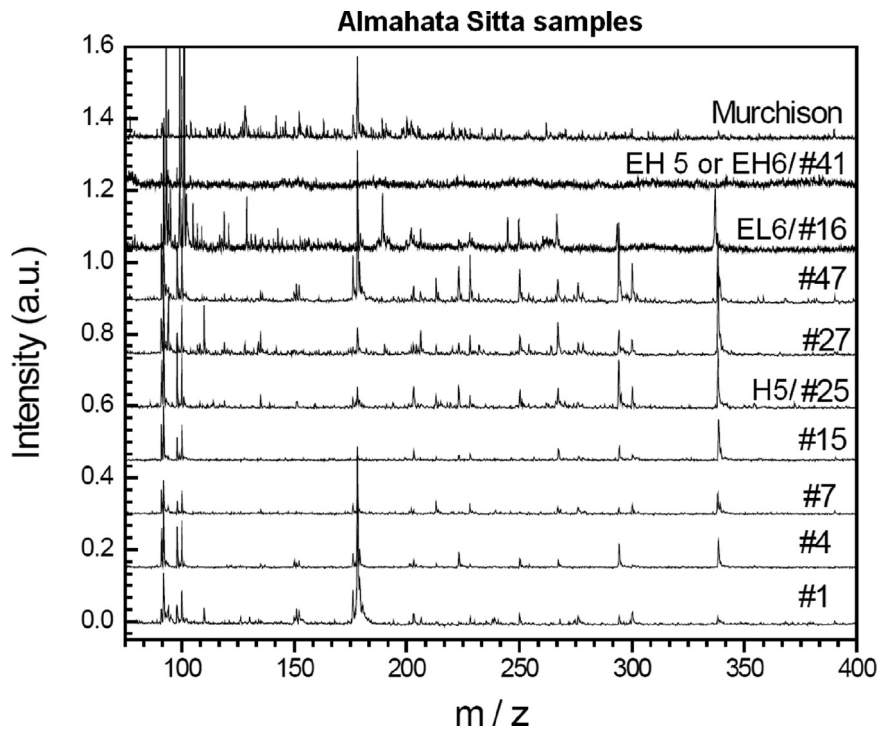

Fig. 14. Laser desorption laser ionization mass spectra of PAHs in nine samples from Almahata Sitta and Murchison. For details see Sabbah et al. (2010); Figure after Sabbah et al. (2010).

results in a higher microporosity estimate of about 20% for Almahata Sitta compared to other ureilites.

Fragment AHS 7 shows porosity ranging from 10 to 25% (Jenniskens et al., 2009b). The average porosity among the different Almahata Sitta specimens varies from fragment to fragment according to the bulk density. With an average ureilite grain density of 3.35 g/cm^3, the calculated Almahata Sitta porosity ranges from 25 to 37% (Jenniskens et al., 2009b) in comparison to an average microporosity of 9% (range 6–20%) in other ureilites (Britt and Consolmagno, 2003).

Kiuru et al. (2011) and Kohout et al. (2011) obtained bulk densities of different Almahata Sitta ureilites in the range of 2.9–3.3 g/cm^3 (average 3.1 g/cm^3, equivalent to the upper limit for the bulk density of asteroid 2008 TC_3), which are higher than those reported by Jenniskens et al. (2009b), but similar to values reported from other ureilites (Consolmagno et al., 2008; Macke et al., 2011). Kohout et al. (2011) determined a grain density of 3.5 g/cm^3 for AHS 15, which translates into a microporosity of 6%, given its bulk density of 3.3 g/cm^3.

Estimates of the total mass of asteroid 2008 TC_3 range from 8 to 27 t (Kohout et al., 2011) to ~60–100 t (Jenniskens et al., 2009b). This wide mass range is mainly due to the uncertainty in the absolute size (volume) of this asteroid, which is not well known, even though its absolute magnitude (Jenniskens et al., 2009a,b) and irregular shape are relatively well constrained (Scheirich et al., 2010). However, the latter authors showed that the total volume, mass and porosity are all strongly dependent on the average albedo of asteroid 2008 TC_3 (Fig. 17). This value is not known from the observations of asteroid 2008 TC_3 before its impact, but can only be estimated from albedo measurements of the surviving meteorites (which may not necessarily be representative for the asteroid itself). While the average albedo of F-type asteroids is ~0.05, the measured albedo of the Almahata Sitta meteorites ranges from 0.046 to 0.12 for the ureilite fragments (Jenniskens et al., 2009a,b; Hiroi et al., 2010a,b) to 0.23 for one of the chondrites (Hiroi et al., 2010a,b). Welten et al. (2010a,b) showed that the cosmogenic radionuclides yield one additional size constraint, i.e., an average (radius × density) of 300 ± 30 g/cm^2. Assuming an asteroid volume of 25 m^3 (corresponding to an albedo of ~0.05), they constrained the total mass of asteroid 2008 TC_3 to 41 ± 8 t, corresponding to a bulk density of 1.66 ± 0.25 g/cm^3 and a total porosity of 50 ± 7%, respectively. However, it should be noted that an average albedo of 0.10 (instead of 0.05) would yield a volume of 8.6 m^3, corresponding to a mass of 20 t, a bulk density of 2.4 g/cm^3 and a porosity of 30 ± 5%.

Using the average meteorite density of 3.1 g/cm^3, albedo estimates of 0.09–0.2 by Hiroi et al. (2010a), the shape model of Scheirich et al. (2010), and assuming macroporosities of 20–50%, Kohout et al. (2011) estimate a mass range of 8–27 t, but presume that it was probably below 20 t based on its albedo and macroporosity of about 50%. These values are generally lower than values of 83 ± 25 t and 35–65 t, reported by Jenniskens et al. (2009b) and Borovička and Charvát (2008), respectively. However, they are consistent with the estimates by Welten et al. (2011) if we adopt an albedo of 0.10 for asteroid 2008 TC_3 instead of the initial value of ~0.05 proposed by Jenniskens et al. (2009a,b) and Scheirich et al. (2010).

6.4. Magnetic characteristics

Hoffmann et al. (2010, 2011a,b) studied magnetism and opaque mineralogy of AHS 4 and 39 (both coarse-grained ureilites, Table 2). They found a variety of magnetic phases including kamacite(s) (low-Ni), troilite, daubreelite (-like phase), suessite, and most likely schreibersite. The natural magnetic remanence is 15.4 and 2.99×10^{-3} Am^2 kg^{-1}; the isothermal magnetic remanence is 1.67 and 1.57×10^{-1} Am^2 kg^{-1} for AHS 4 and 39, respectively. Magnetic susceptibility values were given as log χ 4.84 and 4.93×10^{-9} kg m^{-3}, respectively. Hoffmann et al. (2011a) additionally gave values of 4.92 and 4.98×10^{-1} Am^2 kg^{-1} for small subsamples of AHS 4 and 39, respectively. They concluded that the magnetic fabric observed is most probably impact related, as the

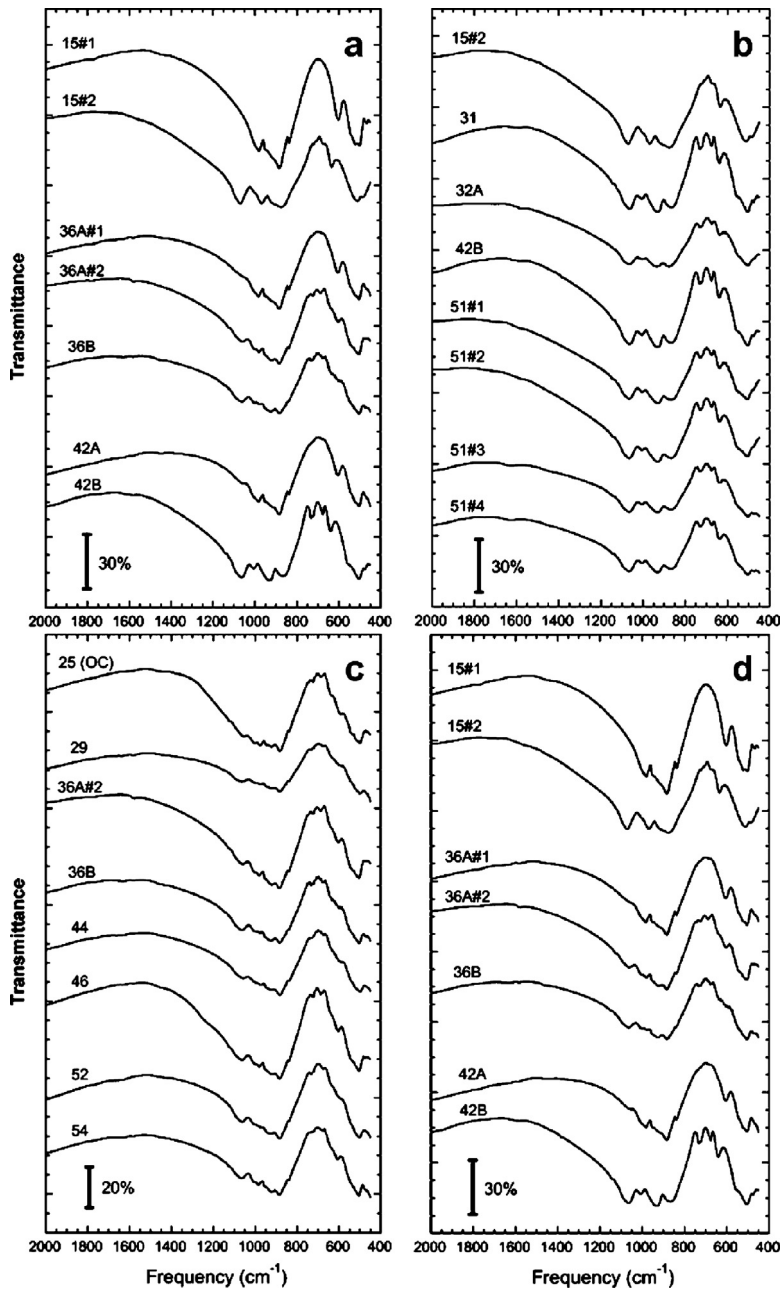

Fig. 15. The 2000–450 cm^{-1} (5.0–22.2) infrared transmission spectra of (a) olivine-dominated, (b) pyroxene-dominated, (c) pyroxene- and olivine-rich fragments from Almahata Sitta. (d) Spectra of these three rocks show dramatic variations, clearly indicating portions with significant differences in mineralogy. See original figures and details in Sandford et al. (2010b).

anisotropy of magnetic susceptibility is an indicator for the degree of shock. However, it is, e.g., also influenced by grain shapes, thus being no unequivocal proof for an impact relation. They report P values (degree of anisotropy) of 1.315 and 1.531 for AHS 4 and 39, respectively, which are significantly higher than those of HED and Martian meteorites. Magnetic hysteresis data show complex magnetization behavior for AHS 4, indicating strong magnetic interactions, and normal hysteresis for AHS 39. They identified four magnetic components based on isothermal magnetic remanence, pointing to a multi-domain phase (presumably kamacite), suessite/kamacite in micron-sized particles, and intergrown magnetic phases such as daubreelite-troilite-kamacite. Low-Ni kamacite, two populations of kamacite with slightly different Ni- and Si-contents, suessite-like phases, probably schreibersite, and a probable Fe-oxy-hydroxide as a terrestrial alteration product were identified using low and high field thermomagnetic runs in air and Ar on AHS 4 and 39. The magnetic record of AHS 4 and 39 is dominated by kamacite. More precisely, Hoffmann and co-workers concluded that the induced magnetization of AHS 4 is dominated by coarse-grained kamacite and probably minor cohenite and/or suessite similar to AHS 39. The (paleo-)magnetic record of the latter, however, is characterized by fine-grained kamacite and some contribution from suessite, cohenite, and schreibersite. Additionally, there are indications for the presence of daubreelite-heideite-like phases as a Fe-Cr sulfide phase intergrown with troilite. Daubreelite has been reported from ureilites before. Hoffmann et al. (2010, 2011a) concluded that the observed (paleo-)magnetic signature of Almahata Sitta is undoubtedly extraterrestrial and most probably represents a ureilite parent body magnetic record.

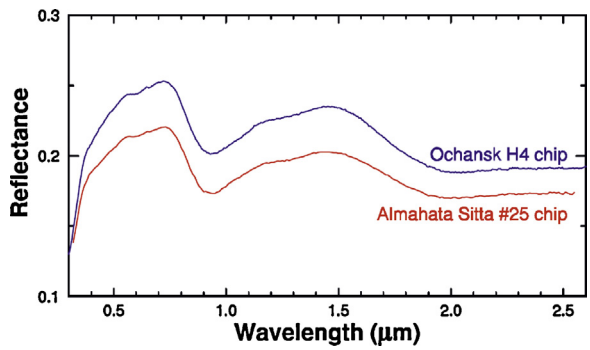

Fig. 16. Comparison of the visible-near infrared reflectance spectra of Almahata Sitta sample AHS 25 and the H4 chondrite Ochansk (modified after Hiroi et al., 2010a).

Kohout et al. (2010a) found magnetic susceptibilities for many Almahata Sitta samples in the narrow range of $4.96 \pm 0.12 \log 10^{-9}\,Am^2\,kg^{-1}$ identical to the range of other ureilite falls with $4.95 \pm 0.14 \log 10^{-9}\,Am^2\,kg^{-1}$ (Table 12). Kohout et al. (2010b) report similar values based on analyzing a total of 62 samples, and distinguished three groups based on magnetic susceptibility. The first group (a total of 15 samples found in the first four months after the fall and prior to rain exposure) gave $4.92 \pm 0.08 \log 10^{-9}\,Am^2\,kg^{-1}$ for samples with ureilite appearance (7 rocks). The ureilitic samples (7 out of 13 rocks) of the second group (samples collected one year after the fall) gave $4.90 \pm 0.06 \log 10^{-9}\,Am^2\,kg^{-1}$, indicating no severe effect of terrestrial weathering. The remaining samples in both groups deviate and are non-ureilitic in appearance. The third group comprised all small meteorites collected in the tail of the strewn field, giving an average of $4.97 \pm 0.34 \log 10^{-9}\,Am^2\,kg^{-1}$ for all samples, and $4.89 \pm 0.20 \log 10^{-9}\,Am^2\,kg^{-1}$ excluding those with high susceptibilities. The large number of samples with anomalously high susceptibilities and distinct textural appearance [about half of all samples analyzed by Kohout et al. (2010b)] mostly belong to ordinary and E chondrites. Most of these have fresh appearances and susceptibilities similar to other fresh meteorites from their respective class (ureilites, E chondrites, ordinary chondrites), pointing to a common impact origin with the ureilites. AHS 33 shows an unusual susceptibility ($5.7 \log 10^{-9}\,Am^2\,kg^{-1}$), which can be attributed to it being a ureilite with a shock melt-produced metal-sulfide assemblage. Several other samples showing unusual susceptibility values (Table 12) are, e.g., AHS 14 and S194 with values in the range of ureilites and H chondrites, and H or E chondrites, respectively. The very small samples (<5 g) show a large scatter of susceptibility data and thus reveal lithological inhomogeneity within asteroid 2008 TC_3 materials below a fragment size of 1–3 cm, due to both various ureilitic and non-ureilitic materials. However, some of this inhomogeneity may result from slight terrestrial weathering. Kohout et al. (2010a) concluded that "asteroid 2008 TC_3 may represent a compositionally heterogeneous body composed of ureilites with mix of chondrite materials and most likely an assemblage of material left after the catastrophic collision between ureilite and chondrite parent bodies".

Hoffmann et al. (2012a) examined the magnetic signatures of two samples from MS-150. They found that the MS-150 samples (EL6 IMR) show significantly lower magnetic susceptibility values than the average of all EL6 chondrite falls with a value of $5.46 \times 10^{-9}\,m^3\,kg^{-1}$, which might be the result of terrestrial oxidation. The room temperature properties of MS-150 can be attributed to a near-kamacite phase and cohenite. The origin of a ~120 °C phase is not clear, but daubreelite was found at low-T of ~−150 °C. The isothermal magnetic remanence of MS-150 is higher than that of Neuschwanstein (EL6), the reason for which is also unclear but might originate from differences in metal content or shock stage.

A rock magnetic and paleomagnetic characterization of AHS 22 and 27 revealed the presence of kamacite as the dominant magnetic mineral, although heating curves indicate various Ni contents in metal (Kohout et al., 2010b). Furthermore, indications for minor Ni-free metal, minor cohenite, and large multi-domain kamacite grains were found. The frequency and field amplitude dependence of the magnetic susceptibility was measured for AHS 99, S127, and S129, and turned out to be low, in agreement with previous data on ureilites.

6.5. Other physical properties

Fragment AHS 7 was broken to obtain a fresh surface to determine a tensile strength of only 56 ± 26 MPa (Jenniskens et al., 2009b), which is significantly higher than the tensile strength inferred for the asteroid from the atmospheric break-up estimated as 0.2–0.3 MPa (Popova et al., 2011). This clearly illustrates the weak welding of asteroid 2008 TC_3 compared with fragments from well consolidated lithologies.

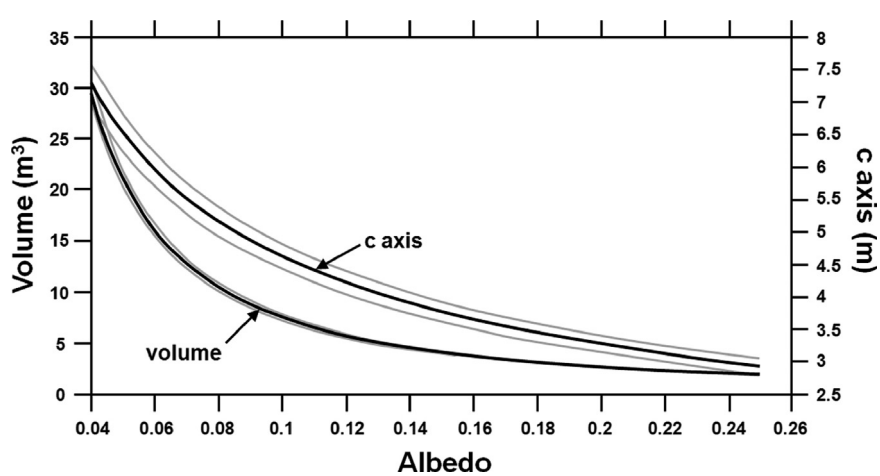

Fig. 17. Volume and the largest axis of the asteroid 2008 TC_3 shape model (3σ errors are indicated by gray lines) as a function of the surface geometric albedo. Modified after Scheirich et al. (2010).

Table 12
List of all Almahata Sitta (AHS) meteorite samples measured for their magnetic susceptibility (given as logarithm) and mass. Anomalous (most likely non-ureilitic) samples are distinguished by difference with typical ureilite values or by their anomalous appearance. For details, see Kohout et al. (2010b).

AHS	Log χ (in 10^{-9} Am^2 kg^{-1})	Mass (g)	Anomalous susceptibility	AHS	Log χ (in 10^{-9} Am^2 kg^{-1})	Mass (g)	Anomalous susceptibility
14	5.21	152.58	X	721	5.13	0.78	
16	5.38	171.08	X	722	4.60	0.99	
25	5.30	190.7	X	723	4.98	2.51	
33	5.69	9.2	X	724	5.39	2.59	X
41	5.47	49.1	X	725	5.37	0.30	X
82	5.02	10.3		726	5.19	0.39	
87	5.55	10.3	X	727	4.93	0.30	
99	4.93	7.8		1104	4.47	1.07	X
S127	4.90	20.6		1105	5.35	0.43	X
S129	5.08	9.3		1106	5.37	0.30	X
S138	4.79	35		1107	5.50	1.82	X
S164	4.95	28.8		1109	4.39	1.82	X
S194	5.43	82.4	X	1110A	4.45	6.88	X
S195	4.91	28.9		1110B	4.40	0.73	X
S195A	4.92	24.9		1111	5.57	0.46	X
603	4.94	17.3		1112	4.69	2.38	
607	4.97	20.9		1113	4.74	3.74	
1001	5.65	48.5	X	1114	5.02	0.38	
1003	4.84	10.8		1115	4.88	1.37	
1004	4.81	13.5		1116	4.63	1.79	
1005	5.39	21.3	X	1118	4.76	0.92	
1006	4.87	12.3		1119	5.30	0.82	
1007	5.32	23.5	X	1120	5.17	1.11	
1008	5.55	23.6	X	1213	5.14	0.77	
1009	5.67	13.8	X	1214	4.82	0.87	
1010	4.94	23.7		1215	5.51	0.44	X
1011	5.66	22	X	1216	4.83	0.70	
1012	4.94	28.7		1217	4.87	2.39	
716	4.94	0.89		1219	4.84	1.88	
717	4.68	1.05		1220	4.88	1.57	
720	5.44	0.36	X	1221	4.61	2.17	

7. Discussion

7.1. Ureilite formation and evolution – further insights from Almahata Sitta

Ureilites comprise the second largest group of differentiated meteorites (337 rocks, uncorrected for pairings) after the HEDs (1215 rocks; *Meteorit. Bull. Database*, 08/26/2013). They are typically ultramafic rocks dominated by olivine and pyroxene, and the majority is unbrecciated (monomict), showing coarse-grained igneous textures (e.g., Mittlefehldt et al., 1998; Goodrich et al., 2004, and references therein). Furthermore, several polymict ureilites containing foreign (chondritic) fragments are known (e.g., Goodrich et al., 2004; Downes et al., 2008; see also Section 7.2). Ureilites lack feldspar, which is only rarely found in ureilitic breccias (e.g., Cohen et al., 2004; Goodrich et al., 2004; Bischoff et al., 2006). The average carbon content is ~3 wt%, although individual ureilites show carbon contents ranging from ~0 to 7 wt% (e.g., Mittlefehldt et al., 1998; Goodrich et al., 2004). Olivine typically has reduced, Mg-rich rims, and is sprinkled with numerous tiny metal grains thought to have formed via smelting (carbon-redox controlled reduction). Ureilites are in several aspects a somewhat enigmatic group of achondrites. They have preserved primordial signatures (e.g., primitive oxygen isotope composition, near-chondritic siderophile trace element abundances), although they appear to be products of asteroidal differentiation processes (e.g., Mittlefehldt et al., 1998, and references therein). The details of ureilite petrogenesis are controversial, but most authors assume that the majority formed as asteroidal mantle restites (e.g., Singletary and Grove, 2003; Goodrich et al., 2004; Warren et al., 2006, and references therein). A detailed presentation of existing ureilite formation models is out of the scope of this review and it is referred to the following references for details (e.g., Boynton et al., 1976; Wasson et al., 1976; Berkley and Jones, 1982; Warren and Kallemeyn, 1992; Scott et al., 1993; Walker and Grove, 1993; Goodrich, 1999; Singletary and Grove, 2003; Goodrich et al., 2004, 2007; Warren and Huber, 2006; Wilson et al., 2008; Warren, 2010). It is the intention of this paragraph to briefly sketch ureilite evolution highlighting results from the study of Almahata Sitta ureilites to provide a framework in which to discuss the formation and evolution of asteroid 2008 TC_3 in more detail (Section 7.4).

Herrin et al. (2010a,b) combined their results on Almahata Sitta ureilites with existing literature to set up a four stage scenario for ureilite thermal history, which will be supplemented here with further constraints from the literature and further recent results from Almahata Sitta.

Stage (I) involved heating and partial melting on the ureilite parent body (UPB), including basaltic magmatism. This is supported by highly fractionated trace element systematics (incompatible element depletion) of bulk ureilites and has been interpreted as ~20–30% loss of partial ("basaltic") silicate melts (e.g., Mittlefehldt et al., 1998; Goodrich et al., 2004; Warren et al., 2006, and references therein). Fragments of this melt are thought to be represented by the feldspathic clasts in polymict ureilite (e.g., Cohen et al., 2004). The first large fragment (individual) of the ureilitic crust (i.e., the missing "basalt") was found among the Almahata Sitta samples (MS-MU-011) and indicates that the mode of silicate melt extraction on the UPB was disequilibrium partial melting with rapid melt extraction, and that at least some of this melt was andesitic in composition (Bischoff et al., 2013b). The ~4.56 Ga U-Pb age (Torigoye-Kita et al., 1995) and studies on short-lived chronometers (Goodrich et al., 2002a; Kita et al., 2003; Lee et al., 2005) indicate that the ureilite parent asteroid differentiated very early in the history of the Solar System.

Stage (II) in ureilite evolution encompassed an impact event that resulted in the catastrophic disruption of the UPB (or at least parts of it including the mantle). This body was presumably a larger C-rich asteroid (>200 km diameter) that existed for a short

period in the early Solar System (e.g., Walker and Grove, 1993; Warren and Huber, 2006). Fragmentation of the UPB occurred while the mantle material (i.e., the ureilites) was (were) still at elevated, presumably close to anatectic temperatures (e.g., Walker and Grove, 1993; Goodrich et al., 2002b, 2004; Herrin et al., 2010a,b; Warren and Rubin, 2010). Two-pyroxene equilibrium temperatures in augite-bearing fragments from Almahata Sitta revealed that final mantle equilibrium was at 1190 ± 65 °C, i.e., at or near temperatures of partial melting. This temperature is similar to that of other augite-bearing ureilites (1185–1255 °C; Herrin et al., 2010a,b). Along with disruption, the reduction textures in coarse-grained ureilites formed as a result of smelting, triggered by the sudden pressure loss along fragmentation (Fig. 6e, f). In regions of more intense reduction and granulation, the fine-grained ureilites common in Almahata Sitta were formed via impact smelting (Fig. 7; Warren and Rubin, 2010; Horstmann et al., 2013b). Furthermore, Almahata Sitta fine-grained ureilites revealed that solid metal–liquid metal fractionation occurred, most likely along with this stage during impact smelting (Horstmann et al., 2013b). Further evidence for metal (re-)processing was reported by Goodrich et al. (2010a).

Stage (III): After disruption of the UPB, the mantle material cooled rapidly, with reduction zoning being preserved at grain margins of coarse-grained ureilite silicates. Herrin et al. (2009, 2010a,b) examined reversely-zoned olivine and pyroxene from Almahata Sitta ureilites. These document minimum cooling rates of 0.05–6 °C h^{-1} from initial temperatures of 1200–1300 °C down to 800 °C, which is consistent with previous estimates from other ureilites (Herrin et al., 2009, 2010a,b). Similar cooling rates (0.2–5 °C h^{-1}) were found by Mikouchi et al. (2010a,b) based on augite exsolution lamellae (10–15 nm wide) in Almahata Sitta pigeonite. In agreement with Herrin et al. (2009, 2010a,b) such rapid cooling was interpreted to record quenching from high temperature on the order of 1240–1280 °C down to approximately 1000 °C due to the UPB impact break-up while still hot (Mikouchi et al., 2010a,b). These rates indicate disruption of the parent lithologies forming "fragments ten meters in size or smaller" (Herrin et al. 2010b). Rapid cooling from high temperature is also suggested based on the metal characteristics of Almahata Sitta ureilites, like the formation of lath martensite in Fe-Ni metal (Mikouchi et al., 2011, 2013).

In stage (IV), the fragmented material re-accreted into smaller daughter asteroids forming one or multiple ureilitic "second generation" asteroids (e.g., Goodrich et al., 2002b, 2004; Downes et al., 2008; Herrin et al., 2010a,b). Based on CRE ages (~0.1 to ~47 Ma; Eugster, 2003; Rai et al., 2003), ureilites are suggested to largely derive from these bodies, on which also the brecciated ureilites formed (e.g., Goodrich et al., 2004; Downes et al., 2008). Asteroid 2008 TC_3 and its remnant meteorites of Almahata Sitta likely derive from such a "second generation" object still preserved in the Solar System, the details of which will be discussed in the following.

7.2. Occurrence and formation of polymict meteorite breccias

Almahata Sitta is an extremely heterogeneous polymict breccia formed by mixing of a variety of independently-formed chondritic and achondritic lithologies. Impact processes occurred and still occur on all planetary bodies of our Solar System, resulting in the formation of shock effects in mineral constituents, in situ fragmentation forming monomict breccias, and brecciation and mixing of different parent body lithologies with or without incorporation of fragments of the projectile (polymict or genomict breccias; e.g., Bischoff et al., 2006). After fragmentation/brecciation and mixing, a subsequent impact in a loose parent body material has formed tough breccias by grain boundary melting and lithification (Kieffer, 1975; Bischoff et al., 1983; Bischoff and Stöffler, 1992). Foreign (xenolithic, exotic) fragments have been found in a great number of polymict meteorite breccias. These breccias can be divided into five groups: (a) brecciated chondrites with chondritic clasts of other chondrite classes, (b) brecciated chondrites with achondritic xenoliths, (c) differentiated meteorite breccias with chondritic clasts, (d) differentiated meteorite breccias with other achondritic clasts, and (e) meteoritic breccias with fragments of different chondrite classes and achondritic clasts. Considering all breccias in general, the occurrence and abundance of foreign clasts in meteorites can be regarded as a good measure of the degree of mixing among asteroids. The relative abundance of different types of material may indicate the availability of certain components (impactors) at different times and places in the asteroid belt.

7.2.1. Brecciated chondrites with chondritic clasts of other chondrite classes

The occurrence of clasts from different ordinary chondrite groups in a specific host ordinary chondrite breccia is relatively rare (Bischoff et al., 2006). For example, in the LL chondrites St. Mesmin and Ngawi, H-group chondrite fragments occur (Dodd, 1974; Fodor and Keil, 1975); in the Dimmitt H chondrite regolith breccia, LL5 clasts (Rubin et al., 1983), and in the brecciated LL chondrite Paragould (Fodor and Keil, 1978) L-group components were encountered. An LL-chondritic xenolith was observed in the Tanezrouft 039 (L3) (Funk et al., 2011). Semenenko et al. (2001) identified fine-grained chondritic, accretionary objects in Krymka (LL3).

CM- or CI-like chondrite clasts bearing phyllosilicates, magnetites, and/or carbonates were observed in several H-group ordinary chondrites (e.g., MacPherson et al., 1993; Rubin and Bottke, 2009; Funk et al., 2011) and in CR- and CH-chondrites (e.g., Bischoff et al., 1993b,c, 2006; Endress et al., 1994).

7.2.2. Brecciated chondrites with achondritic xenoliths

Troctolitic, pyroxenitic, noritic, dunitic, or harzburgitic clasts have been reported from several ordinary chondrites [e.g., Hedjaz (L3.7), Barwell (L6), Yamato (Y-) 75097 (L6), Y-794046 (H5), Y-793241 (L6); e.g., Prinz et al., 1984; Hutchison et al., 1988; Nakamura et al., 1990; Misawa et al., 1992; Nagao, 1994; Mittlefehldt et al., 1995]. Igneous-textured fragments have also been found in Julesberg (L3), Vishnupur (LL4–6), and Parnallee (LL3) (Kennedy et al., 1992; Ruzicka et al., 1998; Bridges and Hutchison, 1997). A fragment in the polymict Villalbeto de la Peña L6 meteorite breccia is related to the winonaites based on oxygen isotope composition (Dyl et al., 2012; Bischoff et al., 2013c).

7.2.3. Differentiated meteorite breccias with chondritic clasts

Considering ureilitic breccias, chondrite fragments and chondrules showing certain relationships to ordinary and Rumuruti chondrites have been reported by Jaques and Fitzgerald (1982), Prinz et al. (1986, 1987, 1988), Ikeda et al. (2000, 2003), and Downes et al. (2008) from North Haig, Nilpena, EET83309, and Dar al Gani (DaG) 319. Downes et al. (2008) identified a single, nearly pure enstatite clast in EET 83309, with oxygen isotopes similar to E chondrites (and aubrites). Also, dark carbonaceous chondrite-like clasts are reported from several polymict ureilities (e.g., North Haig, Nilpena, DaG 319; DaG 165; Prinz et al., 1987; Brearley and Prinz, 1992; Brearley and Jones, 1998; Ikeda et al., 2000, 2003; Goodrich and Keil, 2002). The fragments in DaG 165 largely consist of phyllosilicates and grains of sulfide and magnetite (Goodrich and Keil, 2002).

In some polymict HED breccias carbonaceous chondritic clasts have been found, e.g., in Kapoeta and LEW 85300 (Wilkening, 1973; Zolensky et al., 1992, 1996), some of which are mineralogically similar to CM and CV3 chondrites. The occurrence of chondritic clasts

in HED breccias was also reported by, e.g., Bunch et al. (1979), Kozul and Hewins (1988), Mittlefehldt and Lindstrom (1988), Hewins (1990), Olsen et al. (1990), Reid et al. (1990), Buchanan et al. (1993), Pun et al. (1998), and Buchanan and Mittlefehldt (2003). Similarly, foreign clasts are also present in some aubrites: Cumberland Falls and ALH A78113, contain abundant FeO-bearing, chondritic clasts that have oxygen isotopic compositions related to ordinary chondrites. Their origin, however, is controversial (Lipschutz et al., 1988; Wasson et al., 1993).

7.2.4. Differentiated meteorite breccias with other achondritic clasts

In ureilitic breccias, rare ferroan, anorthitic clasts were found in Nilpena, DaG 319, and North Haig that are similar to angrite meteorites (Jaques and Fitzgerald, 1982; Prinz et al., 1986, 1987; Ikeda et al., 2000). Kita et al. (2003) showed that one ferroan, anorthite-rich clast in DaG 319 has an oxygen isotope composition similar to the Angra dos Reis angrite.

The Norton County aubrite contains igneous-textured pyroxenitic clasts composed of orthoenstatite, pigeonite, and diopside, and impact melt breccia clasts (e.g., Okada et al., 1988). These authors also found a fragment having diopside, plagioclase, and silica, and olivine and feldspathic clasts that are probably derived from separate lithologies (e.g., Okada et al., 1988), which may be foreign in our view.

7.2.5. Meteoritic breccias with fragments of different chondrite classes and achondritic clasts

The most prominent meteorite belonging to this group is certainly Kaidun, which contains all different kinds of chondritic and achondritic clasts (see Section 7.3). Among the chondritic breccias, Adzhi Bogdo (LL3-6) is an excellent example. In Adzhi-Bogdo (Bischoff et al., 1993a, 1996) L-group components were encountered as well as granitic clasts (Bischoff et al., 1993a; Sokol et al., 2007a; Terada and Bischoff, 2009), but the oxygen isotope compositions of the latter were similar to those obtained for ordinary chondrites (Sokol et al., 2007b).

For details regarding further exotic clasts identified in polymict ureilite breccias, it is referred to the comprehensive review by Goodrich et al. (2004).

7.3. Kaidun and Almahata Sitta – two extreme cases of polymict breccia formation

Extreme compositional and lithological inhomogeneities in meteorites exist in the cases of Kaidun (Zolensky and Ivanov, 2003) and Almahata Sitta. A combination of different processes (e.g., accretion, metamorphism, differentiation, brecciation, destruction, and re-accretion) is certainly responsible for producing this kind of multifaceted polymict breccias. Before Almahata Sitta, Kaidun has been regarded as the most impressive and fascinating meteoritic breccia, consisting of abundant millimeter and sub-millimeter-sized fragments (e.g., EH3-5, EL3, CV3, CM1-2 and R chondrites; Zolensky and Ivanov, 2003, and references therein). Also C1 and C2 lithologies, new enstatite-bearing clasts, fragments of impact melt products and Ca-rich achondritic materials, as well as phosphide-bearing clasts were encountered. Some alkaline-enriched clasts were observed that are similar to granitoidal clasts found in the Adzhi-Bogdo ordinary chondrite regolith breccia (Bischoff et al., 1993a). Zolensky and Ivanov (2003) suggest that Kaidun may derive from an especially large asteroid like Ceres, or an unusually located one like Phobos, the larger moon of Mars. By comparison, the variety of different lithologies is quite similar between Kaidun and Almahata Sitta; however, the ingredients are quite different, since ureilitic lithologies are dominating in Almahata Sitta.

Beyond that, there is another significant difference between the Almahata Sitta/asteroid 2008 TC_3 polymict breccia and Kaidun: Kaidun is a well-consolidated breccia and the relationship between different lithologies can be studied in great detail on the thin section scale, which is not the case for Almahata Sitta showing only meteorite individuals, which broke apart from each other during atmospheric entry of a loosely consolidated breccia. In this respect Almahata Sitta is also very different from other polymict ureilites, in which ureilitic and exotic (chondritic) fragments are well-consolidated in one thin section (e.g., Goodrich et al., 2004). In addition, as stated in Bischoff et al. (2010b), other polymict ureilites do not contain such an apparent abundance of "exotic" clasts.

Several other interesting facts regarding the nature of asteroid 2008 TC_3/Almahata Sitta can be observed [some of which have been listed in Bischoff et al. (2010b)]: (a) CB_a chondrites (Bischoff et al., 2012) have never before been reported to occur as clasts in polymict ureilites; (b) the unusual R chondrite-like fragment (Horstmann et al., 2010) extends the number of R chondrite(-related) fragments in polymict ureilites; (c) although a single enstatite clast related to enstatite meteorites is known from polymict ureilites (Downes et al., 2008), the quantity, size, and textural and chemical variability of E chondrites in Almahata Sitta is unique; (d) no information on the strength and lithological connections of the various chondritic and achondritic components can be inferred; (e) asteroid 2008 TC_3 was much more loosely lithified and porous than typical polymict ureilite breccias and Kaidun; (f) asteroid 2008 TC_3 may have consisted of loosely agglomerated components that disintegrated into monolithic fragments along their original boundaries during explosion in the atmosphere (Horstmann and Bischoff, 2010b; Fig. 18; see also below).

7.4. Late accretion and evolution of asteroid 2008 TC_3 – a summary

The formation and evolution of asteroid 2008 TC_3 has been discussed to various extents by several workers (e.g., Bischoff et al., 2010b; Herrin et al., 2010a,b; Horstmann and Bischoff, 2010b; Hartmann et al., 2011; Gayon-Markt et al., 2012).

As a starting point for the formation and evolutionary pathway of asteroid 2008 TC_3 (Fig. 18), the final catastrophic disruption of the UPB delivering various ureilitic materials in terms of texture and mineral composition is chosen (equivalent to the aftermath of Stage III in Section 7.1). This approach is based on this largely accepted view established in, e.g., Goodrich et al. (2004), Downes et al. (2008), and references therein. Fig. 18 illustrates two distinct evolutionary pathways that are proposed for asteroid 2008 TC_3.

Bischoff et al. (2010b) and Horstmann and Bischoff (2010b) suggested that the highly variable ureilitic materials delivered and dispersed by the impact re-accreted to second-generation asteroids upon which various chondritic materials found in the Almahata Sitta strewn field could have been mixed into these bodies (Fig. 18). This gave rise to polymict second generation asteroids, a fragment of which is represented by asteroid 2008 TC_3. Similarly, Herrin et al. (2010a,b) suggested that the ureilitic fragments formed a debris cloud around the former UPB and were mixed with various chondritic materials, finally forming "polylithologic aggregate objects such as asteroid 2008 TC_3". Meteorites bearing foreign clasts are typically regolith breccias. However, the absence of solar wind gases argues against a regolith nature of asteroid 2008 TC_3 (Ott et al., 2010) and suggests that it was shielded at greater depth in a larger body. This is supported by Meier et al. (2010, 2012) and Welten et al. (2011), who showed that the chondritic constituents were apparently shielded in a larger body (after >8 Ma pre-exposure) before delivery of asteroid 2008 TC_3 to Earth. Sabbah et al. (2010) supported the common derivation of ureilites and chondrites from one mixed parent body by analysis of PAHs.

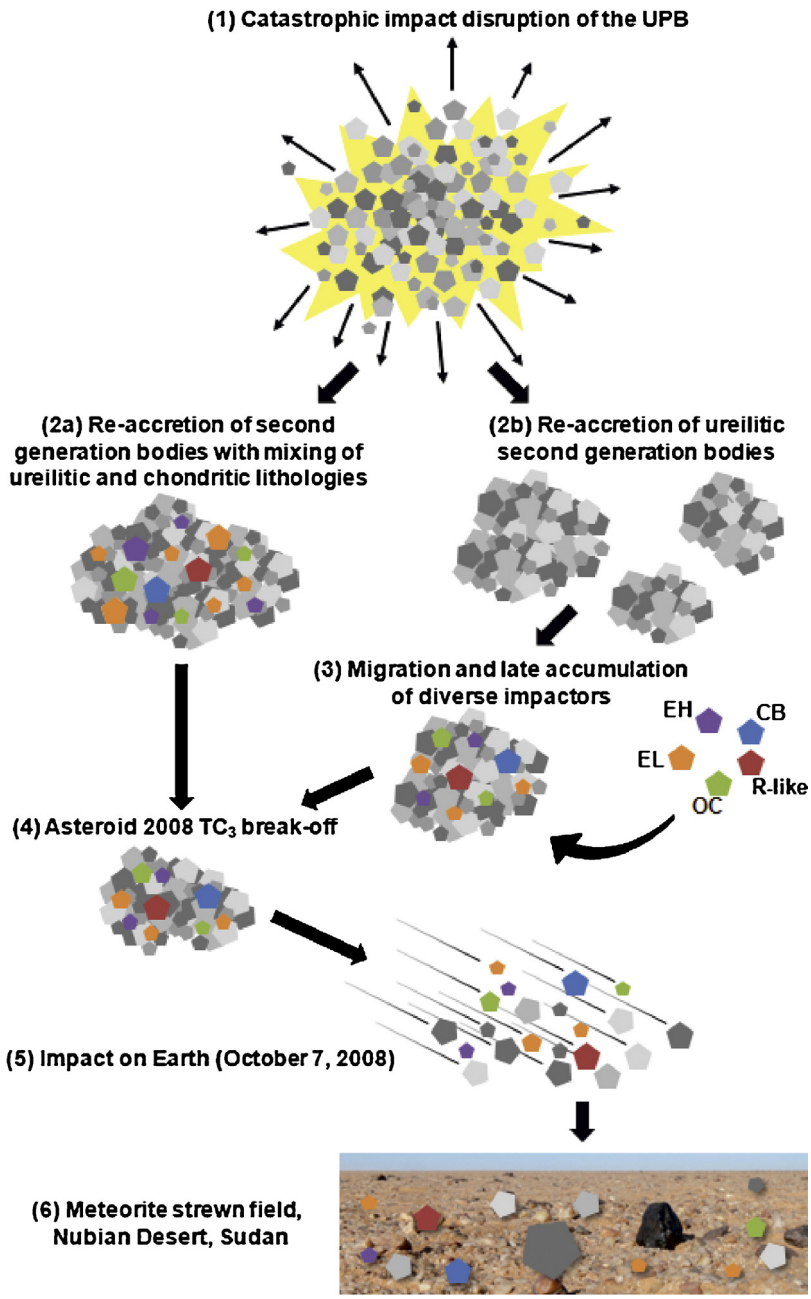

Fig. 18. Schematic illustration of a possible formation scenario of the late-accreted, second generation-ureilite asteroid, the break-off of asteroid 2008 TC_3, and the origin of the Almahata Sitta strewn field. Picture of the strewn field modified after http://apod.nasa.gov/apod/ap090328.html, accessed 08/12/2013.

Following Hartmann et al. (2011) in assuming that the UPB accreted and disrupted in the outer asteroid belt, and considering the presence of chondritic material in asteroid 2008 TC_3 formed in the inner regions of the Solar System (E and O chondrites), the scenario envisioned by Bischoff and co-workers (Bischoff et al., 2010b; Horstmann and Bischoff, 2010b) appears unlikely, as it requires considerable migration of material. Hartmann et al. (2011) also conclude that a chondrite-rich regolith developed on a ureilitic second generation asteroid in the outer belt is also unlikely, which is in agreement with the results of Ott et al. (2010). Hartmann et al. (2011) deduce that "the UPB daughter must have spent sufficient time in the inner asteroid belt and/or the terrestrial region in order to accrete this [chondritic] material". Alternatively, they suggest that the intact UPB could have migrated inwards and broke up in the inner asteroid belt. Either formed or emplaced in the inner belt, the ureilitic second generation body was gardened via bombardment with various local (chondritic) materials (Fig. 18). The body developed deep regolith of intimately mixed various ureilitic and chondritic fragments over time. These authors envision that asteroid 2008 TC_3 would derive from shallow regolith with small grain size and high abundance of foreign materials. Other polymict ureilites might originate from deeper regolith portions, common coarse-grained ureilites from the interior of these bodies.

However, there are (potentially) several problematic issues with Hartmann et al. (2011) model as recognized by the authors themselves, like low impact velocities not present in the main belt required to allow non-destructive integration of impactors (also noted by Gayon-Markt et al., 2012), the apparent abundance of E chondrites in the present-day inner belt (considering the apparent high E to O chondrite ratio in Almahata Sitta), or the difference

in clast types between Almahata Sitta and normal polymict ureilites. Furthermore, the lack of solar wind implanted gases (Ott et al., 2010) argues for an origin from a greater depth on the asteroid 2008 TC_3 parent body, which is not in agreement with a surficial regolith-nature of the object. Regarding the impact velocities, however, Hartmann et al. (2013) speculate that many asteroidal fragments in the diameter range of approximately 1–500 m are masses of loosely consolidated regolith, and that some would have captured multiple, intact impactors of different meteorite types at relatively low velocities. Concerning the evolution of small, rapidly rotating asteroids in the context of the meteoroid impact of 2008 TC_3, see details in Scheeres and Sánchez (2011). With respect to the apparent high abundance of E chondrite in Almahata Sitta, Hartmann et al. (2011) speculate that the break-up of the UPB might have involved an E chondrite breccia impactor.

The nature and characteristics of the various chondritic fragments in asteroid 2008 TC_3 clearly show that these fragments were incorporated into the asteroid 2008 TC_3 parent body as already completely processed objects. This means that, e.g., the H5 chondrite clast derives from an H chondrite parent body that accreted after chondrule formation, experienced thermal metamorphism for some million years, and collided with some other body. The body was (partly) disrupted and the material delivered into space. Similar processes can/have to be invoked with respect to EL6 and basically all other metamorphosed chondritic components of Almahata Sitta. Between the formation of Ca,Al-rich inclusions and chondrules, and the accretion of asteroid 2008 TC_3 considerable time has passed. Meier et al. (2012) reported a pre-irradiation of Almahata Sitta ordinary chondrites of roughly 10–20 Ma. This shows that the samples clearly migrated as individual meteoroids in space for some time, prior to incorporation into a larger body (the asteroid 2008 TC_3 parent body), in which they were shielded (Ott et al., 2010). Furthermore, Meier et al. (2012) could show that the accretion of the asteroid 2008 TC_3 parent asteroid (incorporation of chondritic components) took place no later than ~3.8 Ga ago, around the time of the proposed late heavy bombardment. Gayon-Markt et al. (2012) also suggest that the heterogeneous composition of asteroid 2008 TC_3 has to be inherited from processes in the very early Solar System. They conclude that asteroid 2008 TC_3 "seems to be an agglomeration of meteorite-sized (i.e., a few dm) pebbles of different nature" and formed in a phase of the Solar System in which collisional erosion and collisional accretion overlapped for some time in the primordial asteroid belt.

Since about 25–40% of (intact) non-ureilitic fragments have been encountered (which might not be truly representative of bulk 2008 TC_3), a re-accretion process for the formation of asteroid 2008 TC_3 over an incorporation of the chondritic components as projectiles into a regolith (Hartmann et al., 2011) is favored here: All sorts of chondritic fragments may have been present as "meteorite-sized pebbles" (Gayon-Markt et al., 2012) in a debris disk around the sun at the time of accretion of the asteroid 2008 TC_3 parent body and were mixed into it at low collisional velocities. Derivation from greater depth from the parent body is supported by the lack of solar wind implanted gases (Ott et al., 2010).

Accretion of asteroids was accompanied by mixing of material that originated over a range of heliocentric distances (Weidenschilling, 2013). This author also suggests that at least some of the large scale compositional heterogeneities in the asteroid belt (radial zoning) and small scale heterogeneities in meteorites documented by polymict breccias probably occurred after the excitation and mass depletion of the main belt in the early Solar System during ~4 Ga of high-velocity collisional evolution. In the case of asteroid 2008 TC_3, however, its parent body did not experience a large impact in the last ~3.8 Ga (Meier et al., 2012).

Anyway, a polymict second generation asteroid broke up as a result of an impact liberating, among others, asteroid 2008 TC_3 (Fig. 18) that ended up in an Earth-crossing orbit ultimately impacting Earth in the Nubian Desert, northern Sudan. The time span asteroid 2008 TC_3 traveled through space after its break-off can be given as on the order of ~20 Ma (Welten et al., 2010a,b, 2011). Thus, asteroid 2008 TC_3 clearly represents a fragment from a (ureilitic) second generation asteroid, which formed late in Solar System evolution.

Based on the orbital calculations, Jenniskens et al. (2009b) suggested that there might be a link between asteroid 2008 TC_3 and the 2.6-km sized asteroid 1998 KU_2, the only other known F-class asteroid in space close to its evolutionary pathway. Jenniskens et al. (2010) performed a detailed study to reconstruct the source region of asteroid 2008 TC_3. Although they found a population of near-Earth asteroids with spectra similar to asteroid 2008 TC_3 – the source region of which can be either in the main, inner, or outer asteroid belt – there is no strong evidence for either option. Gayon-Markt et al. (2012) conclude-based on spectroscopic and dynamical investigations – that the most likely source region of asteroid 2008 TC_3 is the inner main belt at low inclination ($i < 8°$). Regions of the main belt including the Nysa-Polana family and background objects were found by Gayon-Markt et al. (2012) to contain asteroids of spectroscopic classes that can be associated with different Almahata Sitta meteorite types.

Due to its high porosity and weak lithification, asteroid 2008 TC_3 broke up at a relatively high altitude of ~37 km, spreading a meteorite shower over the desert close to train station 6, south of Wadi Halfa (Figs. 1b, 2, and 18). Popova et al. (2011) suggest that as a result of the apparent massive dust release upon detonation, the recovery of only a small fraction of the mass as Almahata Sitta fragments, the different lithologies of achondritic and chondritic rocks, and the rotational evidence against a cohesionless rubble pile, asteroid 2008 TC_3 must have been weakly bonded by fine-grained matrix. Bischoff et al. (2010b) suggested that the highly porous, fine-grained ureilite material of AHS 7 classified by Jenniskens et al. (2009b) may represent the weak and relatively unconsolidated matrix which surrounded the monolithic clasts. However, from all studies of the Almahata Sitta fragments, no information could be gathered whether primordial dust was present in the region of re-accretion, since most of the fragments studied consist of a single lithology and the total material (~10 kg) represents <0.1% of the initial asteroid mass (for which most estimates now range from 20 to 50 t). The fine-grained material, however, which may have been generated in a parent body regolith, was lost during the fragmentation event in the atmosphere (Popova et al., 2011) and, hence, is most likely different from the fine-grained ureilites, which rather represent a distinct lithology.

8. Concluding remarks

More than 600 recovered samples have been gathered in the collection of the Almahata Sitta consortium and are stored in Khartoum. However, only a very limited number of samples from this collection have so far been studied in detail (Table 2). Mineral-chemical data are only available for 25 samples, though some more samples have at least been generally classified (Shaddad et al., 2010; Kohout et al., 2010a,b). It should be of great interest for international science to study as many of these samples as possible, because based on the results obtained so far on Almahata Sitta, it is suggested that Almahata Sitta is – from the petrological and cosmochemical point of view – the most important meteorite shower after that of Allende almost 50 years ago. Almahata Sitta was shown to and still bears significant potential to considerably further our understanding of, e.g., the thermal histories of different meteorite classes (especially ureilites and E chondrites) and the formation and evolution of asteroids, i.e., migration, collision, and mixing in the

asteroid belt. Additionally, not all meteoritic ingredients residing in the samples that remained in the collection so far may have been found in previous studies on Almahata Sitta and in meteoritics in general, as exemplified by the ureilite-related andesite and sulfide-metal assemblages. In particular, studying the complete range of Almahata Sitta samples will probably allow to learn much more about the formation of ureilites and the evolution of the UPB than it would ever be possible based on the study of all other known individual ureilites together.

Another aspect that should not be underestimated is the direct link of meteorite samples and remote sensing data of their parental asteroid 2008 TC_3. This could substantially contribute to gain new insights into the understanding of spectral data obtained by remote sensing and actual asteroid samples and, hence, might allow to link certain meteorite classes more confidently to certain asteroidal parent bodies.

Acknowledgements

We thank Mona Weyrauch and Moritz Barth (both Münster) for assistance with data compilation, and Steve Haumersen (Wyk auf Föhr) for help during crosschecking of tables and references. We thank the reviewers Kees Welten, and Mike Zolensky, and Associate Editor Klaus Keil for their thorough reviews, and useful comments and suggestions. This work was partly supported by the German Research Foundation (DFG) within the Priority Program "The first 10 Million Years – a Planetary Materials Approach" (SPP 1385). We thank Associate Editor Klaus Keil for soliciting and handling this Invited Review.

References

Aoyagi, Y., Mikouchi, T., Goodrich, C.A., 2013a. New observations on grain boundary metal in ureilitic fragments of Almahata Sitta. Lunar Planet. Sci. 44 (abstract #1448).

Aoyagi, Y., Mikouchi, T., Goodrich, C.A., Zolensky, M.E., 2013b. Mineralogy of grain boundary metal in ureilitic fragments of Almahata Sitta. Meteorit. Planet. Sci. 48, 5231.

Beard, S.P., Swindle, T.D., Isachsen, C., Jenniskens, P., Shaddad, M., 2013. Ar–Ar analysis of Almahata Sitta ordinary chondrites. Lunar Planet. Sci., 44 (abstract #2311).

Berkley, J.L., Jones, J.H., 1982. Primary igneous carbon in ureilites: Petrological implications. In: Proc. 13th Lunar Planet. Sci. Conf, pp. A353–A364.

Bischoff, A., Stöffler, D., 1992. Shock metamorphism as a fundamental process in the evolution of planetary bodies: information from meteorites. Eur. J. Mineral. 4, 707–755.

Bischoff, A., Rubin, A.E., Keil, K., Stöffler, D., 1983. Lithification of gas-rich chondrite regolith breccias by grain boundary and localized shock melting. Earth Planet. Sci. Lett. 66, 1–10.

Bischoff, A., Geiger, T., Palme, H., Spettel, B., Schultz, L., Scherer, P., Schlüter, J., Lkhamsuren, J., 1993a. Mineralogy, chemistry, and noble gas contents of Adzhi-Bogdo – an LL3-6 chondritic breccia with L-chondritic and granitoidal clasts. Meteoritics 28, 570–578.

Bischoff, A., Palme, H., Ash, R.D., Clayton, R.N., Schultz, L., Herpers, U., Stöffler, D., Grady, M.M., Pillinger, C.T., Spettel, B., Weber, H., Grund, T., Endreß, M., Weber, D., 1993b. Paired Renazzo-type (CR) carbonaceous chondrites from the Sahara. Geochim. Cosmochim. Acta 57, 1587–1603.

Bischoff, A., Palme, H., Schultz, L., Weber, D., Weber, H.W., Spettel, B., 1993c. Acfer 182 and paired samples, an iron-rich carbonaceous chondrite: similarities with ALH 85085 and relationship to CR chondrites. Geochim. Cosmochim. Acta 57, 2631–2648.

Bischoff, A., Geiger, T., Palme, H., Spettel, B., Schultz, L., Scherer, P., Loeken, T., Bland, P., Clayton, R.N., Mayeda, T.K., Herpers, U., Meltzow, B., Michel, R., Dittrich-Hannen, B., 1994. Acfer 217 – a new member of the Rumuruti chondrite group (R). Meteoritics 29, 264–274.

Bischoff, A., Gerel, O., Buchwald, V.F., Spettel, B., Loeken, T., Schultz, L., Weber, H.W., Schlüter, J., Baljinnyam, L., Borchuluun, D., Byambaa, C., Garamjav, D., 1996. Meteorites from Mongolia. Meteorit. Planet. Sci. 31, 152–157.

Bischoff, A., Goodrich, C.A., Grund, T., 1999. Shock-induced origin of diamonds in ureilites. Lunar Planet. Sci., 30 (abstract #1100).

Bischoff, A., Scott, E.R.D., Metzler, K., Goodrich, C.A., 2006. Nature and origins of meteoritic breccias. In: Lauretta, D.S., McSween Jr., H.Y. (Eds.), Meteorites and the Early Solar System II. Univ. of Arizona, Tucson, pp. 679–712.

Bischoff, A., Horstmann, M., Laubenstein, M., Haberer, S., 2010a. Asteroid 2008 TC_3 Almahata Sitta: Not only a ureilitic meteorite, but a breccia containing many different achondritic and chondritic lithologies. Lunar Planet. Sci. 41 (abstract #1763).

Bischoff, A., Horstmann, M., Pack, A., Laubenstein, M., Haberer, S., 2010b. Asteroid 2008 TC_3—Almahata Sitta: a spectacular breccia containing many different ureilitic and chondritic lithologies. Meteorit. Planet. Sci. 45, 1638–1656.

Bischoff, A., Vogel, N., Roszjar, J., 2011. The Rumuruti chondrite group – invited review. Chem. Erde Geochem. 71, 101–133.

Bischoff, A., Horstmann, M., Heusser, G., Pack, A., Albrecht, N., 2012. Almahata Sitta sample MS-181: the first carbonaceous chondrite (CBa) from asteroid 2008 TC3. Meteorit. Planet. Sci. 47, A71.

Bischoff, A., Horstmann, M., Pack, A., Herwatz, D., Decker, S., 2013a. Almahata Sitta sample MS-MU-011: a rapidly crystallized basalt from the crust of the ureilite parent body (abstract No. 5104). Meteorit. Planet. Sci. 48, A60.

Bischoff, A., Horstmann, M., Barrat, J.-A., Chaussidon, M., Pack, A., Herwartz, D., Ward, D., Vollmer, C., Decker, S., 2013b. Andesitic volcanism in the early Solar System - constraints from the ureilite parent body (submitted).

Bischoff, A., Dyl, K.A., Horstmann, M., Ziegler, K., Wimmer, K., Young, E.D., 2013c. Reclassification of Villalbeto de la Peña – occurrence of a winonaite-related fragment in a hydrothermally metamorphosed polymict L-chondritic breccias. Meteorit. Planet. Sci. 48, 628–640.

Borovička, J., Charvát, Z., 2008. In: Green, D.W.E. (Ed.), 2008 TC3. IAU Circular 8994. Central Bureau for Astronomical Telegrams (October 8, 2008), Cambridge, MA.

Borovička, J., Charvát, Z., 2009. Meteosat observation of the atmospheric entry of 2008 TC_3 over Sudan and the associated dust cloud. A&A 507, 1015–1022.

Boynton, W.V., Starzyk, P.M., Schmitt, R.A., 1976. Chemical evidence for genesis of ureilites, achondrite chassigny, and nakhlites. Geochim. Cosmochim. Acta 40, 1439–1447.

Brearley, A.J., Jones, R.H., 1998. In: Papike, J.J. (Ed.), Chondritic Meteorites. Planetary Materials – Reviews in Mineralogy, 26. Mineralogical Society of America, Washington, pp. 3-01–3-398.

Brearley, A.J., Prinz, M., 1992. CI chondrite-like clasts in the Nilpena polymict ureilite. Implications for aqueous alteration processes in CI chondrites. Geochim. Cosmochim. Acta 56, 1373–1386.

Bridges, J.C., Hutchison, R., 1997. A survey of clasts and chondrules in ordinary chondrites. Meteorit. Planet. Sci. 32, 389–394.

Britt, D.T., Consolmagno, G.J., 2003. Stony meteorite porosities and densities: a review of the data through 2001. Meteorit. Planet. Sci. 38, 1161–1180.

Brown, P., 2008. http://aquarid.physics.uwo.ca/~pbrown/usaf/usg282.txt (University of Western Ontario, Canada).

Brown, P.G., ReVelle, D.O., Tagliaferri, E., Hildebrand, A.R., 2002. An entrymodel for the TagishLake fireball using seismic, satellite and infrasound records. Meteorit. Planet. Sci. 37, 661–675.

Buchanan, P.C., Mittlefehldt, D.W., 2003. Lithic components in the paired howardites EET 87503 and EET 87513: Characterization of the regolith of 4 Vesta. Antarctic Meteor. Res. 16, 128–151.

Buchanan, P.C., Zolensky, M.E., Reid, A.M., 1993. Carbonaceous chondrite clasts in the howardites Bholghati and EET 87513. Meteoritics 28, 659–669.

Bunch, T.E., Chang, S., Frick, U., Neil, J., Moreland, G., 1979. Carbonaceous chondrites. I. Characterization and significance of carbonaceous chondrite (CM) xenoliths in the Jodzie howardite. Geochim. Cosmochim. Acta 43, 1727–1742.

Burbine, T.H., McCoy, T.J., Meibom, A., Gladman, B., Keil, K., 2002. Meteoritic parent bodies: their number and identification. In: Bottke, W., Cellino, A., Paolicchi, C., Binzel, R.P. (Eds.), Asteroids III. Univ. of Arizona, Tucson, pp. 653–667.

Burton, A.S., Glavin, D.P., Callahan, M.P., Dworkin, J.P., Jenniskens, P., Shaddad, M.H., 2011a. Extraterrestrial amino acids in ureilites including Almahata Sitta. Lunar Planet. Sci., 42 (abstract #2815).

Burton, A.S., Glavin, D.P., Callahan, M.P., Dworkin, J.P., Jenniskens, P., Shaddad, M.H., 2011b. Heterogeneous distributions of amino acids provide evidence of multiple sources within the Almahata Sitta parent body, asteroid 2008 TC3. Meteorit. Planet. Sci. 46, 1703–1712.

Ceplecha, Z., McCrosky, R.E., 1976. Fireball end heights: a diagnostic for the structure of meteoric material. J. Geophys. Res. 81, 6257–6275.

Chesley, S., Codas, P., Yeomans, D., 2008. Asteroid 2008 TC3 strikes Earth: Predictions and observations agree, http://neo.jpl.nasa.gov./news/2008TC3.html (NASA/JPL, near Earth Object Program).

Cloutis, E.A., Hudon, P., Romanek, C.S., Bishop, J.L., Reddy, V., Gaffey, M.J., Hardersen, P.S., 2010. Spectral reflectance properties of ureilites. Meteorit. Planet. Sci. 45, 1668–1694.

Cohen, B.A., Goodrich, C.A., Keil, K., 2004. Feldspathic clast populations in polymict ureilites: stalking the missing basalts from the ureilite parent body. Geochim. Cosmochim. Acta 68, 4249–4266.

Consolmagno, G.J., Britt, D.T., Macke, R.J., 2008. The significance of meteorite density and porosity. Chem. Erde Geochem. 68, 1–29.

Dodd, R.T., 1974. Petrology of the St. Mesmin chondrite. Contrib. Mineral. Petro. 46, 129–145.

Downes, H., Mittlefehldt, D.W., Kita, N.T., Valley, J.W., 2008. Evidence from polymict ureilite meteorites for a disrupted and re-accreted single ureilite parent asteroid gardened by several distinct impactors. Geochim. Cosmochim. Acta 72, 4825–4844.

Dyl, K.A., Bischoff, A., Ziegler, K., Young, E.D., Wimmer, K., Bland, P.A., 2012. Early Solar System hydrothermal activity in chondritic asteroids on 1-10-year timescales. Proc. Natl. Acad. Sci. 109, 18306–18311.

El Goresy, A., Boyet, M., Miyahara, M., 2011. Almahatta Sitta MS-17 EL-3 chondrite fragment: contrasting oldhamite assemblages in chondrules and matrix and significant oldhamite REE-patterns. Meteorit. Planet. Sci. 46, A63.

El Goresy, A., Lin, Y., Feng, L., Boyet, M., Hao, J., Zhang, J., Dubrovinsky, L., 2012. Almahata Sitta EL-3 chondrites: Sinoite, graphite, and oldhamite (CaS) assemblages C- and N-isotopic compositions and REE patterns. Meteorit. Planet. Sci. 47, A125.

Endress, M., Keil, K., Bischoff, A., Spettel, B., Clayton, R.N., Mayeda, T.K., 1994. Origin of dark clasts in the Acfer 059/El Djouf 001 CR2 chondrite. Meteoritics 29, 26–40.
Eugster, O., 2003. Cosmic-ray exposure ages of meteorites and lunar rocks and their significance. Chem. Erde Geochem. 63, 3–30.
Feng, L., El Goresy, A., Zhang, J., Hao, J., Boyet, M., Yang, L., 2012. Excess ^{36}S in lawrencite and nitrogen isotopic compositions of sinoite from Almahata Sitta MS-17 EL3 chondrite fragment. Lunar Planet. Sci., 43 (abstract #1766).
Fodor, R.V., Keil, K., 1975. Implications of poikilitic textures in LL-group chondrites. Meteoritics 10, 325–340.
Fodor, R.V., Keil, K., 1978. Catalog of lithic fragments in LL-Group chondrites. Special Publication No. 19. Uiverity of New Mexico, Institute of Meteoritics, 38 pp.
Friedrich, J.M., Wolf, S.F., Rumble, D., Troiano, J., Gagnon, C.J.L., Compton, J.R., Jenniskens, P., Shaddad, M.H., 2010. The elemental composition of Almahata Sitta. Meteorit. Planet. Sci. 45, 1718–1727.
Funk, C., Bischoff, A., Schlüter, J., 2011. Xenoliths in carbonaceous and ordinary chondrites. Meteorit. Planet. Sci. 46, A71.
Gaffey, M.J., Burbine, T.H., Binzel, R.P., 1993. Asteroid spectroscopy: progress and perspectives. Meteorit. Planet. Sci. 28, 161–187.
Gayon-Markt, J., Delbo, M., Morbidelli, A., Marchi, S., 2012. On the origin of the Almahata Sitta meteorite and 2008 TC_3 asteroid. Mon. Not. R. Astron. Soc. 424, 508–518.
Glavin, D.P., Aubrey, A.D., Callahan, M.P., Dworkin, J.P., Elsila, J.E., Parker, E.T., Bada, J.L., 2010a. Extraterrestrial amino acids in the Almahata Sitta meteorite. Lunar Planet. Sci., 41 (abstract #1042).
Glavin, D.P., Aubrey, A.D., Callahan, M.P., Dworkin, J.P., Elsila, J.E., Parker, E.T., Bada, J.L., Jenniskens, P., Shaddad, M.H., 2010b. Extraterrestrial amino acids in the Almahata Sitta meteorite. Meteorit. Planet. Sci. 45, 1695–1709.
Goodrich, C.A., 1999. Are ureilites residues from partial melting of chondritic material? The answer from MAGPOX. Meteorit. Planet. Sci. 34, 109–119.
Goodrich, C.A., Keil, K., 2002. Feldspathic and other unusual clasts in polymict ureilite DaG 165. Lunar Planet. Sci., 33 (abstract #1777).
Goodrich, C.A., Hutcheon, I.D., Keil, K., 2002a. ^{53}Mn-^{53}Cr age of a highly evolved, igneous lithology in polymict ureilite DaG 165. Meteorit. Planet. Sci. 37, A54 (abstract).
Goodrich, C.A., Krot, A.N., Scott, E.R.D., Taylor, G.J., Fioretti, A.M., Keil, K., 2002b. Formation and evolution of the ureilite parent body and its offspring. Lunar Planet. Sci., 33 (abstract #1379).
Goodrich, C.A., Scott, E.R.D., Fioretti, A.M., 2004. Ureilitic breccias: clues to the petrologic structure and impact disruption of the ureilite parent asteroid. Chem. Erde Geochem. 64, 283–327.
Goodrich, C.A., Van Orman, J., Wilson, L., 2007. Fractional melting and smelting on the ureilite parent body. Geochim. Cosmochim. Acta 71, 2876–2895.
Goodrich, C.A., Goldstein, J., Kita, N.T., Mikouchi, T., Zolensky, M., Herrin, J., Ash, R.D., McDonough, W.F., Jenniskens, P.M., 2010a. Metal in ureilitic fragments of Almahata Sitta. Meteorit. Planet. Sci. 45, A66.
Goodrich, C.A., Hutcheon, I.D., Kita, N.T., Huss, G.R., Cohen, B.A., Keil, K., 2010b. ^{53}Mn-^{53}Cr and ^{26}Al-^{26}Mg ages of a feldspathic lithology in polymict ureilites. Earth Planet. Sci. Lett. 295, 531–540.
Goodrich, C.A., Bischoff, A., O'Brien, D.P., 2014. Asteroid 2008 TC3 and the fall of Almahata Sitta, a unique meteorite breccia. Elements 10, 31–37.
Grund, T., Bischoff, A., 1999. Cathodoluminescence properties of diamonds in ureilites: further evidence for a shock-induced origin. Meteorit. Planet. Sci. 34, A48–A49.
Hain, H., (Bachelor thesis) 2012. Characterization of different meteorite samples from the Almahata Sitta strewn field. Insitut für Planetologie, Westfälische Wilhelms-Universität Münster, Germany, 66 pp.
Hartmann, W.K., Goodrich, C.A., O'Brien, D.P., Michel, P., Weidenschilling, S.J., Sykes, M.V., 2011. Breakup and reassembly of the ureilite Parent Body, formation of 2008 TC_3/Almahata Sitta, and delivery of ureilites to Earth. Lunar Planet. Sci. 42 (abstract #1360).
Hartmann, W.K., Popova, O., Joseph, E.C.S., 2013. From Almahata Sitta to crater clusters on Mars. Lunar Planet. Sci., 44 (abstract #1580).
Herrin, J.S., Zolensky, M.E., Ito, M., Jenniskens, P., Shaddad, M.H., 2009. Fossilized smelting; reduction textures in Almahata Sitta ureilite. Meteorit. Planet. Sci. 44, A89.
Herrin, J.S., Ito, M., Zolensky, M.E., Mittlefehldt, D.W., Jenniskens, P.M., Shaddad, M.H., 2010a. Thermal history and fragmentation of ureilitic asteroids; insights from the Almahata Sitta fall. Lunar Planet. Sci., 41 (abstract #1095).
Herrin, J.S., Zolensky, M.E., Ito, M., Le, L., Mittlefehldt, D.W., Jenniskens, P., Ross, A.J., Shaddad, M.H., 2010b. Thermal and fragmentation history of ureilitic asteroids: insights from the Almahata Sitta fall. Meteorit. Planet. Sci. 45, 1789–1803.
Hewins, R.H., 1990. Geologic history of LEW 85300, 85302 and 85303 polymict eucrites (abstract). Lunar Planet. Sci. 21, 509–510.
Hiroi, T., Jenniskens, P.M., Bishop, J.L., Shatir, T., 2010a. Reflectance spectroscopy of Almahata Sitta meteorite samples from Asteroid 2008 TC_3. Lunar Planet. Sci., 41 (abstract #1148).
Hiroi, T., Jenniskens, P., Bishop, J.L., Shatir, T.S.M., Kudoda, A.M., Shaddad, M.H., 2010b. Bidirectional visible-NIR and biconical FT-IR reflectance spectra of Almahata Sitta meteorite samples. Meteorit. Planet. Sci. 45, 1836–1845.
Hochleitner, R., Hoffmann, V.H., Kaliwoda, M., Mikouchi, T., 2010. Mineralogy of opaque phases in Almahata Sitta ureilite. DMG Meeting, 2010 (abstract #P3-01).
Hoffmann, V.H., Hochleitner, R., Torii, M., Funaki, M., Mikouchi, T., Almahata Sitta Consortium, 2010. Magnetism and mineralogy of Almahata Sitta. Lunar Planet. Sci., 41 (abstract #2120).
Hoffmann, V.H., Hochleitner, R., Torii, M., Funaki, M., Mikouchi, T., Kaliwoda, M., Jenniskens, P., Shaddad, M.H., 2011a. Magnetism and mineralogy of Almahata Sitta polymict ureilite (= asteroid 2008 TC_3): implications for the ureilite parent body magnetic field. Meteorit. Planet. Sci. 46, 1551–1564.
Hoffmann, V.H., Torii, M., Funaki, M., Hochleitner, R., Kaliwoda, M., Mikouchi, T., Zolensky, M., 2011b. Magnetic phases of Almahata Sitta: new results. Lunar Planet. Sci., 42 (abstract #2191).
Hoffmann, V.H., Mikouchi, T., Torii, M., Funaki, M., Kaliwoda, M., Hochleitner, R., Horstmann, M., Bischoff, A., Gnos, E., Hofmann, B., Yamamoto, Y., Kodama, K., 2012a. Almahata Sitta magnetism a compilation. In: Asteroids, Comets, Meteors 2012, Houston (abstract #6346).
Hoffmann, V.H., Hochleitner, R., Kaliwoda, M., Torii, M., Funaki, M., Mikouchi, T., 2012b. Magnetic signature of E chondritic lithologies of Almahata Sitta and comparison with Neuschwanstein (EL6). Lunar Planet. Sci., 43 (abstract #2342).
Horstmann, M., (Master thesis) 2010. Mineralogy and chemistry of selected components in meteorites. Institut für Planetologie, Westfälische Wilhelms-Universität Münster, Germany, 307 pp.
Horstmann, M., (PhD thesis) 2013. The Almahata Sitta meteorites: Insights into the nature of selected chondritic and achondritic lithologies and possible genetic relations. Institut für Planetologie, Westfälische Wilhelms-Universität Münster, Germany, 225 pp.
Horstmann, M., Bischoff, A., 2010a. Characterization of spectacular lithologies from the Almahata Sitta breccia. Lunar Planet. Sci., 41 (abstract #1784).
Horstmann, M., Bischoff, A., 2010b. Formation and evolution of the highly unconsolidated Asteroid 2008 TC3. Meteorit. Planet. Sci. 45, A83.
Horstmann, M., Bischoff, A., Pack, A., Laubenstein, M., 2010. Almahata Sitta—fragment MS-CH: characterization of a new chondrite type. Meteorit. Planet. Sci. 45, 1657–1667.
Horstmann, M., Humayun, M., Bischoff, A., 2011a. Rare Earth Element (REE) abundances of sulfides from E chondrite lithologies of the Almahata Sitta Polymict breccia. Meteorit. Planet. Sci. 46, A102.
Horstmann, M., Humayun, M., Bischoff, A., 2011b. Siderophile element patterns of sulfide-metal assemblages from the Almahata Sitta polymict breccia. Meteorit. Planet. Sci. 46, A101.
Horstmann, M., Bischoff, A., Pack, A., Albrecht, N., Weyrauch, M., Hain, H., Roggon, L., Schneider, K., 2012a. Mineralogy and oxygen isotope composition of new samples from the Almahata Sitta strewn field. Meteorit. Planet. Sci. 47, A193.
Horstmann, M., Humayun, M., Harries, D., Langenhorst, F., Chabot, N.L., Bischoff, A., 2012b. Wüstite in the Almahata Sitta polymict ureilite: implications for oxygen during asteroidal differentiation. Lunar Planet. Sci., 43 (abstract #1876).
Horstmann, M., Humayun, M., Harries, D., Langenhorst, F., Chabot, N.L., Bischoff, A., Zolensky, M.E., 2012c. Wüstite in the fusion crust of the MS-166 Almahata Sitta metal-sulfide assemblage. Meteorit. Planet. Sci. 47, A194.
Horstmann, M., Humayun, M., Harries, D., Langenhorst, F., Chabot, N.L., Bischoff, A., Zolensky, M.E., 2013a. Wüstite in the fusion crust of Almahata Sitta sulfide-metal assemblage MS-166: evidence for oxygen in metallic melts. Meteorit. Planet. Sci. 48, 730–743.
Horstmann, M., Humayun, M., Fischer-Gödde, M., Bischoff, A., 2013b. Enstatite chondrite-like metal and sulfide in Almahata Sitta fine-grained ureilites and indications for partial metallic melts on the ureilite parent body. Meteorit. Planet. Sci., in revision.
Hutchins, K.I., Agee, C.B., 2012. Microprobe analyses of two Almahata Sitta ureilites. Lunar Planet. Sci., 43 (abstract #2435).
Hutchison, R., Williams, C.T., Din, V.K., Clayton, R.N., Kirschbaum, C., Paul, R.L., Lipschutz, M.E., 1988. A planetary, H-group pebble in the Barwell, L6, unshocked chondritic meteorite. Earth Planet. Sci. Lett. 90, 105–118.
Ikeda, Y., Prinz, M., Nehru, C.E., 2000. Lithic and mineral clasts in the Dar al Gani (DAG) 319 polymict ureilite. Antarct. Meteor. Res. 13, 177–221.
Ikeda, Y., Kita, N.T., Morishita, Y., Weisberg, M.K., 2003. Primitive clasts in the Dar al Gani 319 polymict ureilite: precursors of the ureilites. Antarct. Meteor. Res. 16, 105–127.
Jaques, A.L., Fitzgerald, M.J., 1982. The Nilpena ureilite, an unusual polymict breccia – implications for origin. Geochim. Cosmochim. Acta 46, 893–900.
Jenniskens, P., Shaddad, M.H., and the Almahata Sitta Consortium, 2009a. The unusually frail asteroid 2008 TC3. In: Proc. Int. Astron. Union 5, pp. 227–230.
Jenniskens, P., Shaddad, M.H., Numan, D., Elsir, S., Kudoda, A.M., Zolensky, M.E., Le, L., Robinson, G.A., Friedrich, J.M., Rumble, D., Steele, A., Chesley, S.R., Fitzsimmons, A., Duddy, S., Hsieh, H.H., Ramsay, G., Brown, P.G., Edwards, W.N., Tagliaferri, E., Boslough, M.B., Spalding, R.E., Dantowitz, R., Kozubal, M., Pravec, P., Borovicka, J., Charvat, Z., Vaubaillon, J., Kuiper, J., Albers, J., Bishop, J.L., Mancinelli, R.L., Sandford, S.A., Milam, S.N., Nuevo, M., Worden, S.P., 2009b. The impact and recovery of asteroid 2008 TC3. Nature 458, 485–488.
Jenniskens, P., Vaubaillon, J., Binzel, R.P., DeMeo, F.E., NesvornÝ, D., Bottke, W.F., Fitzsimmons, A., Hiroi, T., Marchis, F., Bishop, J.L., Vernazza, P., Zolensky, M.E., Herrin, J.S., Welten, K.C., Meier, M.M.M., Shaddad, M.H., 2010. Almahata Sitta (=asteroid 2008 TC_3) and the search for the ureilite parent body. Meteorit. Planet. Sci. 45, 1590–1617.
Kaliwoda, M., Hochleitner, R., Hoffmann, V.H., Mikouchi, T., Gigler, A.M., Schmahl, W.W., 2011a. New Raman spectroscopic data of Almahata Sitta meteorite. In: Conf. Micro-Raman Spectrosc Luminescence Studies Earth Planet. Sci. (CORALS II), Houston (abstract #4037).
Kaliwoda, M., Hoffmann, V.H., Hochleitner, R., Mikouchi, T., Gigler, A., 2011b. New Raman spectroscopy data of Almahata Sitta. Lunar Planet. Sci., 42 (abstract #2225).
Kaliwoda, M., Hochleitner, R., Hoffmann, V.H., Mikouchi, T., Gigler, A.M., Schmahl, W.W., 2013. New Raman spectroscopic data of the Almahata Sitta meteorite. Spectrosc. Lett. 46, 141–146.

Kennedy, A.K., Hutchison, R., Hutcheon, I.D., Agrell, S.O., 1992. A unique high Mn/Fe microgabbro in the Parnallee (LL3) ordinary chondrite: Nebular micture or planetary differentiate form a previously unrecognized planetary body? Earth Planet. Sci. Lett. 113, 191–205.

Kieffer, S.W., 1975. From regolith to rock by shock. The Moon 13, 301–320.

Kita, N.T., Ikeda, Y., Shimoda, H., Morishita, Y., Weisberg, M.K., 2003. Timing of basaltic volcanism in ureilite parent body inferred from the ^{26}Al ages of plagioclase-bearing clasts in DAG 319 polymict ureilite. Lunar Planet. Sci., 34 (abstract #1557).

Kita, N.T., Ikeda, Y., Togashi, S., Liu, Y., Morishita, Y., Weisberg, M.K., 2004. Origin of ureilites inferred from a SIMS oxygen isotopic and trace element study of clasts in the Dar al Gani 319 polymict ureilite. Geochim. Cosmochim. Acta 68, 4213–4235.

Kita, N.T., Goodrich, C.A., Zolensky, M.E., Herrin, J.S., Shaddad, M.H., Jenniskens, P., 2011. Oxygen isotope systematics of Almahata Sitta. Lunar Planet. Sci., 42 (abstract #1491).

Kiuru, R., Kohout, T., Montonen, M., Britt, D., Macke, R., Scheirich, P., Consolmagno, G., 2011. Limits for asteroid 2008 TC_3 size and mass based on densities of Almahata Sitta meteorites. Meteorit. Planet. Sci. 46, A126.

Kohout, T., Jenniskens, P., Haloda, J., Britt, D., 2010a. Inhomogeneity of the 2008 TC_3 asteroid material (Almahata Sitta meteorites) revealed through physical properties measurements. Meteorit. Planet. Sci. 45, A108.

Kohout, T., Jenniskens, P., Shaddad, M.H., Haloda, J., 2010b. Inhomogeneity of asteroid 2008 TC_3 (Almahata Sitta meteorites) revealed through magnetic susceptibility measurements. Meteorit. Planet. Sci. 45, 1778–1788.

Kohout, T., Kiuru, R., Montonen, M., Scheirich, P., Britt, D., Macke, R., Consolmagno, G., 2011. Internal structure and physical properties of the Asteroid 2008 TC_3 inferred from a study of the Almahata Sitta meteorites. Icarus 212, 697–700.

Kong, P., Mori, T., Ebihara, M., 1997. Compositional continuity of enstatite chondrites and implications for heterogeneous accretion of the enstatite chondrite parent body. Geochim. Cosmochim. Acta 61, 4895–4914.

Kowalski, R.A., 2008. 2008 TC3. In: Williams, G.V. (Ed.), MPEC 2008-T50. Minor Planet Center, Smithsonian Astrophysical Observatory, Cambridge, MA, p. 1.

Kozubal, M.J., Gasdia, F.W., Dantowitz, R.F., Scheirich, P., Harris, A.W., 2011. Photometric observations of earth-impacting asteroid 2008 TC3. Meteorit. Planet. Sci. 46, 534–542.

Kozul, J., Hewins, R.H., 1988. LEW 85300,02,03 polymict eucrites consortium – II: Breccia clasts, CM inclusions, glassy matrix and assembly history (abstract). Lunar Planet. Sci. 19, 647–648.

Krot, A.N., Ivanova, M.A., Ulyanov, A.A., 2007. Chondrules in the CB/CH-like carbonaceous chondrite Isheyevo: evidence for various chondrule-forming mechanisms and multiple chondrule generations. Chem. Erde Geochem. 67, 283–300.

Kwok, R., 2009. The rock that fell to Earth. Nature 458, 401–404.

Lee, D.C., Halliday, A.N., Singletary, S.J., Grove, T.L., 2005. ^{182}Hf-^{182}W chronometry and an early differentiation in the parent body of ureilites. Lunar Planet. Sci., 36 (abstract #1638).

Lin, Y., El Goresy, A., Boyet, M., Feng, L., Zhang, J., Hao, J., 2011. Earliest solid condensates consisting of the assemblage oldhamite, sinoite, graphite and excess 36S in lawrencite from Almahata Sitta MS-17 EL3 chondrite fragment. In: Workshop on Formation of the First Solids in the Solar System, Houston (abstract #9040).

Lipschutz, M.E., Verkouteren, R.M., Sears, D.W.G., Hasan, F., Prinz, M., Weisberg, M.K., Nehru, C.E., Delaney, J.S., Grossman, L., Boily, M., 1988. Cumberland falls chondritic inclusions: III. Consortium study of relationship to inclusions in Allan Hills 78113 aubrite. Geochim. Cosmochim. Acta 52, 1835–1848.

Macke, R.J., Britt, D.T., Consolmagno, G.J., 2011. Density, porosity, and magnetic suscepotibility of achondritic meteorites. Meteorit. Planet. Sci. 46, 311–326.

MacPherson, G.J., Jarosewich, E., Lowenstein, P., 1993. Magombedze: a new H-chondrite with light–dark structure. Meteoritics 28, 138–142.

McGaha, J.E., Jacques, C., Pimentel, E., 2008. 2008 TC3. In: Williams, G.V. (Ed.), Minor planet electronic circular 2008-TC50. Minor Planet Center, Smithsonian Astrophysical Observatory, Cambridge, MA, p. 1 (Issued October 6, 14:59 UT).

McSween Jr., H.J., Mittlefehldt, D.W., Beck, A.W., Mayne, R.G., McCoy, T.J., 2010. HED meteorites and their relationship to the geology of Vesta and the Dawn Mission. Space Sci. Rev. 163, 141–174.

Meadni, H.T., Taha, G.M., 2011. Analysis of Almahata Sitta meteorite. Meteorit. Planet. Sci. 46, A156.

Meier, M.M.M., Welten, K.C., Jenniskens, P., Baur, H., Wieler, R., 2010. Cosmic ray exposure ages for Almahata Sitta non-ureilite samples. Meteorit. Planet. Sci. 45, A135.

Meier, M.M.M., Welten, K.C., Caffee, M.W., Friedrich, J.M., Jenniskens, P., Nishiizumi, K., Shaddad, M.H., Wieler, R., 2012. A noble gas and cosmogenic radionuclide analysis of two ordinary chondrites from Almahata Sitta. Meteorit. Planet. Sci. 47, 1075–1086.

Mikouchi, T., Zolensky, M., Takeda, H., Hagiya, K., Ohsumi, K., Satake, W., Kurihara, T., Jenniskens, P., Shaddad, M.H., 2010a. Mineralogy of pyroxene and olivine in the Almahata Sitta ureilite. Lunar Planet. Sci., 41 (abstract #2344).

Mikouchi, T., Zolensky, M.E., Ohnishi, I., Suzuki, T., Takeda, H., Jenniskens, P., Shaddad, M.H., 2010b. Electron microscopy of pyroxene in the Almahata Sitta ureilite. Meteorit. Planet. Sci. 45, 1812–1820.

Mikouchi, T., Zolensky, M.E., Ohnishi, I., Suzuki, T., Takeda, H., Jenniskens, P., Shaddad, M.H., 2010c. Transmission electron microscopy of pyroxenes in the Almahata Sitta Ureilite. Meteorit. Planet. Sci. 45, A138.

Mikouchi, T., Goodrich, C.A., Hoffmann, V.H., Zolensky, M.E., Sugiyama, K., 2011. Electron back-scatter diffraction study of iron metal in Almahata Sitta ureilite. Meteorit. Planet. Sci. 46, A161.

Mikouchi, T., Aoyagi, Y., Goodrich, C.A., Yubuta, K., Sugiyama, K., Zolensky, M.E., Goldstein, J.I., 2013. Cooling history of Almahata Sitta ureilite as inferred from transmission electron microscopy of iron metal. Meteorit. Planet. Sci. 48, 5205.

Misawa, K., Watanabe, S., Kitamura, M., Nakamura, N., Yamamoto, K., Masuda, A., 1992. A noritic clast from the Hedjaz chondritic breccia: implications for melting events in the early solar system. Geochem. J. 26, 435–446.

Mittlefehldt, D.W., Lindstrom, M.M., 1988. Geochemistry of diverse lithologies in antarctic eucrites (abstract). Lunar Planet. Sci. 19, 790–791.

Mittlefehldt, D.W., Lindstrom, M.M., Wang, M.-S., Lipschutz, M.E., 1995. Geochemistry and Origin of achondritic inclusions in Yamato-75097,-793241 and-794046 chondrites. In: Proc. NIPR Symp. Antarct. Meteorites 8, pp. 251–271.

Mittlefehldt, D.W., McCoy, T.J., Goodrich, C.A., Kracher, A., 1998. Non-chondritic meteorites from asteroidal bodies. In: Papike, J.J. (Ed.), Planetary Materials—Reviews in Mineralogy, 26. Mineralogical Society of America, Washington, pp. 4-01–4-170.

Miyahara, M., Ohtani, E., El Goresy, A., Lin, Y.T., Feng, L., Zhang, J.C., Gillet, P., Nagase, T., Muto, J., Nishijima, M., 2013. A huge single diamond in Almahata Sitta coarse-grained ureilite. Lunar Planet. Sci., 44 (abstract #1425).

Murty, S.V.S., Mahajan, R.R., Jenniskens, P., Shaddad, M.H., Eldien, B., 2010a. Noble gases and nitrogen in the Almahata Sitta ureilite. Meteorit. Planet. Sci. 45, 1751–1764.

Murty, S.V.S., Mahajan, R.R., Jenniskens, P., 2010b. Trapped nitrogen and noble gases in Almahata Sitta ureilite. Meteorit. Planet. Sci. 45, A144.

Nagao, K., 1994. Noble gases in hosts and inclusions from Yamato-75097 (L6),-793241 (L6) and–794046 (H5). In: Proc. NIPR Symp. Antarct. Meteorites 7, pp. 197–216.

Nakamura, N., Misawa, K., Kitamura, M., Masuda, A., Watanabe, S., Yamamoto, K., 1990. Highly fractionated REE in the Hedjaz (L) chondrite: implications for nebular and planetary processes. Earth Planet. Sci. Lett. 99, 290–302.

Nakamura, T., Noguchi, T., Tanaka, M., Zolensky, M.E., Kimura, M., Tsuchiyama, A., Nakato, A., Ogami, T., Ishida, H., Uesugu, M., Yada, T., Shirai, K., Fujimura, A., Okazaki, R., Sandford, S.A., Ishibashi, Y., Abe, M., Okada, T., Ueno, M., Mukai, T., Yoshikawa, M., Kawaguchi, J., 2011. Itokawa dust particles: a direct link between S-type asteroids and ordinary chondrites. Science 333, 1113–1116.

Okada, A., Keil, K., Taylor, G.J., Newsom, H., 1988. Igneous history of the aubrite parent asteroid: evidence from the Norton County enstatite achondrite. Meteoritics 23, 59–74.

Olsen, E.J., Fredriksson, K., Rajan, S., Noonan, A., 1990. Chondrule-like objects and brown glasses in howardites. Meteoritics 25, 187–194.

Ott, U., Herrmann, S., Jenniskens, P.M., Shaddad, M., 2010. A noble gas study of two stones from the Almahata Sitta Meteorite. Lunar Planet. Sci., 41 (abstract #1195).

Popova, O., Borovicka, J., Hartmann, W.K., Spurny, P., Gnos, E., Nemtchinov, I., Trigo-Rodriguez, J.M., 2011. Very low strengths of interplanetary meteoroids and small asteroids. Meteorit. Planet. Sci. 46, 1525–1550.

Pravec, P., Harris, A.W., 2007. Binary asteroid population. I. Angular momentum content. Icarus 190, 250–259.

Prinz, M., Nehru, C.E., Weisberg, M.K., Delany, J.S., Yanai, K., Kojima, H., 1984. H-chondritic clasts in a Yamato L6 chondrite: implications for metamorphism. Meteoritics 19, 292–293.

Prinz, M., Weisberg, M.K., Nehru, C.E., Delaney, J.S., 1986. North Haig and Nilpena: paired polymict ureilites with Angra dos Reis-related and other clasts (abstract). Lunar Planet. Sci. 17, 681–682.

Prinz, M., Weisberg, M.K., Nehru, C.E., Delaney, J.S., 1987. EET83309, a polymict ureilite: recognition of a new group (abstract). Lunar Planet. Sci. 18, 802–803.

Prinz, M., Weisberg, M.K., Nehru, C.E., 1988. Feldspathic components in polymict ureilites (abstract). Lunar Planet. Sci. 19, 947–948.

Pun, A., Keil, K., Taylor, G.J., Wieler, R., 1998. The Kapoeta howardite: implications for the regolith evolution of the howardite-eucrite-diogenite parent body. Meteorit. Planet. Sci. 33, 835–851.

Qin, L., Rumble, D., Alexander, C.M.O.D., Carlson, R.W., Jenniskens, P., Shaddad, M.H., 2010a. Chromium isotopic composition of Almahata Sitta. Lunar Planet. Sci., 41 (abstract #1910).

Qin, L., Rumble, D., Alexander, C.M.O.D., Carlson, R.W., Jenniskens, P., Shaddad, M.H., 2010b. The chromium isotopic composition of Almahata Sitta. Meteorit. Planet. Sci. 45, 1771–1777.

Rai, V.K., Murty, A.V.S., Ott, U., 2003. Noble gases in ureilites: cosmogenic, radiogenic, and trapped components. Geochim. Cosmochim. Acta 67, 4435–4456.

Reid, A.M., Buchanan, P., Zolensky, M.E., Barrett, R.A., 1990. The Bholghati howardite: petrography and mineral chemistry. Geochim. Cosmochim. Acta 54, 2161–2166.

Roggon, L., (Bachelor thesis) 2012. Charakterisierung ureilitischer Proben aus dem Almahata Sitta Meteoriten-Streufeld. Insitut für Planetologie, Westfälische Wilhelms-Universität Münster, Germany, 71 pp.

Ross, A.J., Steele, A., Downes, H., Fries, M., Jones, A.P., Kater, L., Smith, C.L., Jenniskens, P., Shaddad, M., Zolensky, M., 2010. Raman analysis of diamond in Almahata Sitta and other ureilites. Meteorit. Planet. Sci. 45, A174.

Ross, A.J., Herrin, J.S., Mittlefehldt, D.W., Downes, H., Smith, C.L., Lee, M.R., Jones, A.P., Jenniskens, P., Shaddad, M.H., 2011a. Petrography and geochemistry of metals in Almahata Sitta ureilites. Lunar Planet. Sci., 42 (abstract #2720).

Ross, A.J., Hezel, D.C., Howard, L.E., Smith, C.L., Downes, H., Herrin, J.S., Jenniskens, P., Shaddad, M., 2011b. Petrography and modal abundance of metal in ureilites: a combined 2D and 3D study. Meteorit. Planet. Sci. 46, A199.

Ross, A.J., Steele, A., Fries, M.D., Kater, L., Downes, H., Jones, A.P., Smith, C.L., Jenniskens, P.M., Zolensky, M.E., Shaddad, M.H., 2011c. MicroRaman spectroscopy of diamond and graphite in Almahata Sitta and comparison with other ureilites. Meteorit. Planet. Sci. 46, 364–378.

Rubin, A.E., Bottke, W.F., 2009. On the origin of shocked and unshocked CM clasts in H-chondrite regolith breccias. Meteorit. Planet. Sci. 44, 701–724.
Rubin, A.E., Scott, E.R.D., Taylor, G.J., Keil, K., Allen, J.S.B., Mayeda, T.K., Clayton, R.N., Bogard, D.D., 1983. Nature of the H chondrite parent body regolith: evidence from the Dimmitt breccia. In: Proc. 14th Lunar Planet. Sci. Conf, pp. A741–A754.
Rubin, A.E., Scott, E.R.D., Keil, K., 1997. Shock metamorphism of enstatite chondrites. Geochim. Cosmochim. Acta 61, 847–858.
Rubin, A.E., Kallemeyn, G.W., Wasson, J.T., Clayton, R.N., Mayeda, T.K., Grady, M., Verchovsky, A.B., Eugster, O., Lorenzetti, S., 2003. Formation of metal and silicate globules in Gujba: a new Bencubbin-like meteorite fall. Geochim. Cosmochim. Acta 67, 3283–3298.
Rumble, D., Zolensky, M.E., Friedrich, J.M., Jenniskens, P., Shaddad, M.H., 2010a. Oxygen isotope composition of Almahata Sitta. Lunar Planet. Sci., 41 (abstract #1245).
Rumble, D., Zolensky, M.E., Friedrich, J.M., Jenniskens, P., Shaddad, M.H., 2010b. The oxygen isotope composition of Almahata Sitta. Meteorit. Planet. Sci. 45, 1765–1770.
Ruzicka, A., Snyder, G.A., Taylor, L.A., 1998. Mega-chondrules and large, igneous-textured clasts in Julesberg (L3) and other ordinary chondrites: vapor-fractionation, shock-melting, and chondrule formation. Geochim. Cosmochim. Acta 62, 1419–1442.
Sabbah, H., Morrow, A.L., Jenniskens, P., Shaddad, M.H., Zare, R.N., 2010. Polycyclic aromatic hydrocarbons in asteroid 2008 TC_3: dispersion of organic compounds inside asteroids. Meteorit. Planet. Sci. 45, 1710–1717.
Sandford, S.A., Milam, S.N., Nuevo, M., Jenniskens, P., Shaddad, M.H., 2010a. Infrared spectroscopy of samples from multiple stones from the Almahata Sitta meteorite. Lunar Planet. Sci., 41 (abstract #1229).
Sandford, S.A., Milam, S.N., Nuevo, M., Jenniskens, P., Shaddad, M.H., 2010b. Infrared spectroscopy of multiple samples from the Almahata Sitta meteorite. Meteorit. Planet. Sci. 45, A179.
Sandford, S.A., Milam, S.N., Nuevo, M., Jenniskens, P., Shaddad, M.H., 2010c. The mid-infrared transmission spectra of multiple stones from the Almahata Sitta meteorite. Meteorit. Planet. Sci. 45, 1821–1835.
Scheeres, D.J., Sánchez, P., 2011. Evolution of small, rapidly rotating asteroids. Lunar Planet. Sci. 42 (abstract #2307).
Scheirich, P., Ďurech, J., Pravec, P., Kozubal, M., Dantowitz, R., Kaasalainen, M., Betzler, A.S., Beltrame, P., Muler, G., Birtwhistle, P., Kugel, F., 2010. The shape and rotation of asteroid 2008 TC3. Meteorit. Planet. Sci. 45, 1804–1811.
Scott, E.R.D., Taylor, G.J., Keil, K., 1993. Origin of ureilite meteorites and implications for planetary accretion. Geophys. Res. Lett. 20, 415–418.
Semenenko, V.P., Bischoff, A., Weber, I., Perron, C., Girich, A.L., 2001. Mineralogy of fine-grained material in the Krymka (LL3.1) chondrite. Meteorit. Planet. Sci. 36, 1067–1085.
Shaddad, M.H., Jenniskens, P., Numan, D., Kudoda, A.M., Elsir, S., Riyad, I.F., Ali, A.E., Alameen, M., Alameen, N.M., Eid, O., Osman, A.T., AbuBaker, M.I., Yousif, M., Chesley, S.R., Chodas, P.W., Albers, J., Edwards, W.N., Brown, P.G., Kuiper, J., Friedrich, J.M., 2010. The recovery of asteroid 2008 TC3. Meteorit. Planet. Sci. 45, 1557–1589.
Singletary, S.J., Grove, T.L., 2003. Early petrologic processes on the ureilite parent body. Meteorit. Planet. Sci. 38, 95–108.
Sokol, A.K., Bischoff, A., Marhas, K.K., Mezger, K., Zinner, E., 2007a. Late accretion and lithification of chondritic parent bodies: Mg isotope studies on fragments from primitive chondrites and chondritic breccias. Meteorit. Planet. Sci. 42, 1291–1308.
Sokol, A.K., Chaussidon, M., Bischoff, A., Mezger, K., 2007b. Occurrence and origin of igneous fragments in chondritic breccias. Geochim. Cosmochim. Acta 71 (Suppl. 1), A952.
Stöffler, D., Keil, K., Scott, E.R.D., 1991. Shock metamorphism of ordinary chondrites. Geochim. Cosmochim. Acta 55, 3845–3867.
Taricco, C., Bhandari, N., Colombetti, P., Romero, A., Vivaldo, G., Sinha, N., Jenniskens, P., Shaddad, M.H., Ballabh, G.M., 2010. Cosmogenic radioisotopes in the Almahata Sitta ureilite. Meteorit. Planet. Sci. 45, 1743–1750.
Terada, K., Bischoff, A., 2009. Asteroidal granite-like magmatism 4.53 Gyr ago. Astrophys. J. 699, L68–L71.
Tholen, D.J., 1989. Asteroid taxonomic classifications. In: Mathews, M.S., Binzel, R.P., Gehrels, T. (Eds.), Asteroids II. The University of Arizona Press, Tucson, pp. 1139–1150.
Torigoye-Kita, N., Tatsumoto, M., Meeker, G.P., Yanai, K., 1995. The 4.65 Ga U-Pb age of the MET 78008 ureilite. Geochim. Cosmochim. Acta 59, 2319–2329.
Treutler, J., (Bachelor thesis) 2013. Minerlogische und gefügekundliche Charakterisierung von Meteoritenbruckstücken aus dem Almahata Sitta Streufeld. Insitut für Planetologie, Westfälische Wilhelms-Universität Münster, Germany, 55 pp.
Trinquier, A., Birck, J.-L., Allègre, C.J., 2007. Widespread ^{54}Cr heterogeneity in the inner solar system. Astrophys. J. 655, 1179–1185.
Turrin, B.D., Herzog, G.F., Park, J., Lindsay, F.N., Delaney, J.S., Swisher, C.C., 2013. 40Ar/39Ar ages of H5 and L4 chondrites from Almahata Sitta. Meteorit. Planet. Sci. 48, 5335.
van Niekerk, D., Keil, K., 2011. Metal/sulfide-silicate intergrowth textures in EL3 meteorites: Origin by impact melting on the EL parent body. Meteorit. Planet. Sci. 46, 1484–1497.
Vdovykin, G.P., 1972. Forms of carbon in the new Haverö ureilite of Finland. Meteoritics 7, 547–552.
Walker, D., Grove, T., 1993. Ureilite smelting. Meteoritics 28, 629–636.
Warren, P.H., 2010. Asteroidal depth-pressure relationships and the style of the ureilite anatexis. Meteorit. Planet. Sci. 45, A120.
Warren, P.H., Kallemeyn, G.W., 1992. Explosive volcanism and the graphite oxygen fugacity buffer on the parent asteroid(s) of the ureilite meteorites. Icarus 100, 110–126.
Warren, P.H., Huber, H., 2006. Ureilite petrogenesis: a limited role for smelting during anatexis and catastrophic disruption. Meteorit. Planet. Sci. 41, 835–849.
Warren, P.H., Rubin, A.E., 2010. Pyroxene-selective impact smelting in ureilites. Geochim. Cosmochim. Acta 74, 5109–5133.
Warren, P.H., Ulff-Møller, F., Huber, H., Kallemeyn, G.W., 2006. Siderophile geochemistry of ureilites: a record of early stages of planetesimal core formation. Geochim. Cosmochim. Acta 70, 2104–2126.
Wasson, J.T., Chou, C.L., Bild, R.W., Baedecker, P.A., 1976. Classification of and elemental fractionation among ureilites. Geochim. Cosmochim. Acta 40, 1449–1458.
Wasson, J.T., Rubin, A.E., Kallemeyn, G.W., 1993. Reduction during metamorphism of four ordinary chondrites. Geochim. Cosmochim. Acta 57, 1867–1878.
Weidenschilling, S.J., 2013. Gravitational diffusion and mixing during accretion of the asteroids. Lunar Planet. Sci., 44 (abstract #2704).
Weisberg, M.K., Fogel, R.A., Prinz, M., 1997. Kamacite-enstatite intergrowths in enstatite chondrites. Lunar Planet. Sci., 28 (abstract #1768).
Weisberg, M.K., Smith, C., Benedix, G., Herd, C.D.K., Righter, K., Haack, H., Yamaguchi, A., Chennaoui Aoudjehane, H., Grossman, J.N., 2009. Almahata Sitta. The Meteoritical Bulletin, No. 96. Meteorit. Planet. Sci. 44, 1355–1397.
Weisberg, M.K., Ebel, D.S., Connolly, H.C.J., 2013. EL3 chondrites: Primitive nebular materials, not products of asteroidal processing. Lunar Planet. Sci., 44 (abstract #2871).
Welten, K.C., Meier, M.M.M., Caffee, M.W., Nishiizumi, K., Wieler, R., Jenniskens, P., Shaddad, M.H., 2010a. Cosmogenic nuclides in Almahata Sitta ureilites: cosmic-ray exposure age, preatmospheric mass, and bulk density of asteroid 2008 TC3. Meteorit. Planet. Sci. 45, 1728–1742.
Welten, K.C., Meier, M.M.M., Caffee, M.W., Nishiizumi, K., Wieler, R., Jenniskens, P., Shaddad, M.H., 2010b. High porosity and cosmic-ray exposure age of Asteroid 2008 TC_3 derived from cosmogenic nuclides. Lunar Planet. Sci., 41 (abstract #2256).
Welten, K.C., Meier, M.M.M., Caffee, M.W., Nishiizumi, K., Wieler, R., Jenniskens, P., Shaddad, M.H., 2011. Cosmogenic nuclides and noble gas evidence that Almahata Sitta chondrites represent fragments of asteroid 2008 TC_3. Lunar Planet. Sci., 42 (abstract #2667).
Wilkening, L.L., 1973. Foreign inclusions in stony meteorites. I. Carbonaceous chondritic xenoliths in the Kapoeta howardite. Geochim. Cosmochim. Acta 37, 1985–1989.
Wilson, L., Goodrich, C.A., Van Orman, J.A., 2008. Thermal evolution and physics of melt extraction on the ureilite parent body. Geochim. Cosmochim. Acta 72, 6154–6176.
Wlotzka, F., 1993. A weathering scale for ordinary chondrites (abstract). Meteoritics 28, 460.
Yeomans, D., 2008. NASA/JPL Near-Earth Object Program Office Statement, http://neo.jpl.nasa.gov/news/2008tc3.html (4th November 2008).
Yin, Q.-Z., Yamashita, K., Yamakawa, A., Tanaka, R., Jacobsen, B., Ebel, D., Hutcheon, I.D., Nakamura, E., 2009. ^{53}Mn–^{53}Cr systematic of Allende chondrules and ε^{54}Cr-Δ^{17}O correlation in bulk carbonaceous chondrites. Lunar Planet. Sci. 40 (abstract #2006).
Zolensky, M.E., Ivanov, A., 2003. The Kaidun microbreccia meteorite: a harvest from the inner and outer asteroid belt. Chem. Erde Geochem. 63, 185–246.
Zolensky, M.E., Hewins, R.H., Mittlefehldt, D.W., Lindstrom, M.M., Xiao, X., Lipschutz, M.E., 1992. Mineralogy, petrology and geochemistry of carbonaceous chondritic clasts in the LEW 85300 polymict eucrite. Meteoritics 27, 596–604.
Zolensky, M.E., Weisberg, M.K., Buchanan, P.C., Mittlefehldt, D.W., 1996. Mineralogy of carbonaceous chondrite clasts in HED achondrites and the moon. Meteorit. Planet. Sci. 31, 518–537.
Zolensky, M.E., Herrin, J., Jenniskens, P., Friedrich, J.M., Rumble, D., Steele, A., Sandford, S.A., Shaddad, M.H., Le, L., Robinson, G.A., Morris, R.V., 2009. Mineralogy of the Almahata Sitta ureilite. Meteorit. Planet. Sci. 44, A227.
Zolensky, M.E., Herrin, J., Mikouchi, T., Satake, W., Kurihara, T., Sandford, S.A., Milam, S.N., Hagiya, K., Ohsumi, K., Friedrich, J.M., Jenniskens, P., Shaddad, M.H., Le, L., Robinson, G.A., 2010a. Olivine in Almahata Sitta – curiouser and curiouser. Lunar Planet. Sci., 41 (abstract #2306).
Zolensky, M., Herrin, J., Mikouchi, T., Ohsumi, K., Friedrich, J., Steele, A., Rumble, D., Fries, M., Sandford, S., Milam, S., Hagiya, K., Takeda, H., Satake, W., Kurihara, T., Colbert, M., Hanna, R., Maisano, J., Ketcham, R., Goodrich, C., Le, L., Robinson, G., Martinez, J., Ross, K., Jenniskens, P., Shaddad, M.H., 2010b. Mineralogy and petrography of the Almahata Sitta ureilite. Meteorit. Planet. Sci. 45, 1618–1637.